The Specialist Committee on Hydrodynamic Noise

Final Report and Recommendations to the 29th ITTC

1. OVERVIEW

This report summarizes the work of the Specialist Committee on Hydrodynamic Noise for the 29th ITTC.

1.1 Membership and Meetings

The 28th ITTC appointed the following members to serve on the Specialist Committee on Hydrodynamic Noise:

- Johan Bosschers (chair), MARIN, Netherlands
- Romuald Boucheron, DGA/H, France
- Yezhen Pang, CSSRC, China
- Cheolsoo Park, KRISO, Korea
- Bryce Pearce (secretary), AMC, Australia
- Kei Sato, MHI, Japan
- Tuomas Sipilä, VTT, Finland, (resigned in February 2020 due to job change).
- Claudio Testa, CNR/INM, Italy
- Michele Viviani, UNIGE, Italy

The committee held three face-to-face meetings at the following locations:

- Wageningen, Netherlands, at MARIN on February 7-8, 2018
- Launceston, Australia, at AMC, on March 27-28, 2019
- Rome, Italy, at CNR/INM on February 30-31, 2020

Figure 1. Photograph of the Specialist Committee on Hydrodynamic Noise at its first meeting.

Video conferences were held on June 27, 2018; August 1, 2019; July 30, 2020; September 24, 2020; October 29, 2020; and January 27+28, 2021.

1.2 Recommendations of the 28th ITTC

The 28th ITTC recommended the Specialist Committee on Hydrodynamic Noise for the 29th ITTC to address the following activities:

1. Present ITTC procedures and our community's capabilities to predict emitted noise from ships to the IMO. Specifically, an informative submission shall be made to MEPC 72 (Spring, 2018) of Guideline 7.5-02-01-05 Model-scale propeller cavitation noise measurements.
2. Monitor progress on shipping noise measurement procedures for shallow water and regulations as developed by ISO, classification societies and regulatory agencies.
3. Monitor progress on model-scale noise measurements with emphasis on facility reverberation and scaling of vortex cavitation noise.
4. Monitor progress on computational prediction of propeller noise with emphasis on methods using the acoustic analogy such as coupling CFD with FWHE.
5. Identify a benchmarking case for model-scale noise measurements that has,
   a) full-scale underwater radiated noise measurements available,
   b) that is a representative merchant vessel.
   c) of which geometry and measurement data can be shared with the ITTC community.
6. Maintain and update ITTC guideline 7.5-02-01-05: Model-Scale Propeller Cavitation Noise Measurements and guideline 7.5-04-04-01: Underwater Noise from Ships, Full-Scale Measurements.

For various reasons, the Specialist Committee decided to not prepare an informative submission to the IMO MEPC 72 to be held in Spring 2018. However, an informative document was submitted by the Secretary of the ITTC without input from the Specialist Committee. For that reason, term of reference no. 1 is not further addressed in this report.

2. INTRODUCTION

Noise is described as unwanted sound which interferes with the normal functioning of a system. The noise that is described in this report is the underwater radiated noise of ships in general and of the cavitating propeller in particular. Ship noise is considered as unwanted sound as it increases the signature of naval vessels in relation to threats such as submarines, mines, and torpedoes. It may also interfere with the ability of marine mammals (Southall *et al.*, 2008) and fish (Popper & Hastings, 2009) to hear a sound of interest (masking). A significant number of studies have been and are being performed on the impact of shipping noise on marine life as shown in Figure 2. An extensive review of these studies has been given by Duarte *et al*. (2021).

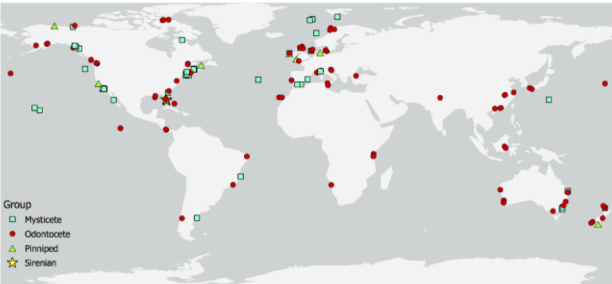

Figure 2. Map showing locations where the effect of ship noise on marine mammals has been or is being studied (Erbe, 2019).

In response to the concern of the effect of underwater noise by shipping on aquatic life, the IMO, class societies, governmental bodies and other organizations have addressed the underwater radiated noise (URN) of merchant vessels as further reviewed in this report.

The various mechanisms that contribute to the URN of ships are discussed by Ross (1976), Urick (1983), and the reports of the 27th and 28th ITTC Specialist Committee on Hydrodynamic Noise. The most important noise sources are machinery noise comprising propulsion and auxiliary components, and propeller cavitation noise. Machinery noise is typically emitted up to a frequency of about 1 kHz whereas propeller cavitation noise is emitted in the frequency range of the blade passage frequency (say 10 Hz) up to 20 kHz and above. An example of the URN spectrum of a merchant vessel is shown in Figure 3. At and below the cavitation inception speed of 10 knots, the noise is caused by machinery equipment. At higher speeds, the high-frequency noise is fully determined by propeller cavitation while the low-frequency noise is due to both machinery equipment and cavitation, with cavitation fully dominant at 16 knots.

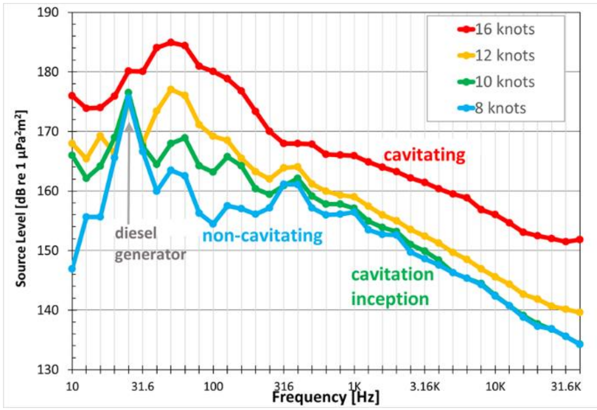

Figure 3. Underwater radiated noise spectrum of a 173 m merchant vessel, data taken from Arveson & Vendittis (2000). Cavitation inception speed is about 10 knots.

Almost all merchant vessels operate with a cavitating propeller at service speed, showing the importance of cavitation noise, with the URN levels decreasing with lower ship speed until the propeller is free from cavitation at shown in Figure 3. However, controllable pitch propellers are known to cavitate at both low and high speed and can be free from cavitation at an intermediate speed.

The interest in the URN of merchant vessels has led to several review studies on URN mitigation measures, such as Renilson (2009), Aquo-Sonic Guidelines for regulation on UW noise from commercial shipping (2015), Chmelnitsky & Gilbert (2016), McHorney *et al*.

(2018), and Kendrick & Terweij (2019). In general, mitigation measures to reduce the source level of the cavitating propeller aim to either reduce ship resistance thereby reducing propeller loading, improving the homogeneity of the ship wake field in which the propeller operates, improved propeller or propulsor design with respect to cavitation extents, or using air bubbles to alleviate the cavity collapse and rebound. Measures such as ship speed reduction and rerouting have also been proposed and investigated, as well as improved manufacturing and maintenance of the propeller.

3. REGULATION

This chapter reviews the recent developments on the regulation of shipping noise at an international and national level. A more extensive review on this topic is provided by Colbert (2020). The rules of classification societies on URN are also discussed.

3.1 International level

The IMO has released non-mandatory 'Guidelines for the Reduction of Underwater Noise from Commercial Shipping' in 2014, but the topic of URN has not been on the agenda of the MEPC since. For the 75th session of the MEPC, scheduled for April 2020, proposal MEPC/75/14 was submitted by Australia, Canada and the United States with as proposed action to review the IMO guidelines and to identify next steps. The proposal was supported by a large number of countries of the EU (document MEPC/75/14/2) in which it was also proposed to address URN on the agenda of MEPC76. However, the 75th session was cancelled due to COVID-19, and was organized as a virtual meeting in November 2020. In that meeting, proposal MEPC/75/14 could not be discussed due to time restrictions and the discussion has been postponed to MEPC76.

Meetings to discuss the impact of underwater anthropogenic noise were also organized by the UN Food and Agriculture Organization (FAO, 2019) and the United Nation Convention of Law of the Sea (UNCLOS, 2018).

The International Quiet Ocean Project [1] (IQOE) aims to promote research, observations, and modelling to improve understanding of ocean soundscapes and effects of sound on marine organisms. The IQOE was founded by the Scientific Committee on Oceanic Research (SCOR) and the Partnership for Observation of the Global Oceans (POGO). The website contains a large number of links to related projects.

3.2 National level

Australia is closely following and endorsing the developments at IMO on URN by shipping and its impact on marine life, largely due to their concern regarding the Great Barrier Reef (GBR). Legislation for Particular Sensitive Sea Areas (such as GBR) allows for speed limits to be set.

The EU has defined the Marine Strategy Frameword Directive 2008/56/EC which aims to achieve good environmental status, including underwater noise, in the European marine waters by 2020. At present, various monitoring campaigns of ambient underwater noise (sound scaping), which includes the noise of shipping, have started on a regional level, being among others the JOMOPANS [2] project in the North Sea, the QuietMED2 [3] project in the Mediterranean Sea, and the JONAS [4] project in the Atlantic Seas. The TANGO project investigates the effect of rerouting shipping lanes in the Kattegat on the soundscape and ecosystem.

Whereas the assessment of the present levels of ambient underwater noise in the European marine waters is well on its way, the critical

[1] https://www.iqoe.org
[2] https://www.northsearegion.eu/jomopans/
[3] https://www.quietmed2.eu
[4] https://www.jonasproject.eu

levels have not yet been determined. The EU Technical Group on Underwater Noise (TG Noise) provides guidance on noise monitoring and an assessment of framework and thresholds for good environmental status for impulsive and continuous noise.

Canada has a number of major shipping routes that overlap with the habitat of endangered animals like the North Atlantic right whale, the beluga whale, and the Southern Resident killer whale. Canada has regulatory mechanisms for the protection of imperilled animals through the Species at Risk Act (SARA). In 2019, measures to reduce underwater noise levels in British Columbia were introduced by the Fisheries and Oceans Canada (DFO) consisting of among others introducing no-go zones for vessels and voluntary guidelines to reduce ship speed to 7 knots or less when within 1000m of killer whales. Also, various noise monitoring programs were initiated by DFO.

Transport Canada has taken several initiatives to reduce shipping noise, such as funding a literature review on ship noise mitigation measures (Kendrick & Terweij, 2019) and organizing an international workshop on 'Quieting ships to protect the marine environment' in London (Bahtiarian, 2019). Both short-term and long-term recommendations for action and future work were defined, such as development of an improved quiet ship design guide, harmonizing the URN limits and measurement methodologies used by class societies, and improving prediction methods for hull and propeller URN prediction.

The Port of Vancouver has introduced in 2017 a discount system, EcoAction, to encourage URN mitigation measures on ships. In 2019, the program was expanded by incorporating rules of more class societies. In 2017, the Port of Prince Rupert has introduced a similar discount system, called Green Wave.

In the US, NOAA has published a roadmap to address ocean noise for a period of 10 years (Gedamke *et al.*, 2016). Marine mammals are protected in the U.S. by the Marine Mammal Protection Act and the Endangered Species Act. NOAA and other organizations are working to better understand underwater sound within the National Marine Sanctuary System[5], see Figure 4 for an example. Sound within seven national marine sanctuaries and one marine national monument will be studied. Standardized measurements will assess sounds produced by marine animals, physical processes (e.g., wind and waves), and human activities, and some results have been published by Haver *et al.* (2019)

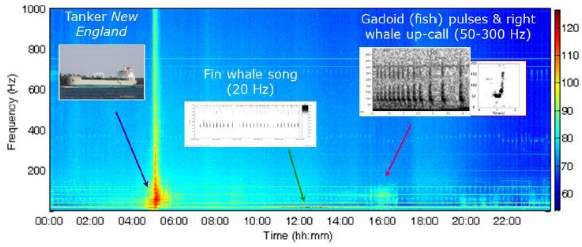

Figure 4. Example of 24-hour soundscape at Stellwagen Bank National Marine Sanctuary (Gedamke *et al.*, 2016).

The Green Marine voluntary certification program for the North American marine industry has also renewed its criteria in 2020 for ports and for ship owners on underwater radiated noise.

3.3 Noise criteria

The first public noise criteria issued for non-military ships is probably the ICES[6] CR209 rule for the URN of fishery research vessels (Mitson, 1995). These noise criteria have also been adopted by classification societies, although sometimes small changes are applied in the lower frequency range.

The first classification society to issue URN rules was DNV through its Silent class in 2010, with its latest version issued in 2019. A

[5] https://sanctuaries.noaa.gov/science/monitoring/sound/ , https://www.pmel.noaa.gov/acoustics/

[6] International Council for the Exploration of the Sea

distinction was made between five different classes of ships, each with a different criterion, being: *i)* Acoustic (ships involved in hydro-acoustic measures); *ii)* Seismic (ships involved in seismic surveys); *iii)* Fishery; *iv)* Research; and *v)* Environmental (any vessel which require controlled environmental noise emission). Other class societies followed with BV releasing rule NR614 on underwater radiated noise in 2014 (with an update in 2017) which specifies noise limits for a "URN – controlled vessel" and a "URN – advanced vessel". Ship speeds or engine load is not specified by BV. The noise limits for a "URN – specified vessel" are specified on a case-by-case study but may for instance consist of the ICES 209 norm. LR issued its noise criteria in 2017 making a distinction between Transit, Quiet and Research levels. The ship speed or engine load at which the criteria is to be met depends on ship type. RINA has released the DOLPHIN class in 2017 in which underwater radiated noise limits are defined for a "Quiet Ship" and for a "Transit Ship" while noise limits are also given for yachts and pleasure yachts. ABS issued its rules for underwater noise (UWN) in 2018 making a distinction between Commercial Vessels (either Transit or Quiet), Research Vessels, and UWN+ requirements for Commercial Vessels (either Transit or Quiet), with noise limits that are 5 dB below those of 'regular' Commercial Vessels. The ship speed for the Quiet condition depends on ship length. CCS issued its criteria in 2018 and also distinguishes three noise levels, designated Underwater Noise 1, Underwater Noise 2, and Underwater Noise 3. The ship speeds are not specified. The list of class rules on URN is given in Table 1.

The noise criteria for commercial vessels corresponding to Quiet and Transit, or similar criteria, of these class societies are presented in Figure 5 and Figure 6. Note that there are small differences in ship speeds for the Quiet condition and the engine load for the Transit condition, and that some classes do not prescribe the ship condition. LR is the only class society that prescribes the noise levels as source levels which explains the higher noise limits at low frequencies, all other class societies use radiated noise levels. BV is the only class society that prescribes the noise levels in spectrum level (i.e., dB re 1 μPa^{2}m^2/Hz), all other class societies use one-third-octave levels. The noise limits by BV have been converted to one-third-octave levels in the figures. The noise limits by ABS correspond to their UWN+ class. The most stringent noise limits are by CCS.

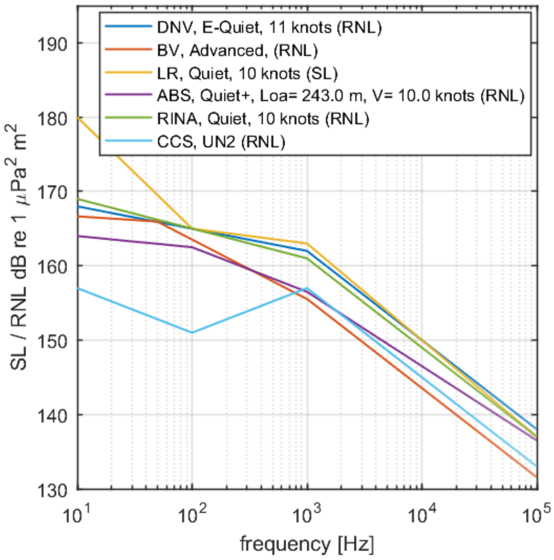

Figure 5. Noise criteria for 'Quiet' condition of commercial ships of various classification societies.

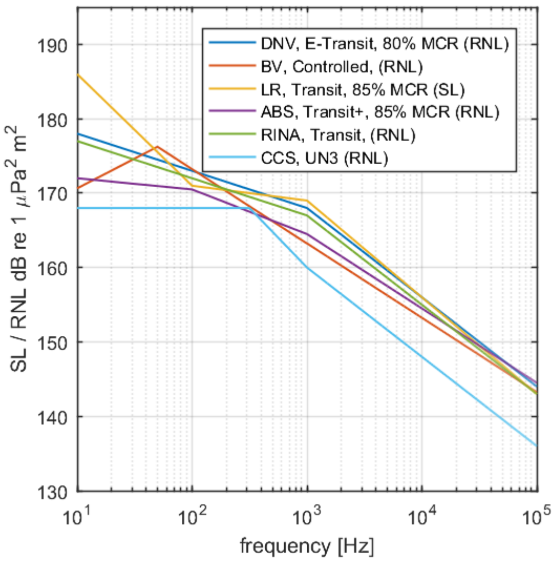

Figure 6. Noise criteria for 'Transit' condition of commercial ships of various classification societies.

Table 1. Standards for the measurement of the underwater radiated noise from ships.

National/International Standards
• ANSI/ASA, 2009, Quantities and procedures for description and measurement of underwater sound from ships, Part 1: General requirements, ANSI/ASA S12.64-2009/Part 1
• ISO 17208-1:2016 Underwater acoustics – Quantities and procedures for description and measurement of underwater sound from ships – Part 1: Requirements for precision measurements in deep water used for comparison purposes
• ISO 17208-2:2019. Underwater acoustics – Quantities and procedures for description and measurement of underwater sound from ships – Part 2: Determination of source level from deep water measurements.
• ISO/NP 17208-3:2017. Underwater acoustics – Quantities and procedures for description and measurement of underwater noise from ships – Part 3: Requirements for measurements in shallow water (under development in ISO/TC43/SC3)
• ISO 18405:2017 Underwater acoustics – Terminology.
Rules of Classification Societies
• DNV-GL (2020), Rules for classification – Ships – DNVGL-RU-Ship Pt.6 Ch.7, Section 6 Underwater Noise Emission - Silent • DNV-GL (2019), Class Guideline DNVGL-CG-0313, Edition July 2019, Measurement procedures for noise emission
• BV (2018), Underwater Radiated Noise (URN), Bureau Veritas Rule Note NR614
• RINA (2017), Amendments to Part A and Part F of “Rules for the Classification of Ships” - New additional class notation: “DOLPHIN QUIET SHIP” and “DOLPHIN TRANSIT SHIP”
• ABS (2018), Guide for the classification notation
• LR (2018), ShipRight - Design and Const-ruction - Additional Design and Construction Procedure for the Determination of a Vessel’s Underwater Radiated Noise
• CCS (2018), Guideline for ship underwater radiated noise

4. FULL-SCALE MEASUREMENT

4.1 Review of standards and procedures

4.1.1 General review

The measured URN of a ship is affected by many factors such as ship operating condition, distance between hydrophone and ship, depth of hydrophone, measurement time, water depth, etc. As the measurement result should not depend on measurement procedures, ANSI/ASA and ISO standards have been developed for the full-scale measurement of the URN of ships. These standards are listed in Table 1. Standards have been released for deep water (from an acoustic point of view) while a standard for shallow water is still in development. Reviews and discussions of aspects relevant for the URN measurements can be found in Moreno (2014), Robinson *et al.* (2014), and the ITTC guideline 7.5-04-04-01 on Underwater Noise from Ships, Full Scale Measurements (ITTC, 2017b).

Six classification societies, such as CCS (China Classification Society), RINA (Italian Classification Society), DNV-GL (Det Norske Veritas - Germanischer Lloyd), BV (Bureau Veritas), ABS (American Bureau of Shipping) and LR (UK Lloyd's Register) have issued rules for underwater noise testing of ships. Here the differences in test requirements, test procedure and underwater noise criteria are reviewed together with ISO standards. An overview of the rules are provided in Appendix A of this report.

Hannay *et al.* (2019) reviewed the methods implemented by five Quiet Ship Certification Procedures considered. Each of the classification societies has defined one or more notations, indicating vessels meet corresponding specified noise emission criteria. In all cases the criteria are a set of 1/3-octave band (or in one case the spectral density distribution) of maximum noise emission levels. Each society also defines a measurement procedure, that includes site/depth requirements, hydrophone geometry, ship track layout, and sound level calculation instructions. Differences in the measurement procedures leads to numeric differences in measured levels between class notations. If measurement configurations are well documented, then it is possible to adjust measurements from one class notation to compare with those of another.

DNV-GL also allows for the measurement of URN using onboard pressure sensors mounted on the hull above the propeller, Figure 7 (see class guideline DNVGL-CG-0313, July 2019). The simplified measurement method is based on pressure measurements in the vicinity of the vessel's propeller(s). The method is not applicable for testing of the Silent(R) requirements or for the thruster condition of Silent(A). Additionally, the method is only applicable for vessels equipped with diesel electric propulsion systems with resiliently mounted diesel generators.

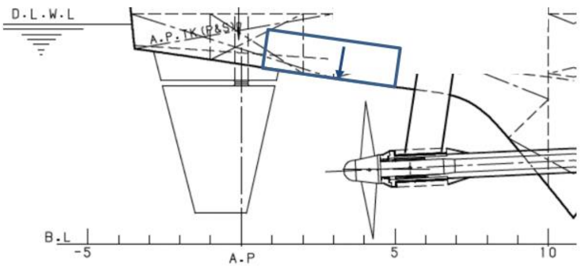

Figure 7. Pressure device locations of DNV's simplified method.

4.1.2 Hydrophone deployment

There are 2 kinds of potential deployment approaches to position the hydrophone: surface-based deployment and bottom based deployment. Practically, it is easier to deploy the hydrophones from an assistant ship or a surface buoy rather than using a bottom anchor. However, bottom anchor deployment may effectively mitigate the effects of cable strum and sea surface effects, which leads to more accurate measurement results especially for low frequencies.

One hydrophone, three hydrophones or more than three hydrophones are used depending on the test method. DNV and CCS use the traditional one hydrophone method for shallow water test. ISO 17208-1 (ISO, 2016) and other classification societies promote three hydrophone methods both in shallow water and deep water. ISO 17208-2 (ISO, 2019a) suggests using more than three hydrophones to improve accuracy. The measurement method with three hydrophones or more reduces the variability caused by Lloyd's mirror surface image coherence and bottom reflections.

The recommendation of ISO 17208-1 standard for the deployment of three hydrophones is that the hydrophones are located at angles of 15°, 30° and 45° to the ship as measured from the sea surface.

In general, it is useful to have more than one hydrophone to create some redundancy in the measurement. If a hydrophone array with more than three hydrophones is used with a specific geometry to get more adequate and accurate measurement data, the hydrophones shall be in line as shown in Figure 8.

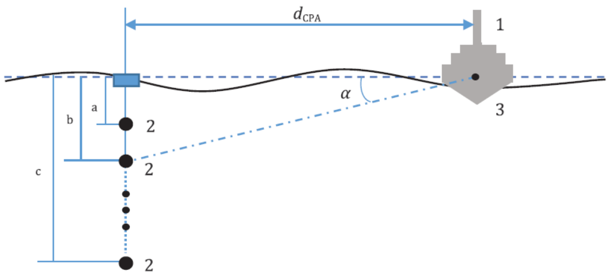

Figure 8. An example of multi-hydrophone deployment.

4.1.3 CPA distance

In ISO 17208-1, the distance for CPA (closest point of approach) is defined as the greater of either 100 m or the ship length. In practical situations, this distance cannot always be strictly controlled. The tolerance of the actual distance at CPA shall no less than -10 % and no greater than +25 % (-10 %/+25 %).

Recommendations from the AQUO project, adopted in the BV rule, specifies an expanded series of such runs past the array to acquire data at multiple CPA to aid in accounting for propagation losses. Six runs are recommended as depicted in Figure 9. Test runs are made for both port and starboard aspect at three different CPA; i) 200 m or distance of 1 ship length, ii) 400 m or distance of 1.5 ship length, iii) 500 m or distance of 2 ship length. Results from these varying CPA aid in assessing source-to-receiver propagation characteristics. Recognition is given of possible issues with low signal-to-noise for quieter ships at the greater CPA. Repeat runs at the closer CPA are recommended to help determine repeatability. Accuracy of CPA distance is specified to be +/- 10 m.

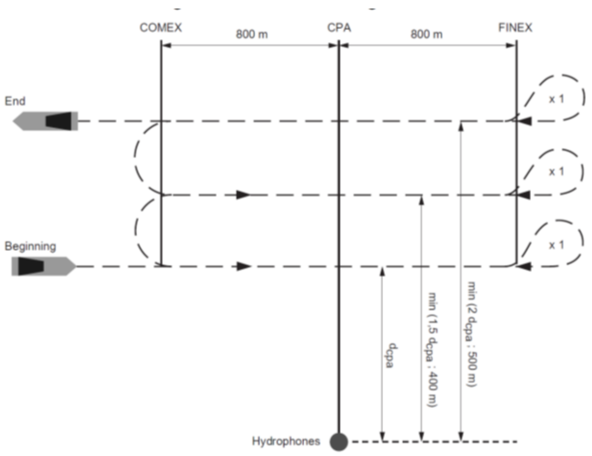

Figure 9. AQUO/BV rule multi-CPA test course configuration (AQUO-SONIC, 2015).

4.1.4 Source Level Correction

Normally, underwater radiated noise level is calculated from measured noise pressure level based on spherical spreading, for which the propagation loss is given by $20\log_{10}R/r_0$, with R the distance between hydrophone and ship, and r_0 the reference distance of 1 m. Some rules take the propagation loss in shallow water as in-between spherical spreading and cylindrical spreading, with the propagation loss given by $18\log_{10}R/r_0$ (DNV) or $19\log_{10}R/r_0$ (BV and CCS).

Since the underwater sound pressure levels are affected by the presence of the free surface (and sometimes the bottom), such quantities are considered "affected source levels" (ANSI/ASA S12.64). To evaluate the source level in the free field, i.e., without the effect of surface reflection and bottom reflection, the term "monopole source level" is introduced in ISO 17208-2. In deep water, the effect of bottom reflection is negligible, and only the Lloyd mirror effect is taken into account.

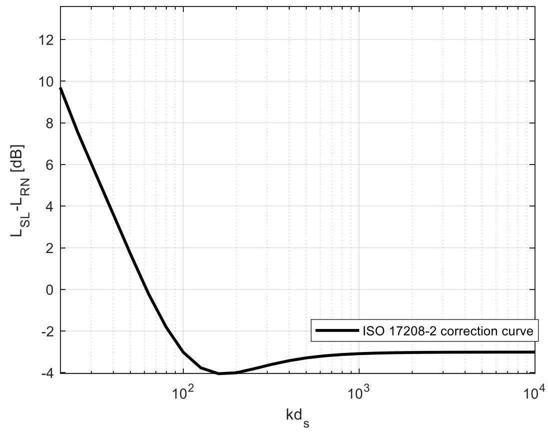

Figure 10. Correction for Lloyd-mirror effect as given by Eq. (1).

For sea trials, where sea surface scattering is influenced by sea state and bubbles, the Lloyd mirror interference pattern is only observed at low frequencies while at high frequencies an incoherent mirror image is assumed leading to a 3 dB correction. The following formulation, as shown in Figure 10, is one of the simplified formulations proposed by ISO 17208-2 for the propagation loss by Lloyd mirror (PL_{LM}) for a single hydrophone:

$$PL_{LM}\ [dB] = \begin{cases} -10log_{10}[4\sin^2(kd_s\sin\theta)] & kd_s\sin\theta \le 3\pi/4 \\ -10log_{10}2 & kd_s\sin\theta > 3\pi/4 \end{cases} \quad (1)$$

where θ corresponds to the depression angle of the hydrophone, k to the acoustic wave number, and d_s to the depth of the source. For wind speeds above approximately 5 m/s, the effect of Lloyd mirror almost disappears for frequencies above 5 kHz and PL_{LM} is close to 0 dB (Audoly & Meyer 2017; He *et al.*, 2020), see Figure 11.

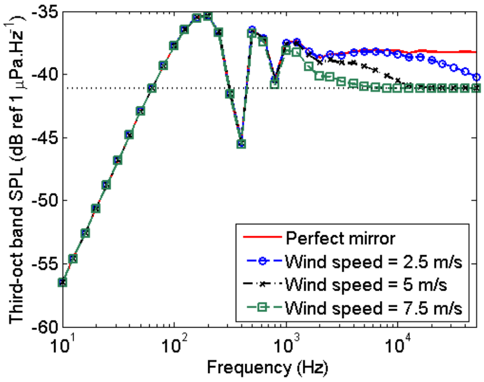

Figure 11. SPL at 100 m distance and 30° slant angle for different wind speed using Kuo's models (Audoly & Meyer, 2017).

Note that as the ship traverses the measurement track, the geometry between the ship and fixed hydrophone(s) continuously changes and hence there are continuous changes in the relative contribution (constructive or destructive) from the surface reflections to the measurements.

If the three-hydrophone geometry is strictly according to ISO 17208-1, the following correction can be applied to the average noise level as published by ISO 17208-2:

$$PL_{LM}\left[dB\right] = -10\log_{10}\left(\frac{2\left(kd_s\right)^4 + 14\left(kd_s\right)^2}{14+2\left(kd_s\right)^2 + \left(kd_s\right)^4}\right) \quad (2)$$

For the source depth d_s, ISO 17208-2 proposes a value of 0.7 times the ship draft, but other depths are in use as well depending on whether machinery noise or cavitation noise is dominant. This formulation is an improvement over those previously used.

4.2 Effect of shallow water

4.2.1 Introduction

In deep water, the effect of sea-surface reflection on sound propagation is much larger than the effect of bottom reflection. The definition of "deep water" is based on the assumption that the effect of bottom reflection could be negligible. In ISO 17208-1, the definition of deep water is "The minimum water depth shall be 150 m or one and one-half times (1.5x) the overall ship length, whichever is greater". DNV GL, LR, RINA and ABS follow this definition of "deep water", while BV's "minimum water depth" is 200m, and CCS has not provided a definition.

However, the depth of the "shallow water" regime for underwater radiated noise tests of ships also has a lower limit. The minimum depth in DNV's rule is at least 30 m under keel, and depth should be larger than 0.64 times ship speed squared (in m/s), while for CCS it is 40 m. Other classification societies follow ISO's requirement in which the minimum depth is defined as 60 m.

Pang *et al.* (2020b) simulated the effect of bottom reflection for various water depths. The maximum variability in sound pressure levels caused by bottom reflection (see Figure 12) is about 28.7 dB for 60 m depth，5.2 dB for 150 m depth，3.2 dB for 300 m depth，3.3 dB for 450 m depth，2.9 dB for 1000 m depth and 0.35dB for 5000 m depth. Most of rules and guidelines define 150 m as the boundary of shallow water and deep water. ANSI/ASA rules define the minimum water depth as 450 m for the class A precise measurement procedure.

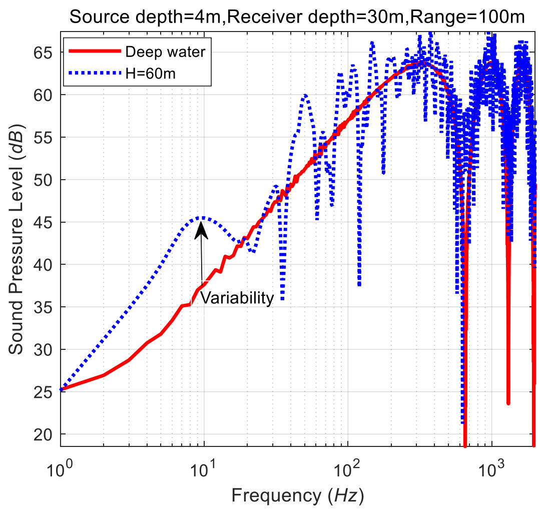

Figure 12. Received sound pressure level of monopole source in deep water and shallow water (data from Pang *et al.* (2020b).

Most of the offshore regions have a water depth less than 150 m, showing the importance of procedures for shallow water. ISO working group "17208-3" aims to develop procedures for URN measurement in shallow water.

4.2.2 Operations in rules and guidelines for shallow water

Alternatively, the propagation loss due to free surface and bottom effects can be calculated by numerical models. BV recommends the use of the range dependent parabolic wave equation model RAM (Collins 1994; Collins *et al.* 1996), or a wave integration model, namely the Scooter/Fields model for low frequencies below 1,000 Hz (Etter 2013), and ray trace-based models, namely Bounce or Bellhop models (Jensen *et al.* 2011), for higher frequencies. Other well validated models such as Weston's intensity model (Weston 1971) can also be used. The propagation models need as inputs the sound velocity profile as a function of depth, noise source depth, hydrophone depth, and sea bottom characteristics. A numerical model that includes near field effects may be needed when ship underwater noise measurements are made for short source-receiver configurations.

According to the BV rule, a noise test with multiple CPA distances is a practical method to analyse the field propagation loss. Pang *et al.* (2020a) have verified this procedure in the China East Sea by measuring the underwater noise of an icebreaker at eight CPA distances. Similar tests have been reported by Sipilä *et al.* (2019), where the underwater noise of another icebreaker is measured at four CPA distances varying between 136 to 174 m.

An empirical formula has been defined to correct for the influence of the environment (Meyer & Audoly, 2019). It has been determined using numerical simulations and depends on water depth and measurement distance. However, this empirical formula is only valid for a sandy sea floor. Additional work aims at extending its validity to other types of sea floor, including hard materials such as basalt (Meyer & Audoly, 2020).

Pang *et al.* (2020b) gives another empirical formula to estimate the source level based on empirical regressed propagation loss factor. Corrections for surface reflection are also taken into account in this formula. Acceptable source-level results can be obtained by simply knowing the type of seafloor and by using typical parameters in these formulas. Validation experiments conducted in a lake show that the deviation between the derived source level and the measured sound pressure level of the reference hydrophone at 1m distance from the projector is less than 3 dB.

4.3 Ship noise monitoring

As discussed in Section 3.2, a large number of programs are dedicated to measuring ambient noise in the sea and the impact of shipping noise on marine mammals, fish and invertebrates. This section presents some of the results presented in recent scientific literature.

Detailed measurements including directivity of the URN from two container ships were reported by Gassman *et al.* (2017b). They show that, for frequencies below 1 kHz, surface reflections cause large variation in measured noise levels depending on hydrophone inclination angle and should be accounted for. The effective source depth required for the correction was estimated from measurements at two separate inclination angles.

As part of a large retrofitting program of MAERSK line, the underwater radiated noise of five container vessels was measured before and after the retrofit (Gassman *et al.*, 2017a). The retrofit included replacing the bulbous bow, derating the engines for low steaming, installing propeller boss cap fins and installing a redesigned propeller. The retrofit resulted in a 6 dB lower source level for frequencies below 100 Hz and 8 dB lower source level for frequencies between 100 Hz and 1 kHz. However, the draft of the ship for the sea trials after the retrofit was

12 to 15 m which is significantly higher than for the sea trials before the retrofit where the draft was in between 9 and 12 m. This effect of this change in draft on propeller cavitation was not further investigated.

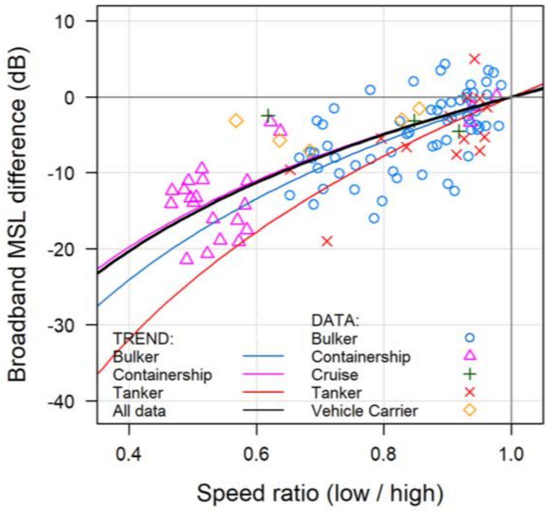

Figure 13. Effect of speed reduction on monopole source levels (MSL), MacGillivray *et al.* (2019).

The Port of Vancouver has set-up the ECHO program in which the effect of voluntary vessel speed slowdown to 11 knots on the underwater radiated noise in the Haro Strait was investigated (MacGillivray *et al.*, 2019). Noise measurements were performed at three hydrophone stations and were combined with AIS data. Measurements were performed during the slowdown trial and pre-trial and post-trial control periods. Results of five categories of piloted vessels have been published, showing a significant reduction of the source levels as shown in Figure 13. The combination of reduced source levels and longer ship passing time leads to a measured median broadband noise reduction of 1.2 dB. The reduction was 2.5 dB when filtering for periods in which the vessels were within 6 km radius of the hydrophone station (Joy *et al.*, 2019).

The reduction in shipping traffic due to COVID19 has resulted in a 1.5 dB reduction in year-over-year mean weekly noise power spectra at a hydrophone station located in the Pacific on the Juan de Fica Ridge in Canada, 60 km from a major shipping lane (Thomson & Barclay, 2020). At other hydrophone locations the reduction was 0.59 dB/week and 0.25 dB/week, whereas no significant changes were reported for another location.

4.4 Typical ship noise levels

The RANDI-3 model (Research Ambient Noise Directionality noise model) was developed based on regression analysis of a large number of measured ship noise levels (Breeding *et al.* 1996). The source level of a ship is defined as

$$L_s(f,v,l) = L_{s0}(f) + c_v \times 10log_{10}(v/v_0) + c_L \times 10log_{10}(l/l_0) + g(f,l) \quad (3)$$

In this formula, c_v and c_L are power-law coefficients for speed and length (taken to be 6 and 2, respectively), v_0 is the reference speed (12 knots), l_0 is the reference length (300 ft), $L_{s0}(f)$ is a mean reference spectrum, and $g(f,l)$ is an additional length-dependent correction to the Ross model (Breeding *et al.*, 1996).

The Institute of Acoustics (IOA) of the Chines Academy of Sciences (CAS) has performed a noise monitoring campaign in the China Yellow Sea from 2015 to 2016 (Jiang *et al.*, 2020). The hydrophone is bottom-mounted and deployed near a shipping lane. A total of 9 cargo ships, 13 container ships and 4 tankers are analyzed. The ship lengths range from 80 to 399 m, and overall source levels (20 Hz～1 kHz) varied between 171.2 dB and 188.3 dB. For the ships whose length is more than 200 m, the calculated results from the RANDI-3 model are generally higher than the measured results and the maximum difference can reach almost 20 dB. For the ships whose length is less than 200 m, there is little gap between the levels given by the RANDI-3 model and by the measured data. The results for all ships are presented in Figure 14.

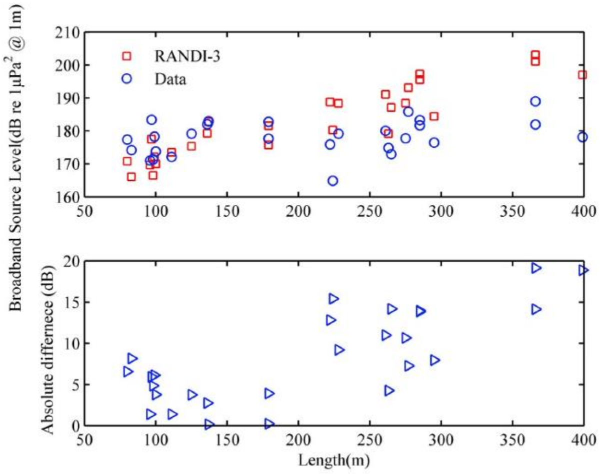

Figure 14. Broadband overall source level and absolute difference between measured data and RANDI-3 versus ship length (Jiang *et al.*, 2020).

5. MODEL-SCALE MEASUREMENT

5.1 Introduction

Performing consistent and reliable noise measurements of cavitating propellers in model-scale test facilities involves many aspects that need to be taken into account, as reviewed in the updated ITTC guideline [7] 7.5-02-03-03.9 on Model-Scale Propeller Cavitation Noise Measurements. This guideline was updated with, among others, the latest knowledge on facility reverberation and Reynolds number scaling of tip-vortex cavitation noise. These topics are discussed in this section in more detail, combined with a discussion on measurement techniques and uncertainty, and a review of water quality measurements. Results of a benchmarking exercise and comparison between model-scale predictions and full-scale data are also presented.

5.2 Measurement techniques

The calibration step is obviously an important measurement that must be performed carefully. The estimate of the sensitivity of a hydrophone is generally given at a distance of 1m in free field environment. This value could be estimated in an anechoic chamber using gated signals to avoid the effect of reflections, or in a lake (or at sea) for very low frequencies. The latter may be costly and difficult to obtain these measurements. Recently, a novel method for calibration has been proposed by Ward & Robinson (2019) to calibrate devices at low frequencies using a small chamber and a Laser interferometer device, as presented in Figure 15. It appears as another solution for measuring the sensitivity with a relative low-cost apparatus and it is able to calibrate the hydrophone system down to 20 Hz as illustrated by Figure 16.

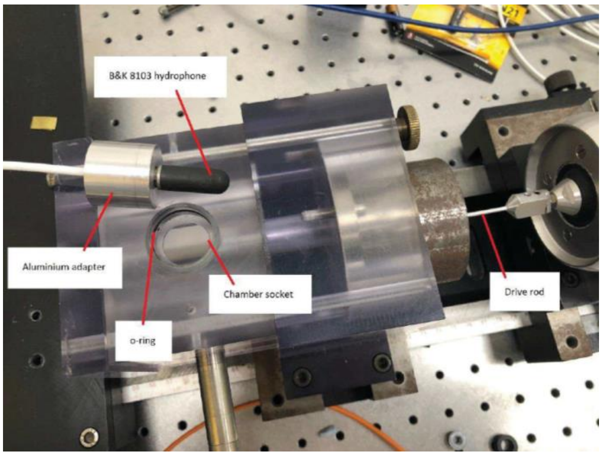

Figure 15. Device for low frequency (20-250 Hz) calibration measurement developed by Ward & Robinson (2019), here with a B&K 8103 hydrophone.

Calibration performed in a free field domain requires the "perfect" knowledge of the distance between the acoustic source and the hydrophone. The determination of the acoustic centre is an important parameter that could be estimated by the time delay of the signal between the source and the hydrophone. This estimate could be done by correlating the two signals (sine burst or sweep as used by Tani *et al.*, 2016a). A dedicated set up with particular signals (based on acoustic Barker codes or Schroeder codes) may also be used (Boucheron, 2017). These techniques permit for example, easier measurement of directivity by

[7] Note that the previous, obsolete, guideline was numbered as 7.5-02-01-5.

refining the real position of the source compared to the sensor.

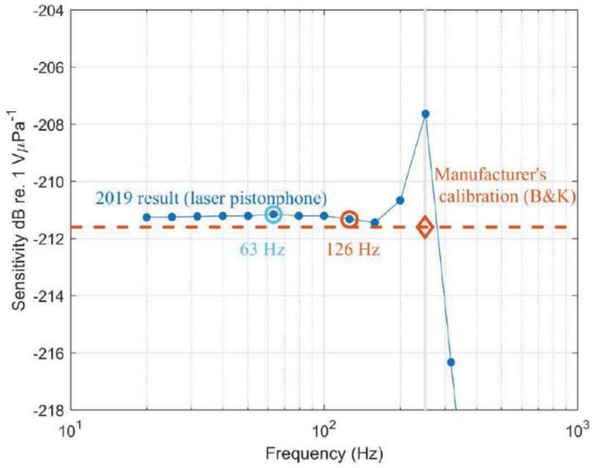

Figure 16. Calibration results obtained by Ward & Robinson (2019). Measurements with the developed technique in blue compared with manufacturer's calibration in orange.

5.2.1 Multiple sensors techniques

Recently, the use of several hydrophones to perform measurements has been investigated by several institutes. The aim of such measurement is not to perform redundant measurements to check the quality of the measurement but to improve the quality by combining the different signals acquired by the sensors and to enhance the estimation.

Among the techniques found in the literature, the array signal processing has been used recently by Park *et al* (2016) with a 45-hydrophone array, localized below the test section, in an application in the Large Cavitation tunnel at KRISO. Figure 17 presents a result obtained by Park *et al.* for localization of acoustic sources in a case of a propeller with cavitation. ISO committee proposes a standard for the array signal processing to localize the noise source (ISO, 2019b).

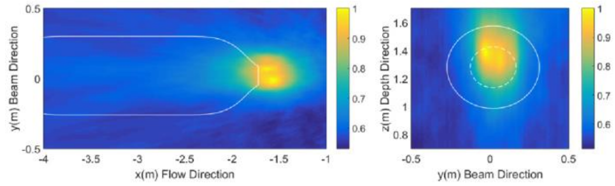

Figure 17. Localization of acoustic sources close to propeller in a cavitation case performed by Park *et al.* (2016).

Figure 18. Flush-mounted transducer set up used by Foerth & Bosschers (2016).

Localization of sources may also be performed with a flush-mounted pressure transducer embedded on the model. Figure 18 presents such a configuration performed by Foeth & Bosschers (2016).

A few transducers located in the hull directly above the propeller can also be used to localize incipient tip vortex cavitation noise in the propeller disc. Kim *et al.* (2015) used a broad-band matched field inversion technique to process these measurements.

It has to be mentioned also that several developments have been recently published in the airborne domain with rotating sources using microphones arrays. As an example, Alexander *et al.* (2020) presented a study on the ingestion of turbulence by a rotor and its consequences in terms of noise radiation and directivity pattern.

5.2.2 Denoising

When the measurement is disturbed by pseudo-noise generated by a boundary layer (typically when the hydrophone is flush mounted in a wall or downstream on a model), different authors have developed techniques to correct the measurement from noise. All these methods are based on measurements with several hydrophones. The cross-spectral matrix is then computed and may be "denoised" with these techniques. Among all the techniques proposed, the recent works from Hald (2017), Gao *et al.* (2019), and Hald (2019) are promising. An application in a hydrodynamic domain has been recently performed by Amailland *et al.* (2018). Figure 19 presents the experimental results obtained in this study. A known source is introduced in the flow inside the test section of the facility. From the raw measurement (acoustic source + flow noise – in blue in Figure 19), the two denoising techniques tested give the curves in grey and black for the estimation of the source level (the reality being the red curve).

A recent study by Dinsenmeyer *et al.* (2020) presents the development of a new technique and a comparison with other denoising methods.

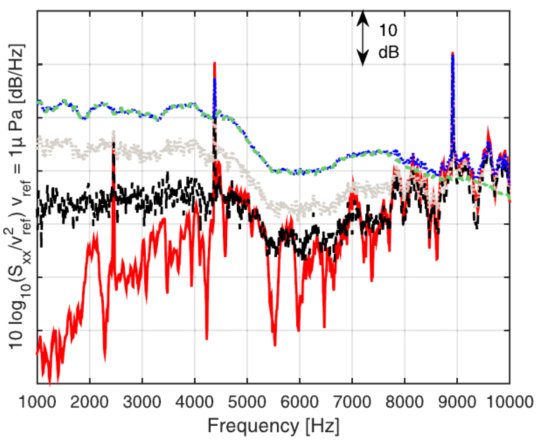

Figure 19. Denoising results from Amailland *et al* (2018). Raw measurement in blue, background noise in flow in green, source level in red. Two denoising techniques results (are given in grey and black).

5.2.3 Doppler Effect

When a given frequency emerges from the spectra, the power measured is disturbed by the Doppler Effect due to the rotation of the source compared to the fixed hydrophone (Morse & Ingard, 1968). Some features of this phenomena have been more recently investigated by Boucheron (2016). The position of the hydrophone is an important parameter as well as the nature of the source. Signal processing techniques may be implemented to remove the Doppler Effect. It is generally required if array processing is intended to be used because the frequency and phase are very important during the combination. The use of a warping time function[8] to perform the "dedopplerization" has been investigated theoretically. A comprehensive knowledge of the environment seems to be required to remove the Doppler effect (Boucheron, 2020c).

5.2.4 Combined methods

In the last decade, several promising approaches have been investigated by Felli *et al* (2014, 2015). One method consists of combining direct pressure fluctuations measurements with flow measurements. Another method combines experimental measurements of the 3D velocity field (obtained with the Tomographic Particle Image Velocimetry technique) and an acoustic analogy as performed in an aeronautical domain, as depicted by Figure 20.

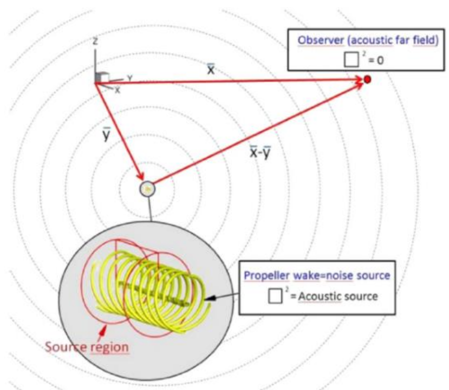

Figure 20. Principle of the acoustic analogy use described by Felli *et al.* (2015).

[8] A warping time function is a relationship that modifies the reception time to mimic a situation with a source and a sensor that do not move. See Baraniuk & Jones (1995) or Feltane *et al* (2018).

5.3 Pressure measurements

In the prospect of future comparisons between experimental and numerical studies (or also with theoretical results), the measurement of the overall pressure is important. This aspect is particularly relevant when the aim of the investigation is to measure the pressure field on a body-surface, like a hull-plate, when impinged by acoustic waves radiated by propellers. The question is: "are pressure transducers able to capture the overall pressure that includes scattering effects too?". In the attempt to answer to this question, a particular focus on both related and main effects is addressed in the following. As shown throughout the paragraph, this measurement must be performed jointly with a calibration step and the control of each step is important. The different steps required and discussed hereafter are,

- Calibration of an acoustic device (source or hydrophone)
- Measurement in free field
- Flush-mounted measurement (wall configuration)
- Transfer function measurement
- Measurement of an unknown source.

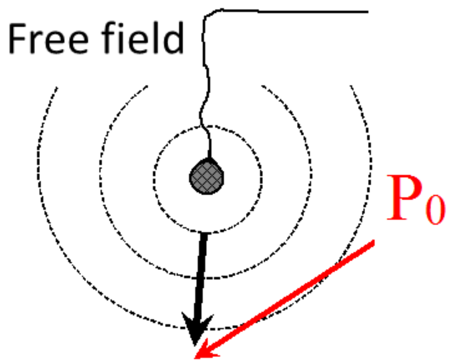

Figure 21. Free field configuration.

The absolute "acoustic" pressure (i.e., the pressure variation around the average pressure) generated at a given distance d from the source is assumed to be P_0 (Figure 21). This pressure wave comes from the source and propagates in a spherical way allowing the use of the following equation available in free field:

$$L_p = L_w - 20\, log_{10}(d) + \mathrm{C} \tag{4}$$

with L_p the sound pressure level, L_w the Acoustic Power Level of the source and C a constant depending on the different propagation medium characteristics and the reference chosen for pressure p_{ref} and power W_{ref}. It could be computed by (see Morse & Ingard, 1968)

$$\mathrm{C} = 10\, log_{10}\left(\frac{\rho\, c\, W_{ref}}{4\, \pi\, p_{ref}^2}\right). \tag{5}$$

With the classical references [9] used in underwater domain, C equals -11 dB.

In the presence of a wall, as described by Figure 22, the incident acoustic wave is reflected by the wall and generates another wave, superimposed to the incident one.

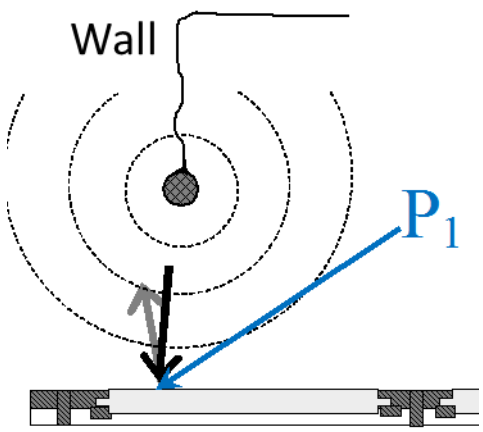

Figure 22. Wall configuration.

At the wall, the pressure P_1 that could be measured is different from P_0. The magnitude of the reflected wave depends mainly on the impedance and curvature of the wall. For the case of infinite impedance and flat wall, the total pressure is roughly twice the incidence amplitude, $P_1 \approx 2\, P_0$.

[9] These are $p_{ref} = 1\text{x}10^{-6}$ Pa and $W_{ref} = 6.67\text{x}10^{-19}$ W. Note that the constant C for airborne noise is computed using $p_{ref} = 20\text{x}10^{-6}$ Pa and $W_{ref} = 1\text{x}10^{-12}$ W. The value for W_{ref} for underwater noise has been computed so as to preserve the same value of the constant C as in air.

The calibration set up is described by Figure 23.

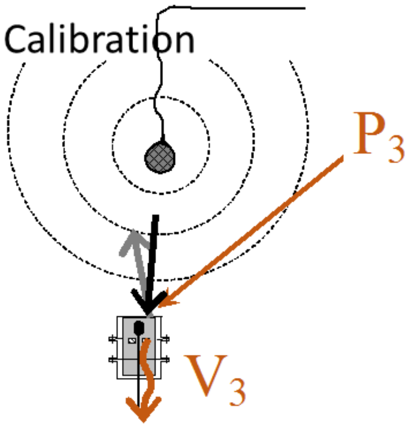

Figure 23. Calibration configuration.

The introduction of the transducer in the acoustic field disturbs the free field propagation. Locally, at the position of the transducer, a reflexion wave is present and the same effect as the one described in Figure 23 appears. The pressure acquired by the transducer, P_3 is then different from P_0. But the aim of such measurement is precisely to adjust the whole acquisition system to estimate the real acoustic pressure that should be at the position of the transducer without it. The output voltage measured by the sensor, denoted V_3 here, allows computing the sensitivity of the sensor M (expressed in Volt by Pascal) by

$$M = \frac{V_3}{P_0} \tag{6}$$

It is worth noticing that the pressure in the last equation is the pressure in free field (because the calibration assumes that the aim of the sensor is measuring the free field, without the presence of the sensor).

After this step of calibration, it is possible to use the sensitivity of the sensor in the same conditions to correct the measurement. The correction step consists of dividing the voltage measurement by the sensitivity to recover the pressure, like described by the following equation,

$$P_3^C = \frac{V_3}{M} = P_0 \tag{7}$$

This correction step, namely known as calibration, allows measuring the real free field acoustic pressure in such environment. However, it is generally not enough to correct a measurement in a hydrodynamic facility because the facility response (or the body-wall in general) is not considered. To overcome this problem, a last step is required inside the environment. This is termed a transfer function and is described by Figure 24 (see also Section 5.4 for a more detailed discussion on transfer function). Let us assume for simplicity the sensing membrane located directly on the surface where pressure has to be measured.

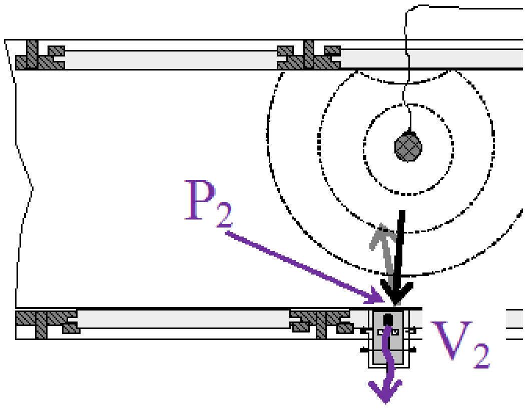

Figure 24. Transfer function configuration

The transfer function uses a calibrated source at a given position inside the environment. The measurement given by the hydrophone P_2 is different from P_0 and P_1. The difference between P_0 and P_2 represents the transfer function *TF*.

$$TF = \frac{V_2}{P_0} \tag{8}$$

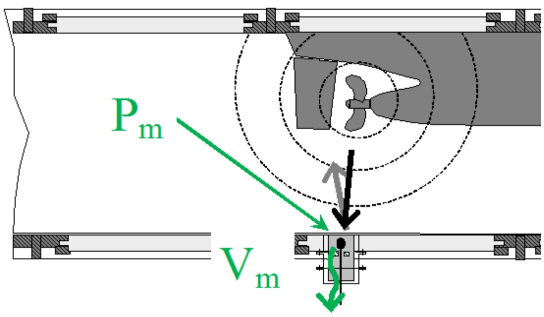

Figure 25. Measurement configuration.

Figure 25 describes the measurement configuration. The measured "raw" pressure P_m does not equal nor P_0 neither P_1 because the pressure at the wall is the superposition of both incident and reflection waves but it is also disturbed by the acoustic response of the facility (reverberation, modal behaviour, etc.). Consequently, it takes account on distance and all the environmental effects. Using this transfer function corrects the measurement V_m, as long as the location of the sources is the same in both configuration (Transfer function and measurement set up).

$$P_m^C = \frac{V_m}{TF} \tag{9}$$

Note that most calibration data are evaluated (or given by manufacturer) at a distance of one meter. This implies that all the estimations made are referenced to 1 meter. The distance plays an important role in the free field and calibration set-ups. The use of a transfer function as described in Figure 24 corrects the measurements and makes the estimation directly at one meter when it is used (because the calibration source data are given at one meter). Fortunately, experimental campaigns to measure the noise emitted by a propeller for example, has the objective to measure the power spectral density (referred to 1 meter) and to estimate this noise at full-scale (also referred to 1 meter). All these equations may also be expressed in the decibel scale, which is generally the most common way of use. The last remark concerns the value of the absolute pressure at the wall during a measurement *Pm*. This real value is never estimated in the tests. It requires the knowledge of both the calibration data of the hydrophone and the measurement of the transfer function.

5.4 Facility reverberation

The problem of facility reverberation was already dealt with by the previous Hydrodynamic Noise Committee, which pointed out the importance of considering this effect. In particular, as indicated in the latest release of the guidelines, when noise is measured in model-scale test facilities, it has to be kept in mind that the test sections do not resemble a free-field environment. The reflections by the walls cause interference between pressure waves which depend on wavelength (and therefore frequency) and lead to acoustic modes in the test section at low frequencies (see e.g., Boucheron *et al.*, 2017; and Hynninen *et al*., 2017). The frequency range of this effect depends on the size of the test section and is larger for the smaller size cavitation tunnels, but the effect is clearly visible for larger size facilities at low frequencies also. The so-called Schroeder cut-off frequency represents the limit below which the measured noise is influenced mainly by the acoustic modes of the facility while for higher frequencies the diffuse domain exists where statistical properties of the acoustic field hold. A formulation for an acoustic measurement in a tank, was given in Kuttruff (2009), while for cavitation tunnel applications a formulation for this cut-off frequency of a test section of infinite length, with source and hydrophone located in the test section, has been derived by Boucheron (2019a, 2020a).

Demodulation techniques can be employed to estimate the magnitude of each mode in the bandwidth where the first modes appear (Boucheron, 2019b). Due to the high number of sensors required when the number of modes increase, the technique is only practicable in a small frequency bandwidth (typically just beyond the first cut-off frequency). The addition of the amplitude of all modes allows the estimate of the whole acoustic field and the acoustic power at each frequency. Figure 26 presents an example of the reconstructed acoustic field estimated experimentally by this technique at each of the three walls of the test section of a cavitation tunnel. However, it is shown that the boundary conditions are one of the key points to ensure good performance of these techniques. A method for the estimate of the impedance of the test section walls has recently been developed (Boucheron, 2020b) and is promising.

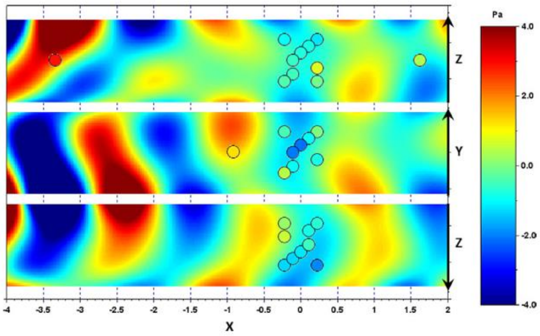

Figure 26. Acoustic field reconstruction by demodulation technique in a test section (Boucheron, 2020b).

The effect of the reflections (or reverberation) can be determined through acoustic transfer function measurements using for example, a sound source with known characteristics put at specific relevant locations in the test section (see Figure 27).

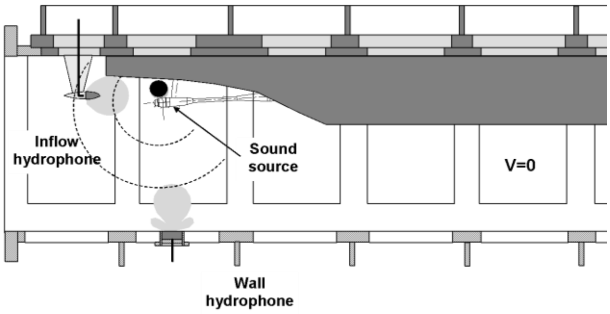

Figure 27. Transfer function measurement set-up in cavitation tunnel.

Examples of measuring the transfer function can be found in Briançon *et al.* (2013), Lafeber *et al.* (2015), Park *et al*. (2016,2018), Tani *et al.* (2016a,b) and Tani *et al.* (2019b).

According to the experiences gained during the period of activity of the Specialist Committee, the Model-Scale Measurements Guidelines have been updated for what regards the effects of facility reverberation; Many different aspects are dealt with, such as:

- Characterisation of transmitting chain, including TVR
- Type of sound projector
- Type of signal
- Position of projector
- Testing conditions, including air content
- Free surface effects
- Further general considerations

Details about these aspects may be found directly in the guidelines and in the above-mentioned references, while in this section some further information is presented about some specific topics.

For what regards the types of signal to be used for the transfer function measurement, many options have been suggested by various authors and have been used in different facilities:

- Pure tones
- White or pink noise
- Chirps
- Sweeps
- Maximum length sequences (MLS)

Basically, the choice is related to the capability of covering large frequency ranges with a single measurement (thus preferring wideband signals) and, in parallel to the need for high signal-to-noise ratio (SNR). Considering the latter, pure tones result in higher SNR, even if they may tend to amplify the waviness of the transfer function, amplifying local singularities.

Different post-processing techniques may be applied to different signals. In Tani *et al.* (2019b), the sweep signal is convolved with an inverse filter to enhance SNR and to separate the linear response of the system from the non-linear distortions that stem from the use of electronic transducers. This procedure may be successfully used to extend the TF also to low frequency ranges where SNR is very low. In Figure 28 the resulting TF using pink noise and a sine sweep (plus convolution with inverse filter) are compared, showing differences at lower frequencies, where the SNR is considerably different, as shown in Figure 29.

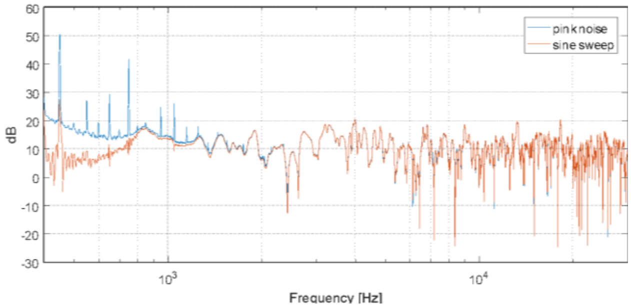

Figure 28. Comparison of transfer function obtained with pink noise and sine sweep with linear deconvolution (Tani *et al.*, 2019a).

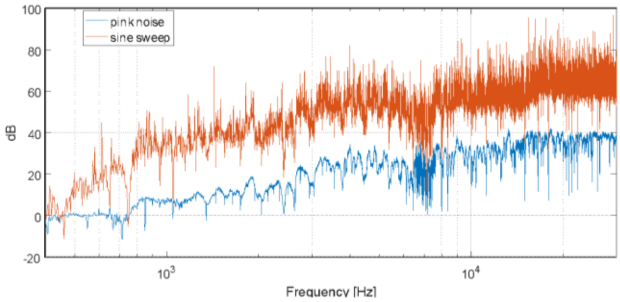

Figure 29. Signal to noise ratio (SNR) in transfer function measurements: pink noise vs sweep with linear deconvolution (Tani *et al.*, 2019b)

Further considerations may arise in the case of a twin-screw ship. This specific topic is discussed in Park *et al.* (2018), where different approaches for the measurement of the transfer function are reported, including the use of single or twin projectors and the signal adopted. Results reported are in favour of the use of a non-deterministic signal (white noise, in the specific case) in order to obtain more accurate results. Although, differences with respect to deterministic signals are anyway rather limited (about 1 dB). In Figure 30 and Figure 31 the effect of using either a non-deterministic or a deterministic signal is shown, comparing the transfer functions obtained with two different ways for evaluating the transfer function (Type 1 and Type 2 in the figures). In Figure 31 a larger (even if still limited) discrepancy between the transfer functions is evident.

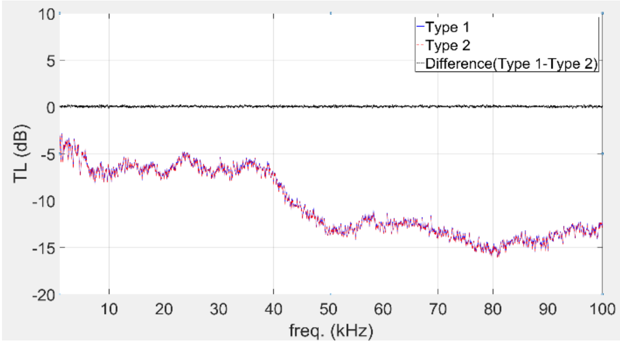

Figure 30. Transfer function comparison with white noise input (Park *et al.*, 2018).

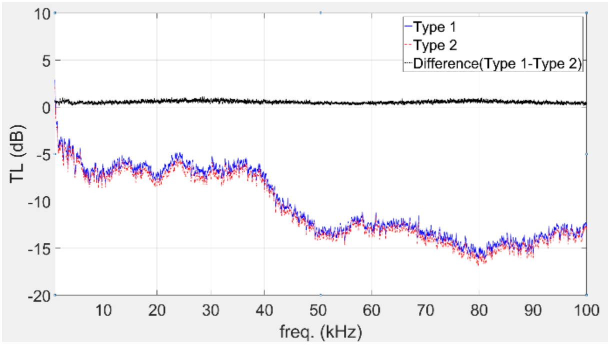

Figure 31. Transfer function comparison with Linear Frequency Modulation (LFM) input (Park *et al.*, 2018).

Additionally, the transducer position is important since it affects the transfer function. Since cavitation is not generally present at a unique position and the characteristics of the transfer function may vary with position, it is preferable to measure the transfer function using multiple transducer positions and averaging the results (Briançon *et al.*, 2013; Tani *et al.*, 2019b). As a possible alternative to the use of multiple positions, in Tani *et al.* (2019b) results obtained with a rotating source are compared with results at different positions of the transducer, as shown in Figure 32.

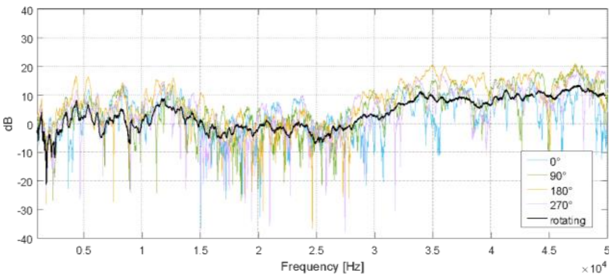

Figure 32. Measured transfer function with fixed and rotating source, narrowband representation (Tani *et al*., 2019b).

This approach seems promising; however, it may pose practical problems and is more complex, especially in the case where the signal has to be emitted only in correspondence to a specific range of angular positions if cavitation phenomena are not present in the whole propeller revolution. In this second case, the relevant angular positions may arise from visual observations or from source localisation techniques.

The use of multiple positions and averaging may also have the advantage of smoothening the transfer function which otherwise tends to present rather large hump and hollows. As an example, this feature is evident in Figure 33 (Tani *et al*., 2019b). Humps and hollows appear to be present in both the transfer function and in the propeller radiated noise levels, which present similar patterns, as expected. However, they seem to be more pronounced in the first case. This suggests that the frequency response of the facility to the cavitation noise, even if presenting similar features, is likely different from the one measured with the electronic noise source, in which the humps and hollows may be amplified. The problem of smoothing is well known in ocean acoustics (Harrison & Harrison, 1995); this is further discussed, for the case of model testing facilities, in Briançon *et al*. (2013).

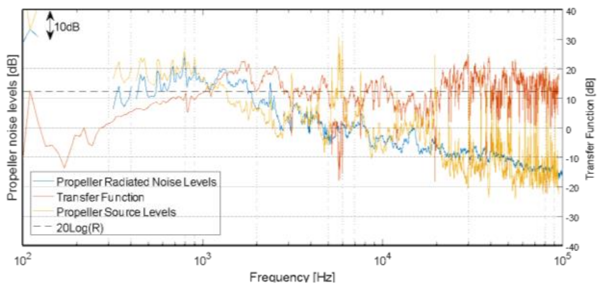

Figure 33. Example of radiated noise levels, transfer function and source levels (Tani *et al*., 2019b).

5.5 Tip-vortex scaling

Various publications have addressed the effect of Reynolds number on the URN of tip-vortex cavitation when performing model tests. Scaling rules for the URN have been proposed by Strasberg (1977), Baiter (1989), and Blake (2017), where various functions of the cavitation number σ and cavitation number at inception σ_i are proposed. Oshima (1990, 1994) shows that high-frequency hull-pressure levels caused by a propeller with a cavitating vortex arising at the face of the propeller are well predicted if the cavitation number in the cavitation tunnel is selected smaller than the cavitation number at full-scale. The ratio of the model-scale and full-scale cavitation number is written as the ratio of the corresponding Reynolds number, *Re*, similar to the scaling rule for cavitation inception by McCormick (1962),

$$\frac{\sigma_m}{\sigma_s} = \left(\frac{\mathrm{Re}_m}{\mathrm{Re}_s}\right)^n \tag{10}$$

where subscript *m* corresponds to the model-scale condition and *s* the full-scale condition. Oshima (1990) shows that good agreement between model-scale and full-scale noise levels are obtained for n = 0.15 while near cavitation inception a value n = 0.35 should be used. Park & Seong (2017) present a relation to scale model-test URN levels to full-scale that includes a correction for the dissimilarity in Reynolds number using the ratio of full-scale and model-scale Reynolds number raised to a power 2.5 n using n = 0.32. A similar correction was also applied to frequencies. This correction method was used by Park *et al*. (2019) who showed that a value of n = 0.1 gives best agreement between sea trial data and model test results.

An alternative approach is proposed by Bosschers (2018a, 2020). The similarity of vortex cavity diameter is investigated using an analytical formulation for the azimuthal velocity distribution of a 2-D vortex, providing a function, f, between ratio of vortex-cavity size, r_c, and viscous core size, r_v, and the ratio of the cavitation number and the cavitation inception number:

$$\frac{r_c}{r_v} = f\left(\frac{\sigma}{\sigma_i}\right). \qquad (11)$$

It was shown that the function f is independent of the vortex strength when the Lamb-Oseen vortex is used. Applying the function to model-scale and full-scale conditions, and using the relation between viscous core size and cavitation inception for the Lamb-Oseen vortex, results into

$$\left(\frac{r_c}{D}\right)_m = \left(\frac{r_c}{D}\right)_s \left(\frac{\sigma_{i,s}}{\sigma_{i,m}}\right)^{1/2} \frac{f\left[\left(\sigma/\sigma_i\right)_m\right]}{f\left[\left(\sigma/\sigma_i\right)_s\right]}. \qquad (12)$$

Through this relation, a cavitation number at model-scale can be obtained from which the non-dimensional cavity size at model-scale is identical that at full-scale. It is then assumed that the resulting URN levels are also similar. Analysis of limiting situations show that near inception, the cavitation number should be adjusted according to the classical McCormick scaling rule while for fully developed cavitation the cavitation number at model-scale should be identical to that at full-scale. If the required change in cavitation number cannot be obtained at model-scale, a semi-empirical correction is applied to the URN levels that makes use of the difference in relative vortex cavity size between model-scale and full-scale. The result of applying this correction procedure to the experimental data of Oshima (1990) is shown in Figure 34.

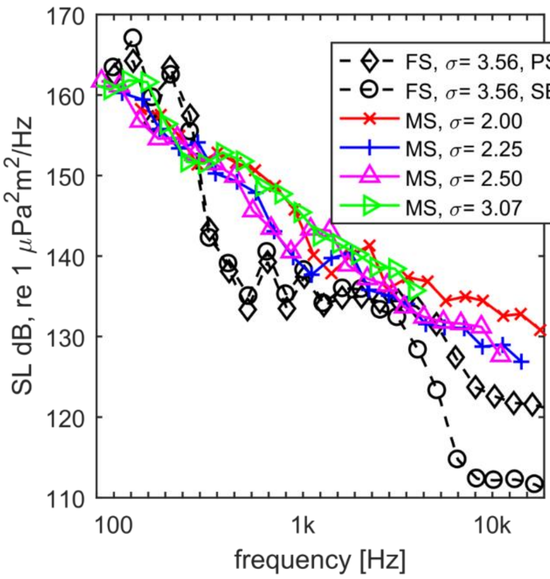

Figure 34. Data of Oshima (1990) corrected by the tip-vortex scaling method of Bosschers (2020).

5.6 Water quality

The influence of water quality, quantified indirectly by dissolved gas level or directly as a microbubble/nuclei population measurement, has long been considered for its impact on the inception and development of cavitation and its scaling, and the associated flow/hull pressure fluctuations and propagation of noise into the surrounding environment (see for example, Arndt & Keller, 1976; Lovik, 1981; Weitendorf, 1981; Bark, 1985). It has been found that nuclei populations can differ between facilities for comparable dissolved gas levels and vary in time within a particular facility (Weitendorf & Tanger, 1999; Heinke *et al.*, 2012). Some water tunnels have been designed to control the nuclei population independent of the dissolved gas level (e.g., Briancon-Marjollet & Michel, 1990; Khoo *et al.*, 2020a) but in general this is not the case.

With respect to hull pressure fluctuations Johannsen (1998) reported that in the large HYKAT facility a high dissolved oxygen content (80% saturation) was required for good agreement between model and full-scale results. At a lower content of 40% the first peak of the model hull pressure signal was substantially higher due to the absence of damping provided by the free bubble population present at the higher saturation level. Similarly, Heinke (2003) and Bosschers & van Wijngaarden (2012) have reported an improved full-scale correlation of high harmonics with a greater gas content (60% saturation rather than 30%).

Little has been published on the effect of water quality on noise propagation in facilities since the 80's (e.g., Blake & Sevik, 1982). Kamiriisa (2001) reported a very significant reduction in sound level from a cavitating propellor above 5 kHz with a variation in dissolved gas level from 70-100%, but no difference below 70%. The main/sole source of recent work assessing the effect of water quality on noise measurement at model-scale is that undertaken by the group at the University of Genoa (Tani *et al*., 2019b). In particular, a possible method for qualitatively assessing the presence of scattering effects is described, despite only giving a rough indication. Possible significant reductions in the sound level (up to 30 dB at most influenced frequencies) are reported in correspondence to worst conditions, showing that this problem has to be considered carefully, especially in facility where presence of free traveling bubbles is more likely to occur. Other than this work, when reported, studies only typically indicate that ITTC recommendations are followed for dissolved gas level and little other comment about water quality is generally made.

Some recent works examining measurement techniques and the influence of nuclei on cavitation inception and nuclei dynamics in test facilities is discussed in further detail below.

5.6.1 About measurements of water quality

Nuclei measurements, or as reported by many authors, the measurement of the quality of water is a crucial aspect regarding cavitation inception. The objective of this measurement is not to have a global overview of the water quality in the whole facility but more to estimate the quality of water that is just upstream of a test model, e.g., a propeller. Both the position and the size of a nucleus has an important influence on cavitation inception and development (Chen *et al.*, 2019; Rijsbergen & Beelen, 2019).

Different techniques have been developed in the past that may be adapted to perform bubble size and concentration measurements. We can cite the cavitation susceptibility meter (see e.g., Lecoffre, 1987; Khoo *et al.*, 2016; Khoo *et al*., 2020a) that make the microbubble cavitate in a Venturi device (see Figure 35). The relationship between the critical radius of a bubble and the pressure allow to compute a cumulative distribution of a microbubble population by modifying the flow rate in the Venturi.

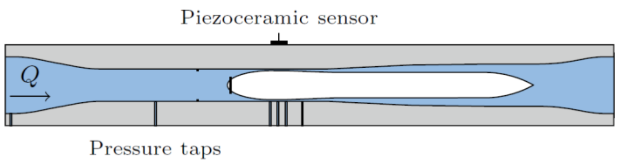

Figure 35. Centerbody Susceptibility Meter schematic principle (adapted from Khoo *et al.*, 2020a).

This technique can measure very low concentration and very small microbubbles but is highly intrusive. It is not suitable for an embedded technique on a whole model dedicated to noise measurements but could be used prior to the noise tests if the water quality conditions are controlled in the facility.

To perform synchronous measurements with noise, only optical techniques are currently available:

- Shadowgraphy: this technique requires the alignment between the light, the measurement volume, and the camera. Particular attention must be paid to the design of the optic and the image processing (see Boucheron *et al*., 2018).

- Phase Doppler Anemometry: this technique could be efficient but requires an optical design at fixed angles (Boucheron *et al.*, 2018). These angles are given by the refractive index of air and water and could not be changed. If the facility provides such angles, this technique could be used efficiently.

- Holography: In-line holography (see Lebrun *et al.*, 2011) may also be used in a small environment. The measurement volume of this technique is very small and the distance between the laser probe and camera must be small.

- Defocus technique: this technique is based on the light scattered by the microbubble and measured with an out-of-focus camera (see the principle described in Figure 36). Note that there is a range of differing acronyms[10] used for this same technique, but all are based on the principle of obtaining an interference pattern from a defocussed optical path (Russell *et al.*, 2020a).

  Birvalski & Rijsbergen (2018a,b) used this technique in a basin with the estimation of both the size distribution and the concentration. The latter is difficult to obtain accurately because it is highly dependent on the measurement of the light power profile of the laser beam. A recent study by Russell *et al.* (2020a,b) details the calibration of the defocus technique for both size and concentration measurements and the application in their tunnel. Ebert *et al.* (2018) have presented an application of such technique at full-scale in the North Sea off Scotland.

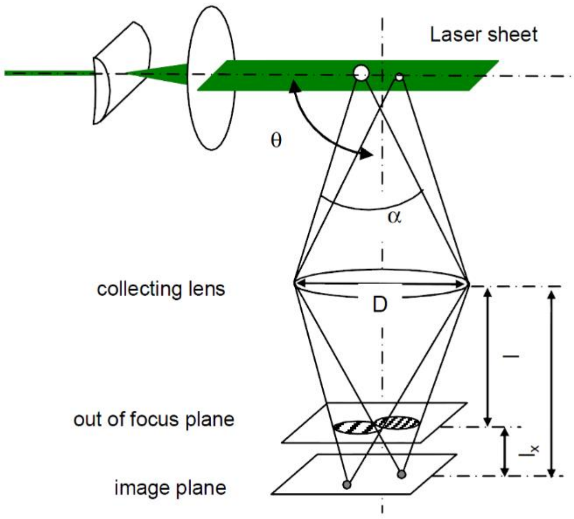

Figure 36. Principle of the defocus technique (from Méès *et al.*, 2010).

The accuracy of these techniques depends on the optical arrangement and on the image processing used. A comparative study for 3 of them has been made in Boucheron *et al.* (2018) exhibiting the spread of results obtained with the same bubbles.

5.7 Uncertainties

The results of noise measurements are usually expressed in decibels, as are the uncertainty of the hydrophones and measurement equipment. However, combining uncertainties of components in the measurement chain is not trivial as briefly shown in this section.

The expanded uncertainty u_i, expressed in percentage, for a given confidence level implies that the range of the signal with mean value x is given for that confidence level by $\left[\left(1-u_i\right)x,\left(1+u_i\right)x\right]$. In decibels, the upper range is given by

[10] Differing acronyms in use include: IMI - Interferometric Mie Imaging, MSI - Mie Scattering Imaging, GPD - Global Phase Doppler, ILIDS - Interferometric Laser Imaging for Droplet Sizing, ILIT - Interferometric Laser Imaging Technique, IPI - Interferometric Particle Imaging

$$\Delta L_{u_i}^{+} = 20\log_{10}\left[(1+u_i)x\right] - 20\log_{10}[x], \\ = 20\log_{10}[1+u_i], \tag{13}$$

and the lower range by

$$\Delta L_{u_i}^{-} = 20\log_{10}[x] - 20\log_{10}\left[(1-u_i)x\right], \\ = -20\log_{10}[1-u_i]. \tag{14}$$

For any given u_i, we have $\Delta L_{u_i}^{+} < \Delta L_{u_i}^{-}$.

However, for small values of the uncertainty, the expressions for the uncertainty in decibels can be linearized which leads to

$$\Delta L_{u_i}^{+} = \frac{20}{\ln 10}\ln[1+u_i] \\ \approx \frac{20}{\ln 10}u_i \quad \forall u_i \ll 1 \tag{15}$$

and similarly

$$\Delta L_{u_i}^{-} \approx \frac{20}{\ln 10}u_i \tag{16}$$

Hence, for small values of the uncertainty, the upper range and lower range are practically equal when expressed in decibels. Computing the combined uncertainty then also becomes straightforward:

$$\Delta L_{U_c} = \frac{20}{\ln 10}\sqrt{\sum_i u_i^2} = \sqrt{\sum_i \Delta L_{u_i}^2} \tag{17}$$

Alternatively, we may also start with a measurement in which the (expanded) uncertainty ΔL_U is directly provided in decibels. The upper and lower bounds, for a given confidence level, are then given by,

$$L_U = \bar{L} \pm \Delta L_U = 20\log_{10}(x) \pm \Delta L_U \tag{18}$$

If we insert the variable inside the logarithm, we find,

$$L_U = 20\log_{10}\left(x \times \left[10^{\Delta L_U/20}\right]^{\pm 1}\right) \tag{19}$$

The Taylor expansion of the power function 10^x gives (assuming that ΔL_U is small)

$$L_U = 20\log_{10}\left(x \times \left[1 \pm \Delta L_U \frac{\ln(10)}{20}\right]\right) \tag{20}$$

We retrieve here the term expressed in equations (15) and (16) available for small uncertainties u, that demonstrates the equivalence of the two approaches when the values are small. Figure 37 presents the relationship between the two situations, assuming a normal distribution of data in linear scale and a small value of the uncertainty u.

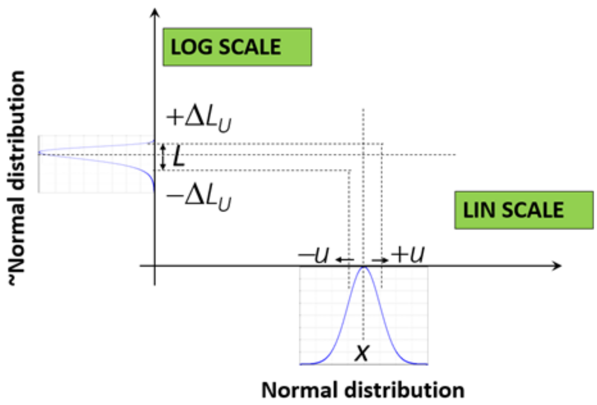

Figure 37. Example of the distributions equivalence between the linear and logarithmic scales, assuming a normal distribution of data in linear scale and a small value of the uncertainty.

Nevertheless, for higher values of the uncertainty, the equivalence is not obtained easily. In this particular case, the equations (15), or (19) if expressed in decibel, cannot be expanded. The equations for the transformation between statistical variables (see for example Papoulis, 2002) shows that one of the distributions is not symmetrical. As an example, Figure 38 presents the relationship between the two distributions assuming a normal distribution in the linear scale. In the logarithmic domain, the distribution looks like Gumbel or Weibull distribution. The upper ΔL^{+}_U and lower ΔL^{-}_U bounds are not equally spaced from the average in the logarithmic domain.

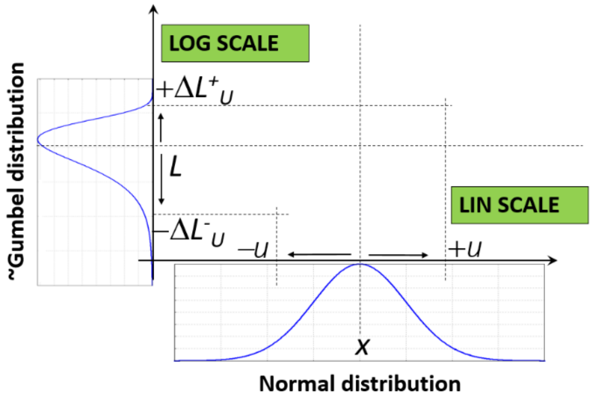

Figure 38. Example of a distribution modification between the linear and logarithmic scales, assuming a normal distribution of data in linear scale and large uncertainties.

Therefore, the distribution of a parameter around its mean value is of principal importance, especially if large uncertainties occur. Combination of uncertainties with equation (17) assumed that data are normally distributed. For small values of all uncertainties, this equation is available. Otherwise, the knowledge of distribution of signals/error of the chain should be used and improve the estimate of the final uncertainties for upper/lower bounds that are not equal.

5.8 Review of HTF benchmark

In the last few years, a benchmarking activity has been carried out by the Community of Practice (CoP) “Noise” of the Hydro Testing Forum (https://www.hydrotestingforum.org/). This followed from the HydroTesting Alliance (European Network of Excellence) with the aim of gaining insight into the key aspects influencing the accuracy and reliability of URN measurements at model-scale, evaluating the impact of different experimental facilities and test procedures on full-scale noise predictions.

A round-robin test programme, involving different propeller scale factors and facility types and dimensions, has been carried out. The programme was carried out in cavitation tunnels of small (UNIGE, NMRI, UNEW) and large size (KRISO, SSPA), a free-surface cavitation channel (INM) and a depressurised wave basin (MARIN). The results of this activity are reported in various papers, such as Aktas *et al.* (2016a), Hallander (2017), Lafeber & Lloyd (2017), Sakamoto *et al.*, (2017), Tani *et al.* (2017), where tests in single facilities are reported, while in Tani *et al.*, (2020) the same results are summarised and compared. In Section 5.8.1 the testing campaign is briefly outlined, while in Section 5.8.2 the main results are summarised.

5.8.1 Presentation of the activity

The activity has been carried out using as test case the five bladed fixed-pitch propeller model (Figure 39) of the research vessel “The Princess Royal”, belonging to Newcastle University and used also in the EU project SONIC. Four different models have been used during the campaign, with diameters ranging from 214 to 250 mm.

Figure 39. Model-scale propeller (Tani *et al*, 2020).

The propeller was tested in open water configuration and without shaft inclination (i.e., uniform inflow), with the aim of making the test as simple as possible. In addition to this, tests were also repeated with inclined shaft (5°) in order to induce non-stationary cavitation. The rather low angle considered did not result in very large variations in terms of radiated noise with respect to the results for 0° shaft inclination, thus the focus in the published articles is on the tests without shaft inclination. The propeller was tested in pulling condition in all cases, except by CNR-INM (pushing condition); this was due to an unexpected stop of tests (linked to the COVID emergency), which did not allow to fully complete the campaign as expected.

For each shaft inclination, six different operational conditions, resulting from two different values of the advance coefficient and three different values of the cavitation number, were considered (see Table 2).

Table 2. Operational conditions (zero shaft inclination)

Loading Condition	J [-]	σ_V [-]
C1	0.4	13.9
C2		8.1
C3		4.5
C4	0.5	13.9
C5		8.1
C6		4.5

This allowed to investigate considerably different cavitation extents, ranging from slightly after inception to fully developed tip vortex and sheet cavitation, as reported in Figure 40 (observations at SSPA).

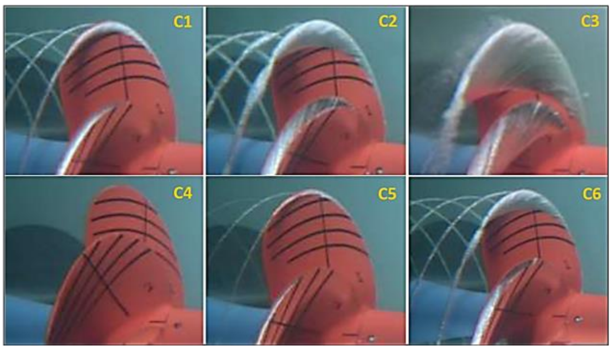

Figure 40. Cavitation extents at different conditions (Tani *et al*, 2020)

5.8.2 Summary of results

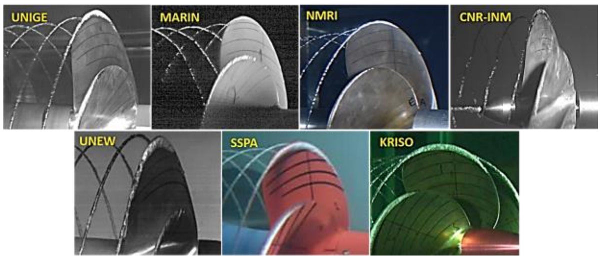

Figure 41. Cavitation extents at C1 condition for different facilities (Tani *et al*, 2020).

Propeller cavitation typologies and extents observed in the different facilities were fairly similar. As an example, in Figure 41 the observations for C1 condition in the different facilities are reported. In this case, the main difference is related to the extent of the sheet cavitation towards the inner radii, ranging from about 0.7R to about 0.8R.

Similar results were obtained also for other conditions, where the most important difference was the radial extent of cavitation (in particular for condition C3); in C4 condition (near inception) different tip vortex dimensions were observed.

These differences have been ascribed to different possible causes, i.e., small discrepancies in the operational conditions (thrust coefficient and cavitation number), different development of boundary layer (Reynolds number and turbulence stimulation), freestream turbulence, blade geometry finishing, and water quality.

For what regards the noise measurements, in Figure 42 and Figure 43, the results for condition C1 and C3 respectively, in terms of one-third octave spectra, are reported.[11]

[11] In order to compare all the results of the campaign, noise spectra were scaled to a common condition in full-scale, resembling one of the functioning conditions of Princess Royal (D_s = 0.75 m, n_s = 19.025 rps, σ_{Ns} = 1.06).

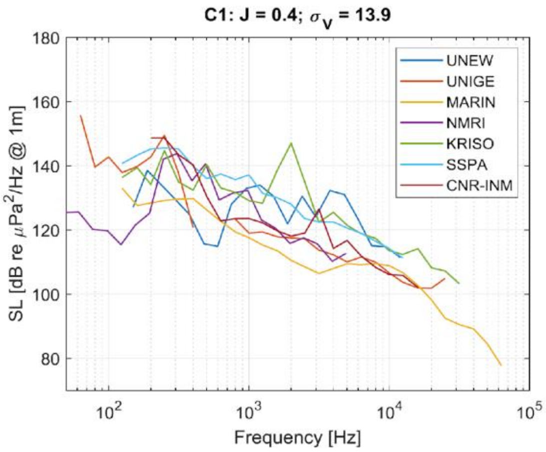

Figure 42. Noise spectra at C1 condition for different facilities (Tani *et al*, 2020).

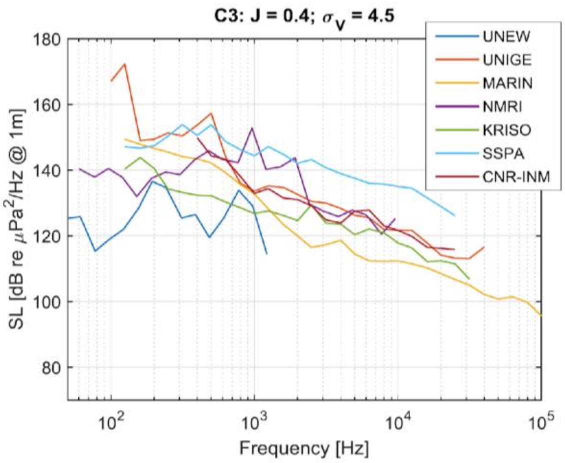

Figure 43. Noise spectra at C3 condition for different facilities (Tani *et al*, 2020).

As it can be seen, a band of variation of about 10 dB of predicted noise levels is observed on average, rising to about 20 dB for condition C3 (similar results were obtained also for condition C4).

Further analyses were devoted to specific parts of the spectra, i.e., the hump (centre frequency and level) and the high frequency part (decay slope and average power content).

Considering the centre frequency of the hump, the agreement observed was better than that visible from noise spectra, with the range of variation mainly below 100 Hz with few exceptions.

The agreement for correspondent peak level was worse, even if common trends might be found especially for conditions at J = 0.6 (C4-C6), while for conditions C1-C3 trends varied for different facilities. The spread in results was in most cases of about 10 dB (lower than the spread in the overall spectrum), except for condition C4, which showed larger variation due to incipient and intermittent cavitation.

Considering the high-frequency spectrum, the decay ratio resulted between 10 and 20 dB per decade, in good agreement with data on cavitation noise available in the literature (Ceccio & Brennen, 1991). However, the spread of results was again appreciable, and it seemed difficult to detect common trends.

Finally, considering the high frequency power content, the trends (for each single participant) agreed rather well with the observed cavitation extent, with higher levels measured in correspondence to higher propeller loading. However, differences of 10 dB are again present for all conditions, with higher discrepancies (up to 20 dB) found for condition C4 and C3, where minimum and maximum cavitation extents were present.

As a whole, the results of this activity are very interesting, providing an overview of the different sources of discrepancy. Among them, cavitation extent and cavitation dynamics, together with facility reverberation, are the most important ones.

Regarding cavitation extent and dynamics, the differences were related both to a not correct reproduction of the operational condition, in terms of thrust coefficient and cavitation number, and to water quality (nuclei content, turbulence levels). The first issue, despite being trivial, has to be considered carefully by each facility; water quality issues are less easy to be controlled, unless dedicated tools are available in the facilities, however it is important to collect as much data as possible in order to understand their effect. Regarding reverb-eration, not all facilities considered it in their measurements; it is very important in the future that all facilities measure the transfer function in accordance to the indications of the model-scale guidelines.

Other possible sources of discrepancy, such as model propeller geometry, bubble scattering, propeller singing, unwanted phenomena on structures inside the facility (e.g., hydrophone supports, screens, etc.), are discussed in Tani *et al*. (2020).

Overall, the HTF results underline that improvements have to be made in the near future and further investigations are needed in order to get a further insight into all the sources of discrepancy between different facilities, with the aim of reducing them. The proposed benchmark activity with the Nawigator ship (see Section 7) represents an opportunity with this aim, allowing to broaden the analysis and involve an even larger number of facilities with respect to those which participated to the HTF round robin. In order to obtain the largest amount of information, the experience of HTF, considering in particular the difficulties encountered, have to be considered carefully.

5.9 Validation studies

The accuracy of the model-scale measurements can be determined from a comparison between model-scale predictions and full-scale noise measurements, as described in the previous report of 28th ITTC specialist committee on hydrodynamic noise. The previous report addressed the importance of the aspects to consider in the model test such as ship wake field, propeller loading, cavitation extents and dynamics, noise measurements, background noise, propagation loss due to facility reverberation, and scaling. The above aspects are revisited in this report and some subjects such as facility reverberation are dealt with in detail.

The papers on the validation studies were reviewed in the previous report. A few papers have been published since the previous report in 2017. Instead of reviewing the individual paper, we summarized the recent validation studies in accordance with categories pertinent to the model-scale and the full-scale measurement methods. Some of papers were already reviewed in the report in 2017.

<u>Ship type (full-scale):</u>

Full-scale underwater radiated noise measurements were performed on various types of ships and the results were compared to model-scale predictions. Among the measured ships, the recently built commercial ships were also included.

Table 3. Review of validation studies of model-scale noise measurements: Arranged according to ship type.

Ship type	Validation studies
Crude Oil Tanker	Lee *et al.* (2012)
Product Carrier	Seol *et al*. (2015)
Oil/Chemical Tanker	Tani *et al*. (2016b), Li *et al*. (2018)
LNG carrier	Park *et al*. (2020)
Container Ship (3,600 TEU)	Kleinsorge *et al*. (2017)
Container Ship (14,000 TEU)	Park *et al*. (2020)
Combi-Freighter	Lloyd *et al*. (2018)
Research vessel (Princess Royal)	Aktas *et al*. (2016a), Gaggero *et al*. (2016), Labefer & Bosschers (2016), Tani *et al*. (2019a)
Research vessel (Nawigator XXI)	Traverso *et al*. (2017)

<u>Cavitation extent observation (full-scale):</u>

Full-scale cavitation extents were presented in many papers, which were helpful for analysis in validation studies. However, there were also some cases where full-scale noise was measured without cavitation observation.

Table 4. Review of validation studies of model-scale noise measurements: Arranged according to full-scale cavitation observations.

Full-scale cavitation	Validation studies
Observed	Aktas *et al*. (2016b), Seol *et al*. (2015), Gaggero *et al*. (2016), Labefer & Bosschers (2016), Tani *et al*. (2016b), Traverso *et al*. (2017), Li *et al*. (2018), Lloyd *et al*. (2018), Tani *et al*. (2019a)
Not observed	Lee *et al*. (2012), Kleinsorge *et al*. (2017), Park *et al*. (2020)

Propagation loss correction (full-scale):

To compare the full-scale measurement with the model-scale prediction, the measured full-scale noise was converted to either the radiated noise level (RNL) or the source level (SL) using various propagation loss corrections.

Table 5. Review of validation studies of model-scale noise measurements arranged according to correction for propagation loss for the full-scale measurements.

Propagation loss (full-scale)	Validation studies
Spherical spreading	Lee *et al*. (2012), Seol *et al*. (2015), Traverso *et al*. (2017), Park *et al*. (2020)
Spherical spreading & Lloyd mirror	Aktas *et al*. (2016b), Labefer & Bosschers (2016), Tani *et al*. (2019a)
Spherical spreading & bottom reflection	Lloyd *et al*. (2018)
Surface & bottom reflection	Kleinsorge *et al*. (2017)
Transmission loss (measured)	Tani *et al*. (2016b), Li *et al*. (2018)
Transmission loss (calculated)	Gaggero *et al*. (2016)

Facility (model-scale):

Most of the model tests were performed in the medium-size and the large cavitation tunnels. The depressurized wave basin in MARIN was also used for the model-scale noise measurement.

Table 6. Review of validation studies of model-scale noise measurements: Arranged according to facility.

Facility	Validation studies
Large cavitation tunnel	Lee *et al*. (2012), Seol *et al*. (2015), Tani *et al*. (2016b), Li *et al*. (2018), Park *et al*. (2020)
Medium-size cavitation tunnel	Aktas *et al*. (2016b), Gaggero *et al*. (2016), Tani *et al*. (2016b), Kleinsorge *et al*. (2017), Traverso *et al*. (2017), Tani *et al*. (2019a)
Depressurized wave basin	Labefer & Bosschers (2016), Lloyd *et al*. (2018)

Ship wake field (model-scale):

The wake fields were generated using a wake screen or a geometrically scaled model of the ship. In general, the former was used in medium-size cavitation tunnels, while the latter was used in the large cavitation tunnels and the depressurized model basin. Sometimes a hybrid method using the wake screen and the dummy body was used for the wake generation in the medium-size cavitation tunnels.

Table 7. Review of validation studies of model-scale noise measurements: Arranged according to simulation method for wake field.

Ship wake	Validation studies
Large-scale model	Lee *et al*. (2012), Seol *et al*. (2015), Labefer & Bosschers (2016), Tani *et al*. (2016b), Li *et al*. (2018), Lloyd *et al*. (2018), Park *et al*. (2020)
Wake screen	Aktas *et al*. (2016b), Gaggero *et al*. (2016), Tani *et al*. (2016b), Traverso *et al*. (2017), Tani *et al*. (2019a)
Dummy body/wake screen	Aktas *et al*. (2016b), Kleinsorge *et al*. (2017)

Propeller loading (model-scale):

In the model-scale measurements, the propeller loading was determined (or prescribed) from the powering tests or from both powering test and sea trial.

Table 8. Review of validation studies of model-scale noise measurements: Arranged according to applied propeller loading.

Propeller loading	Validation studies
Powering test	Lee *et al*. (2012), Labefer & Bosschers (2016), Tani *et al*. (2016), Traverso *et al*. (2017), Li *et al*. (2018)
Powering test + Sea trial	Aktas *et al*. (2016b), Seol *et al*. (2015), Gaggero *et al*. (2016), Kleinsorge *et al*. (2017), Lloyd *et al*. (2018), Tani *et al*. (2019a), Park *et al*. (2020)

Noise measurement (model-scale):

Propeller noise was mostly measured by multiple hydrophones except for Lee *et al.* (2012), Aktas *et al.* (2015b), and Lloyd *et al.* (2018), in which single hydrophone was used.

Propagation loss correction (model-scale):

The propagation loss correction was applied to the measured noise data in most of the validation studies. For the correction, the transfer function was measured or estimated using the spherical spreading of acoustic wave fields. A correction for the Lloyd mirror effect was applied to the measurement data of the Depressurized wave basin.

Table 9. Review of validation studies of model-scale noise measurements: Arranged according to applied correction method for propagation loss in the model-scale measurements.

Propagation loss (model-scale)	Validation studies
Transfer function (measured)	Seol *et al*. (2015), Gaggero *et al*. (2016), Tani *et al*. (2016b), Tani *et al*. (2019a), Park *et al*. (2020)
Spherical spreading	Lee *et al*. (2012), Aktas *et al*. (2016b), Traverso *et al*. (2017), Li *et al*. (2018), Tani *et al*. (2016b),
Transfer function & Spreading	Kleinsorge *et al*. (2017)
Lloyd mirror & spherical spreading	Labefer & Bosschers (2016), Lloyd *et al*. (2018)

Scaling method (model-scale):

Most of the validation studies adopted ITTC’87 low frequency scaling method to estimate the full-scale source level. However, Labefer & Bosschers (2016) applied ITTC’87 high frequency scaling method to the model-scale data. Park *et al.* (2020) and Lloyd et al. (2018) investigated the effects of two ITTC’87 scaling methods on the scaled results. According to their results, the low frequency scaling showed the better correlation to the full-scale measurements than the high frequency scaling. Kleinsorge et al. (2017) investigated both a correction factor for distance between hydrophone and propeller assuming spherical spreading and cylindrical spreading. The spherical spreading correction showed best performance for the low frequency range (f < 100 Hz) and the cylindrical spreading agreed well with full-scale measurement for the high frequency region (f > 100 Hz). Lee *et al.* (2012) scaled the tip vortex cavitation noise and compared the scaled results with the full-scale measured data. According to their study, McCormick exponents of 0.3 showed an acceptable correlation with the full-scale measurement.

Comparison of full-scale & model-scale:

Comparison of the full-scale measurement to the model-scale prediction involves some complexity such as machinery noise, which is only included in the full-scale. It should also be kept in mind that full-scale noise measurement has considerable uncertainty. By simply comparing the levels presented in validation studies, it seems that model-scale tests can predict full-scale noise levels within 5 to 10 dB.

This value of uncertainty is somehow lower than the band of uncertainty reported as a result of the round robin test carried out by Hydro Testing Forum (HTF) members, as reported in Section 5.6.2. That case is, however, different, since an open water propeller was used instead of a propeller operating in a wake field; Some possible reasons for these discrepancies are discussed in Section 5.6.2, showing areas that need further study. It is believed that, starting from that experience, the proposed benchmark study by the Committee will allow to obtain a deeper understanding.

6. COMPUTATIONAL PREDICTION

Some of the aspects on underwater noise prediction methods are discussed in the following sections, providing the *state of the art* in each category. Specifically, Section 6.1 shows hydrodynamic noise prediction, especially from propeller which is an important source of noise. Among of several approaches in Section 6.1, coupled CFD-FWHE technique is picked up as most important numerical approach and its guidelines for utilization are proposed in Section 6.2. Section 6.3 presents structural born noise as another important source of URN, and finally the propagation of URN is shown in Section 6.4.

6.1 Hydrodynamic noise prediction

6.1.1 Empirical and Semi-empirical methods

Overview. Continued from previous committee (28th ITTC specialist committee on hydrodynamic noise), several studies about empirical and semi-empirical prediction methods have been observed. In addition to continuous efforts using classical approaches, adoption of data analysis technique has been rising. Although some of these approaches show fairly good results in the papers, careful attention should be needed to their application considering their modelling phenomena, assumption, based data etc. A schematic view of related phenomena and approach in prediction of URN is shown in Figure 44. Appropriate choice or combination of several methods might be essentially important for reasonable prediction, but no standard methodology has been established up to the present moment.

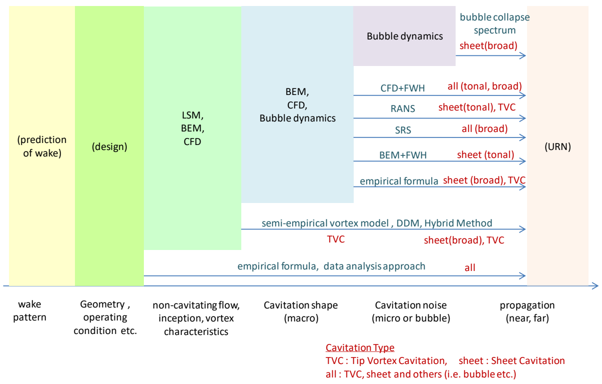

Figure 44. Approaches for predicting hydrodynamic noise from a propeller.

Continuing studies. As shown in previous committee, various approaches using empirical or/and semi-empirical methods have been studied so far. In this committee's period, there have been some further developments of these studies.

One is a combination of bubble dynamics theory and RANS CFD calculation by Ando *et al*. (2018). In this method, radiated noise from sheet cavitation and TVC was predicted by theoretical method modelling bubble collapse of free bubbles from cavitation. Mean initial size of bubble was assumed directly as 2.5 mm, and a normal distribution was adopted to bubble size distribution. Based on these assumptions, the number of bubbles was calculated from volume of sheet cavitation predicted by URANS CFD with cavitation model. For TVC, similar assumption for bubble size was adopted and the length of TVC is assumed as 1.5 D_p (propeller diameter), not based on CFD or other theoretical methods but from observation in model test. The predicted results with TVC showed better agreement to corresponding model test results, than the prediction without TVC.

Another study is by Bosschers (2018b). In this study, a hump-shaped pattern for the noise spectrum was assumed, and the centre frequency and level of this hump was described with an empirical model. This empirical model was obtained using model-scale and full-scale measured hull-pressure data, and described as a function of cavity size, propeller diameter etc. To obtain the cavity size, BEM calculation and semi-empirical vortex strength model was adopted. Even though this method models only for TVC, the results showed some capability for cases with sheet cavitation with adjustment of the empirical parameters.

Both literatures mentioned in above show relatively good agreement between prediction and measurement, but careful attention should be paid to the assumptions or database which are essentially important to utilize these methods.

Adoption of data driven models. In addition to continuous studies in utilizing empirical knowledge and theoretical formulations or calculations, adoption of data driven models has appeared as new approach. This approach shows some possibility to improve the capability of empirical or/and semi-empirical methods.

A relative early study was a simple attempt by Aktas (2016), in which URN levels in several frequencies were modelled directly by Artificial Neural Network (ANN). As input variables, 12 simple parameters including propeller geometry, wake distribution and propeller operating conditions were used, and model tests results of series propeller were employed as training data. In this study, physical knowledge was utilized just in the choice of explanation variables, and only data analysis technique was used for creating prediction formulas. This simple application of ANN left large discrepancy between predictions and measurements.

Another approach was shown by Miglianti *et al.* (2019a,b). In this study, machine learning technique was adopted in following 2 ways. One is called “Data Driven Model” (DDM), which predicts URN directly using propeller geometry, operating conditions, occurring cavitation type etc. as input. Here the cavitation type might be estimated by CFD or other kind of calculation. The other way is called “Hybrid Model” (HM) which uses semi-empirical model similar with Bosschers (2018b), but a DDM approach was also adopted to predict model coefficients in the employed semi-empirical model. In both approaches, URN spectrum was simplified similar with Bosschers (2018b), i.e., characteristic values like URN centre peak frequency, level, etc. in hump-shaped pattern. The predicted results showed a relatively good agreement with measurements, especially in HM the error in centre peek noise level was within 5 dB. One additional interesting point was that HM showed some capability even if the input data for machine learning was only from the outside of range of operating conditions (i.e., thrust coefficient and cavitation number). This suggests the possibility of extrapolation of prediction, which should be useful to estimate the noise in the full-scale condition which is difficult to represent in model-scale.

6.1.2 Potential flow methods

Cavitation-free conditions

a) Bernoulli-based Formulation

Potential flows methods have been largely used in the past for the prediction of the noise field generated by simplified sources of sound like point-sources and vortices (Dowling &

Ffowcs Williams, 1983; Howe, 2002). The extension to non-cavitating propellers is straightforward by assuming operating conditions where the theory of irrotational, inviscid, attached, incompressible three-dimensional (3D) flows is able to capture the flow-field features around lifting/thrusting bodies (Kerwin, 1986; Carlton, 2018) and applying the Bernoulli equation for the prediction of the pressure signals in the fluid medium. Undoubtedly, hydrodynamic solvers based on the Boundary Element Method (BEM) have been proven to be fast and accurate enough in capturing the tonal noise sources localized on the blades and in the flow flow-field surrounding them, whenever the hydrodynamic environment is governed by vorticity fields exhibiting ordered vortex-flow patterns (see for instance: Morino & Gennaretti, 1992; Gennaretti *et al.*, 1997; Seol *et al*., 2002; Testa *et al*., 2008; Salvatore *et al*., 2009b; and Greco *et al*., 2014; just to cite a few). In this context, hydrodynamic effects induced by the hull wake (if present) may be fruitfully described by RANSE (Reynolds Averaged Navier Stokes Equation) computations yielding the main features of the onset-flow incoming the propeller disk, namely, the effective wake field (Rijpkema *et al*., 2013).

However, investigations based on the Bernoulli equation to compute the pressure disturbance in the flow-field have shown their weakness at the light of the recent advances on propeller hydroacoustics (Ianniello *et al*., 2013; Ianniello *et al*., 2014; Ianniello and De Bernardis, 2015; Ianniello *et al*., 2015) proving that non-cavitating propeller noise in open water is an inherently nonlinear problem governed (mainly) by the hydrodynamic sources of sound in the flow-field around the propeller like vortex released at the blade tip, vorticity, turbulence, etc.., which can be very intense and persisting around/downstream the propeller disk. Of course, BEM hydrodynamics is able to capture the noise contribution due to blade(s) kinematics and pressure distribution upon the propeller, including effects coming from the vorticity field convected downstream. Nonetheless, all those hydrodynamic sources of sound due turbulence and interaction among eddies spreading downstream the propeller, are completely lost. As shown in Testa *et al*. (2018b), for a marine propeller in open water at high advancing ratio, potential hydrodynamics is adequate to capture the tonal sources of sound due to cyclic blade passages and trailing vortices convected downstream for observers placed in the near field (0.75 diameters from the hub centre, along the vertical direction), upstream and downstream up to 0.5÷1 diameter far from the disk. Although turbulence-induced noise effects are not captured by BEM coupled with the Bernoulli approach, within this range the noise signals carried out by the potential flow-based approach seems to be a sort of *mean noise signal* with respect to predictions based on the acoustic analogy technique (Ffowcs Williams & Hawkings, 1969). Moving downstream, propeller hydroacoustics is not more dominated by potential wake vorticity effects: important vorticity contributions generated by complex interactions among vortices may give rise to stronger vortex structures inducing, in turns, higher level of noise behind the disk. In addition, the not modelled turbulent structures, evolving in the wake, make the use of BEM hydrodynamics data through the use of the Bernoulli equation inadequate for any hydroacoustic investigation. The range of 0.5÷1 diameter where the potential-flows based methods may provide reasonable results in terms of pressure pulses is expected to reduce for higher blade(s) loads, more intense wake and in the presence of non-uniform inflow to the propeller disk. In fact, in these circumstances the role assumed by the turbulent structures, downstream the propeller disk, grows-up and reduces the limits of applicability of potential methods for hydroacoustic purposes. Note that this approach based on BEM hydrodynamics and the Bernoulli equation does not account for the compressibility delays that, indeed, may alter the overall noise features with respect to prediction in which one assumes that all sources' contributions overlap simultaneously at the observer position. However, the low rotating blade tip Mach number, typical of marine propellers, allows to account for an instantaneous sound propagation because it does not alter the resulting signal in a significant way, at least within a distance of about 10 propeller diameters from the hub (Testa *et. al.*, 2008).

A field of applications where potential flows methods are still accurate for hydroacoustic purposes is in the near field (few diameters from the propeller hub) where the tonal noise components, associated to the blades and vorticity convected downstream, may play an important role. Acoustic scattering problems in which hydro-borne propeller sound interacts with the hull structure, being spread out into reflected and diffracted noise components, fall within this field of application. Details are found in ITTC (2017a). The same considerations may be also valid in the far field, if the acoustic observers are far away from the propeller wake and the rotor blades are subject to a velocity field (due to blade-vortex interaction or high intense wake hull) with high-frequency changes both in time and space.

b) Ffowcs Williams & Hawkings Equation Approach – Linear Acoustics

Several hydroacoustic studies found in literature are based on the so-called *hybrid approach* where noise sources and sound radiation are investigated separately, with the former evaluated by fluid-dynamic computational tools (typically based on BEM) and the latter predicted through a post-processing step based on the use of acoustic analogies. Among them, the Ffowcs Williams & Hawkings Equation (FWHE) for impermeable surfaces has been widely applied for the analysis of rotating blade devices, by assuming that, nonlinear terms (the so-called quadrupole noise) can be neglected because of the low rotational speed of the blade.

For instance, in Seol *et al*. (2002) a noise prediction was carried out for a noncavitating propeller with and without a duct, by coupling the Farassat time-domain formulation 1A (Farassat, 1981) to a hydrodynamic BEM solver based on a potential approach. The robustness of the acoustic analogy and its advantages with respect to a direct pressure estimation by the Bernoulli equation were largely discussed in Testa *et.al*. (2008) by pointing out the role played by the numerical modeling of the propeller wake. From a general standpoint not depending on the CFD (Computational Fluid Dynamics) solver used to detect the sources of sound upon the blades, and for propellers in open-water conditions, the assumption that nonlinear terms can be neglected *a priori* has to be carefully applied, both for the comments at subsection *a)* and in view of the recent analytical study addressed in Ianniello (2016) on the acoustic efficiency of rotating sources in open water conditions, showing that the FWH surface terms from multibladed propellers may vanish underwater in a narrow region with relevant nonlinear phenomena occurring rather far from the body. In particular this paper shows that the blade tip vortex persists in an extended region, and, depending on both the operating conditions and external flow, it is inevitably destined to destabilize and break down, thus increasing the vorticity and turbulence. In other words, the flow nonlinear sources generated by the body motion (and occurring rather far from it) soon get the upper hand, and as a result the hydroacoustic far field may be dominated by the quadrupole term.

Differently, in behind-hull conditions the validity of hydroacoustic predictions based on the 1A Farassat Formulation is an open question because no consensus emerges. Specifically, a substantial margin of uncertainty on the role played by an unsteady loading noise component in case high unsteadiness of the tested operating conditions, remains. Akin to the Bernoulli-based approach, the 1A Farassat Formulation may be well suited in case of acoustic scattering problems in which hydro-borne propeller sound interacts with the hull. This issue is widely discussed in ITTC (2017).

Cavitating propellers

c) Bernoulli-based Formulation

Hydrodynamic cavitation concerns with the formation and collapse of partial vacuums in a liquid by a swiftly moving solid body. Under well-defined physical conditions, cavitation can occur in any hydrodynamic devices operating in liquid when pressure drops below the saturated vapor pressure. Acoustically speaking, cavitation is highly undesirable, as it induces and impulsive sound and deeply modifies the baseline acoustic signature of the propeller. These effects are inherently related to the spectrum of the high-energy radiated noise, that exhibits a low frequency range, governed both by tones (multiple of the blade passage frequency) and broadband hump (due to the large-scale cavity dynamics), and a higher frequency broadband range due to the collapse of vapor bubbles (Brennen, 1995). It is well recognized that the factors causing pressure fluctuation induced by a propeller are classified into three primary parts: changes in the blade loading, rotation of the blade thickness, and the volume change of the propeller cavitation (ITTC, 2014, 2017a; Carlton, 2018). However, pressure fluctuation due to changes in blade loading and blade thickness are very small compared with the pressure fluctuations caused by cavitation.

In principle the goal in the design of hydrodynamic devices is to avoid cavitation; however, few propellers in practice can operate entirely without cavitation due to the non-axisymmetric inflow or unsteady body motion. The occurrence of cavitation makes the detection of the sources of sound a very complicated and partially unsolved problem. In fact, the modern CFD is able to provide a satisfactory estimation of cavitation patterns (Salvatore *et al*., 2009a), but a reliable simulation of important underlying phenomena (especially those related to cavities collapsing stage) is still far from being achieved. Such a modelling uncertainty seems to be less critical in case of a *sheet cavitation*, which frequently occurs on conventional propellers operating in the hull wake field. It consists of a relatively *thin* vapor region which typically forms at blade leading edge, fluctuates in size in a limited azimuth range and eventually collapses, always remaining essentially attached to the blade surface. Under the assumption that: *i*) cavitation pockets remain attached to the blades surface and *ii*) the collapse of the cavity, due to condensation, does not imply violent implosions so that vapor bubble evolves in a smooth way (by progressively reducing its size up to disappear), a potential-flow hydro-dynamics analysis yields a reliable description of the cavity dynamics in terms of inception, growth and collapse (Knapp *et al*., 1970; Brown *et al*., 1976; Franc *et al*., 2004; Salvatore *et al*., 2009a).

In the framework of unsteady propeller cavitation tackled by 3D BEM hydrodynamics, the correlation between flow-field induced pressures and sheet cavitation pattern is obtained by integrating nonlinear sheet cavity models such those described in (Lee, 1987; Kinnas & Fine, 1992; Kinnas & Pyo, 1999; Salvatore & Esposito, 2001; Kinnas *et al*., 2003; Salvatore *et al*., 2003; Bosschers 2018b,) with a boundary integral methodology for the velocity potential (Morino *et al*., 1975) where propeller load-induced vorticity shedding is described by a trailing wake alignment model. In this approach, valid for leading edge cavitation attached to the blade suction side (partial sheet cavitation), the cavity trailing edge region is modelled via a closed–cavity scheme and the cavity shape is determined by a free–cavity length iterative technique. An extension to supercavitation is presented in (Young & Kinnas, 2003). Pressure pulses in the fluid medium is accomplished by means of the Bernoulli theorem once the velocity potential field is known (Gennaretti *et al*., 1997).

An approximated derivation to isolate the pressure field induced by the unsteady cavitation is obtained by noting that any cavity sheet over the blade surface affects the potential field through an additional source distribution known in literature as *cavity source sheet*, whose intensity is governed by the cavity dynamics (Salvatore & Ianniello, 2003). Other simplified approaches typically used to predict the tonal noise induced by the occurrence of sheet cavitation on the blade(s) surface rely on the use of a monopole model where propeller lifting surface methods are coupled to the solution of the Rayleigh-Plesset equation for the detection of the cavitation volume change (Okamura & Asano, 1998).

d) The Ffowcs Williams & Hawkings Equation Approach - Linear Acoustics

Unsteady flows generate pressure fluctuations that partially propagate as acoustic waves throughout the fluid medium. Lighthill's acoustic analogy (Lighthill, 1952) separates sound generation mechanisms from propagation phenomena by arranging the flow governing equations in the form of a wave equation; through the use of generalized functions theory, and by embedding the exterior flow problem in unbounded space, the most general form of the Lighthill's acoustic analogy recasts into the Ffowcs Williams & Hawkings equation (FWHE). In sheet cavitating conditions, a widely used approach followed in the literature (see for instance: Salvatore & Ianniello, 2003; Seol *et al*., 2005; Seol, 2013; Testa *et al*., 2018a) is to predict the noise field through the standard Farassat 1A formulation (Farassat, 2007). This is where: i) the pressure distribution upon blades is provided by a suitable panel code coupled with cavitation modelling such as those briefly mentioned in Section 6.2.2; ii) the bubble dynamics exhibits its noise effect through the variation of the blade shape during a revolution or by imposing suitable boundary conditions on the blade surface assumed as a porous, undeformable body. The two aspects represent the radiated noise by thickness-like effects (Testa *et al*., 2018a) and embody the current state of the art in this field.

In Belibassakis & Politis (2019), a numerical model is developed for the prediction of noise generated from cavitating or non-cavitating marine propellers operating in unsteady inflow conditions in the wake of the ship. The hydrodynamic part is analysed by a velocity-based vortex lattice method, providing the unsteady pressure on the blades and cavitation data. The latter are subsequently used, in conjunction with Farassat formulation, to calculate acoustic radiation from moving surfaces and predict the acoustic spectrum at a distance of several diameters from the propeller, representing the source of marine propeller noise. An approximate model is derived, exploiting information and integrated data concerning the time history of blade sheet cavity volume and the unsteady blade thrust. The latter are used to calculate the monopole and dipole forcing terms of the acoustic equation and derive the propeller acoustic spectrum in the low and moderate frequency band. Also, the directivity characteristics of the propeller noise are calculated, and the effect of nearby boundaries on underwater noise propagation are presented comparatively to the omnidirectional source assumption. In particular, the effect of the free surface as a pressure release boundary (Lloyd mirror effect), and of the ship hull, treated as hard and soft boundary, are illustrated.

In Lampe *et al*. (2019), interaction problems arising from the modelling of the dynamic behaviour of the flexible P1356 marine propeller are presented. The fluid domain is simulated through a potential theory based on BEM with an additional model to take into account sheet cavitation. The structural part of the problem is handled by a high-order finite elements method. Information exchange between the respective sub-problems is managed by a separate coupling tool which employs the Quasi-Newton Least-Squares method to provide a stable and efficient computation method. Acoustic evaluation is performed in a postprocessing fashion using the Ffowcs-Williams Hawkings equation.

In the presence other cavitating phenomena localized in the flow field (bubble cavitation, tip vortex cavitation, etc.) the use of BEM is inadequate and the need of using a CFD solver is mandatory. However, the development and the assessment of reliable two-phase hydrodynamic solvers is well far to be achieved yet, making the prediction of cavitating propeller noise more a hydrodynamic issue than a hydroacoustic one. A brief description on relevant papers concerning the use of CFD solvers to provide the input data to the FWHE for cavitating propellers is found in ITTC (2017a).

6.1.3 Hydroacoustics by CFD-FWHE Coupling

To capture noise induced by the nonlinear sources of sound occurring during the operating conditions for non-cavitating propellers, the FWHE for permeable surfaces is very attractive because no volume integration is needed. Starting from the identification of the sources of sound by high-fidelity CFD tools over a fictitious porous surface *S* that embeds all nonlinear flow effects and physical noise sources, the permeable FWHE yields the noise signatures outside *S* by solving an inhomogeneous wave equation through the Green function technique. However, its drawbacks are: i) the need of accurate CFD simulations as Large Eddy Simulation (LES) or Detached Eddy Simulation (DES) methods; ii) the occurrence of spurious signals when vortical/turbulent eddies pass through the downstream end of the control surface (namely, the end-cap problem); & iii) the need of a careful placement of the porous surface whose dimension must be tailored to enclose all the noise sources. Finally, for CFD finite-volume based solvers relying on the dual (or pseudo) time-stepping approach (Merkle & Athavale, 2012) the need of computations capable to avoid boundary conditions reflections is mandatory (Poinsot & Lele, 1992).

The end-cap problem is caused by truncation of the source terms at the integration boundary. From a physical standpoint, it is strictly related to the differences between acoustic and hydrodynamic pressure distributions that the FWHE describes (as an exact rearrangement of the Navier-Stokes equations). When vortical structures pass across the permeable surface, the integral formulation used to solve the FWHE radiates the hydrodynamic pressure field across it as sound waves, because the free space Green's function technique is applied to solve the FWH-P problem. By including the (neglected) volume term, these contributions are cancelled-out through the Lighthill's stress tensor.

In view of these issues, the use of the FWHE for permeable surfaces is widely applied. For instance, in Ianniello *et al*. (2014), the radiated noise of a complete scaled ship model using incompressible RANS simulation and the FW-H analogy is computed. The direct volume integration and permeable FW-H approach were both used. For the direct volume integration, the averaged contribution of the turbulent fluctuating velocity components to the Lighthill stress was also included. Different permeable surfaces enveloping the whole ship were studied. Good correlation between the acoustic pressures and the RANS pressure signals were obtained.

Lloyd *et al*. (2014), compared two different numerical solvers (ReFRESCO with porous FW-H and EXCALIBUR with Kirchhoff formulation) for the two-bladed model propeller (S6666) in open water condition. The main aim of the study was to verify the FW-H application and investigate the behaviour of the porous surface. It was observed that FW-H results show good agreement with the measurement by underpredicting the first harmonic, whereas Kirchhoff formulation gives slightly better estimation to FW-H formulation.

Lloyd *et al*. (2015b), investigated the propeller hydroacoustic performance using RANS with porous FW-H equation in open water condition. In their study, different grid structure configurations were analysed in order to examine its effects on propeller hydrodynamic and hydroacoustic performance using the steady simulations for the receivers located at the propeller plane. The numerical results showed that both unsteady FW-H and RANS pressures seem to suffer from some numerical disturbances which are attributed to sliding interface or pressure correction methods.

Lloyd *et al.* (2015a), also examined the propeller hydroacoustic performance using RANS with porous FW-H formulation for two receivers located downstream with two different CFD codes (ReFRESCO and OpenFoam). The effects of the permeable surface closure on the propeller hydroacoustic performance were investigated. Testa *et al*. (2018b) examined the INSEAN E779A propeller using BEM and DES with a porous FW-H approach under uniform flow and non-cavitating conditions. The main aim of the study was to show the capabilities of BEM for propeller underwater radiated noise predictions. Due to the absence of capturing the turbulence-induced noise effects, BEM only provides acceptable results in the vicinity of the propeller (0.5-1D) and hence only tonal components can be predicted.

Lidtke *et al*. (2016), used URANS and the FW-H analogy to compute the tonal blade passage noise of the PPTC propeller and used LES (Large Eddy Simulation) and the FW-H analogy for the noise generated by a hydrofoil. In this case cavitation occurrence is simulated using the Schnerr-Sauer model. It was concluded that RANS is unable to accurately account for cavitation dynamics and the associated noise.

Lidtke *et al*. (2019), investigated the INSEAN E779A model propeller underwater radiated noise under non-cavitating and cavitating conditions in the presence of a wakefield with RANS and FW-H analogy. This systematic study might be the first study to test the capabilities of FW-H approach in the realistic configuration in the maritime field. Therefore, the main aim was to understand the definition of the porous surface as well as important parameters such as time step and grid resolution. The results showed that the porous surface definition is important for reliable acoustic simulations.

Li *et al*. (2018), used DDES (Delayed Detached Eddy Simulation) and the permeable FW-H approach to compute the radiated noise of a full-scale ship and compared the results with sea trial measurements.

In Cianferra *et al*. (2019) a numerical computation of the acoustic field generated by an isolated marine propeller, in open water is addressed. The propeller considered corresponds to a benchmark case, for which fluid dynamic data are available in literature and online. The fluid dynamic field, which represents the source of noise, is reproduced through a LES solver, the small scales of motion are modeled through the dynamic Lagrangian model and a wall-layer model allows to avoid the resolution of the viscous sublayer. The acoustic field is reconstructed by the Ffowcs Williams and Hawkings equation, which is composed of surface and volume terms indicating different noise generation mechanisms. By isolating each term contribution, the paper shows that the shaft vortex constitutes a considerable source of low frequencies noise.

6.2 Guidelines for Coupled CFD-FWHE

From the above cited literature works and referring to some relevant papers on jet-noise such as Mendez *et al*. (2009), Mendez *et al*. (2013) and Shur *et al*. (2005) where the use of the permeable FWHE is mature, some useful suggestions may be proposed.

Among them the optimal FWH surface location should be fairly tight around the rotor disk and the wake convected downstream. This would lead to calculating noise by information (only) from the high-quality region of the calculus domain.

Further, both the magnitude of Lighthill's source term and placement of the vorticity/turbulent field downstream the rotor disk should be used as good indicator of correctness of the FWH surface placement; a basic test would be to check that sound is not strongly dependent on the surface used, in terms of diameter and length.

Finally, a warning is made on the common use of open porous surface to overcome the end-cap problem. For observers downstream, omitting the closure disk from the permeable FWHE seems to yield slightly better results than closed surfaces, especially in terms of waveform. Note that several correction techniques have been proposed to alleviate this issue. Among them, the exit-flux concept introduced in Wang *et al*. (1996) has been successfully extended in Nitzkorski & Mahesh (2014) to the FWH methodology for the end-cap correction of porous surfaces in the near field.

For the sake of clarity Figure 45 depicts a sketch of marine propeller enclosed by a permeable closed cylindrical surface. Accounting for the above criteria and looking at the contour plot of the L_2 norm of the Lighthill stress tensor distribution inside the computational domain, the porous surface size (length and width), as well as the placement of closure-end are well suited to compute the noise induced by the propeller, in that outside the acoustic surface the noise sources are negligible, and no vortices cut its boundaries.

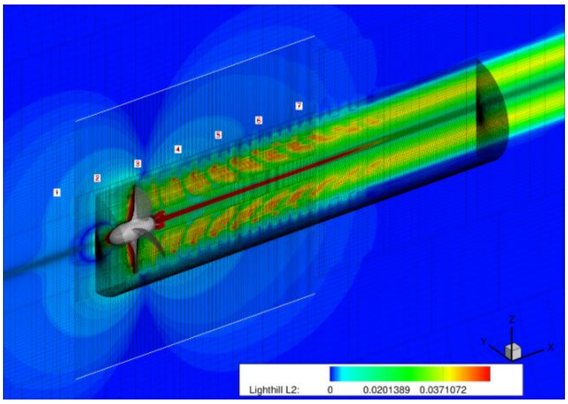

Figure 45. Sketch of FWH-P porous surface and contour of the L2 norm of Lighthill stress tensor.

6.3 Structural borne noise

The noise caused by vibrating machinery onboard is called structural borne noise due to the fact that the vibrations are transmitted through the ship structure to the outer plating and emit as noise to the underwater environment. The most significant machinery noise sources are diesel engines and turbines, generators, propulsion gearboxes, and large pumps.

Any machinery will create both vibration and airborne noise. Figure 46 shows three main paths for noise generated by machinery (Spence *et al*., 2007). The first structure born path relates to the vibration excitation of machinery on the ship structures through the couplings between the source and the structure. The vibrations are carried out through the entire hull. The low frequencies are controlled by the hull resonance modes which also affect the noise directivity (Arveson & Vendittis, 2000).

The secondary structure born path is excited by the airborne noise that impinges at the compartment boundaries and excite structures to vibrate. The vibrations then propagate to the outer plating causing underwater noise. The airborne path describes the noise that passes the ship's outer plating directly. The airborne path applies when the compartment containing machinery source is directly adjacent to the sea. When the machinery is located in the compartment next to the outer plating, the second structure born path has less significance than the airborne path. When the machinery is in inner compartments the situation is vice versa.

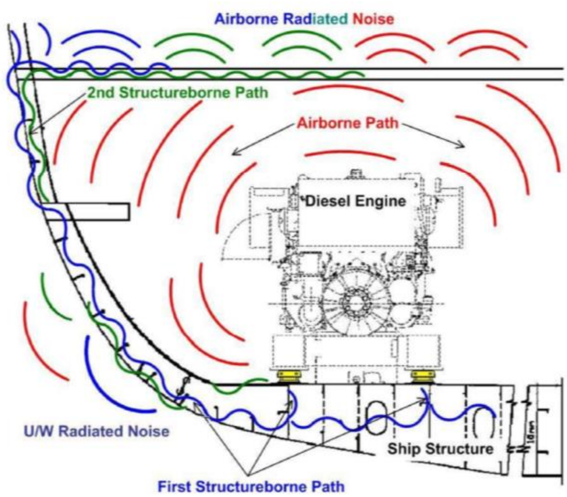

Figure 46. Main paths of structural born noise. Figure taken from Spence *et al.* (2007).

The source levels of vibrations in diesel engines usually scale as (power/weight)^2 (Fisher & Brown, 2005). The heavy low speed diesels have therefore lower source levels compared to medium speed engines. However, medium speed engines can be resiliently mounted which decrease their noise excitation level to water. Other well-known treatments to decrease structural born noise levels are to mount single or multiple items on a common floating deck, use hull decoupling materials, cladding treatments in machinery spaces, machinery enclosures, and flexible piping solutions. Air bubbling layers used to decrease flow friction under the hull also decrease the structural born underwater noise from the ship at a wide range of frequencies.

Vibroacoustic models are used to predict the structural born noise from ships. The models have been developed in other application areas and used for ships by specialist for dedicated purposes. Only few papers exist in open literature on vibroacoustics for underwater noise from ships.

At low frequencies, say up to 100 Hz depending on the size and complicity of the structure, the vibrations are first solved deterministic by FE method. The acoustic radiation is then solved by boundary element method (BEM) using the FEM solution as a forced response boundary condition. The two-step method is significantly less expensive computationally than a strongly coupled FEM-BEM solution.

At high frequencies from 500 Hz upwards, depending on the structure, the vibration behaviour is random. A statistical approach to model the vibrations on a structure is then a feasible choice. Statistical Energy Analysis (SEA) employs statistical descriptions of system components in order to simplify the analysis of complicated vibroacoustic problems (Lyon & De Jong, 1995).

In the frequencies between the feasible frequency limits for pure FEM and SEA approaches, a hybrid FEM/SEA approach can be utilized. FE and SEA subsystems are created for the structure. The FE part can be a larger system or a local junction between two SEA subsystems. The coupling of the FE and SEA methods are described in detail for example in Shorter & Langley (2005a,b).

Not many papers are available in the open literature about underwater structural born noise from ships. Zhang *et al*. (2019) have published a study where they compared different radiation modelling methods for structural born noise of an oil tanker. They compared different acoustic radiation models at low and mid-frequencies with the FE method, namely BEM, infinite element method IFEM, and automatic matching layer AML. The latter two ones require volume mesh for the external acoustic field. All three methods gave relatively similar results, but the authors concluded that the FE-BEM hybrid model is the most suitable one for engineering purposes due to the lowest computational effort and robustness. The authors also studied the directivity of the noise at 50 m depth. The far field was reached at a radius of about half of the ship length around the vessel.

6.4 Noise propagation

Noise propagation models are used to predict propagation loss due to surface and bottom reflections, bathymetry, and celerity profile. Propagation loss models were discussed in detail already in the report of the 28th ITTC specialist committee on hydrodynamic noise and are not repeated here.

NPL (Wang *et al*, 2014) reviewed the existing acoustic propagation models, see Table 10. The parabolic equation solution and the normal mode solution represent the most appropriate model choice at lower frequencies, for high frequency computations ray tracing or energy flux models are generally used.

Table 10. Review of propagation models (Wang et al, 2014)

Shallow water - low frequency	Shallow water - high frequency	Deep water - low frequency	Deep water - high frequency
Ray theory	*Ray theory*	*Ray theory*	*Ray theory*
Normal mode	*Normal mode*	*Normal mode*	*Normal mode*
Wave number integration	*Wave number integration*	*Wave number integration*	*Wave number integration*
Parabolic equation	*Parabolic equation*	*Parabolic equation*	*Parabolic equation*
Energy flux	*Energy flux*	*Energy flux*	*Energy flux*

Green – suitable; Amber – suitable with limitations; Red – not suitable or applicable

Within the project JOMOPANS (the Interreg Joint Monitoring Programme for Ambient Noise North Sea), a wide range of acoustic propagation model implementations from the JOMOPANS project partners are verified by means of a comparison of the output for two well defined benchmark scenarios based on the modelling scenarios developed for the Weston Memorial Workshop (Binnerts *et al*, 2019). The model types considered are based on energy-flux integration, analytical and numerical mode solvers, parabolic equation range step integration, ray tracking and wavenumber integration. Recommendations on the use of these models are given and limitations are discussed. The acoustic metric considered is the depth-averaged sound pressure level in one-third octave (base 10) bands from 10 Hz to 20 kHz. The results show that the majority of the tested models are in agreement for a range independent shallow water environment providing a reliable benchmark solution for the future verification of other propagation models. The observed agreement gives confidence that these models are correctly configured and able to provide numerically correct solutions. For a range-dependent environment however, a significant uncertainty remains. The solutions provided in this paper can be used as a reference to select the optimal compromise between reducing the computational complexity and increasing the model precision for the propagation of sound in shallow water.

Noise propagation models are commonly used for noise mapping. Typically, the modelled ranges are more than 10 km. For example, Cho *et al*. (2018) have modelled noise maps in Korean waters by combining empirical formula for source levels of ships, AIS data for shipping density, and propagation modelling. The transmission loss was calculated by a range-dependent ray-based propagation model. The authors found that the highest uncertainty in their calculation was the empirical model predicting the source level of ships. Halliday *et al*. (2017) simulated a region affected by underwater noise of a vessel in the western Canadian Arctic in order to estimate the potential impacts of underwater noise to whales. The source level was measured in the sea area and transmission loss was calculated by propagation models. A coupled normal modes model for a range-dependent environment (for frequencies between 50 Hz and 1.5 kHz), and a ray trace model (for frequencies between 1.5 and 24 kHz) were used in the study.

Propagation modelling can be used to predict transmission loss also at distances relevant in noise trials. Especially, the effect of shallow water on noise source level analyses can be estimated with propagation models. The Bureau Veritas (2014) URN rule notifications suggest as the first option to calculate the transmission loss at the noise trials at low frequencies (<1000 Hz) using a range independent wave integration model, and at higher frequencies (>1000 Hz) a range dependent ray trace-based model. One may also use other models if appropriate validation references are available.

Kozaczka & Grelowska (2018) have studied noise propagation in shallow water of about 20 meters using the normal mode theory. The authors have investigated the transmission loss at distances from 100 to 10 000 meters from the source. The paper investigates transmission loss at frequencies between 200 and 1000 Hz, and with different bottom sediment types. The bathymetry in the sea area was flat. The effect of shallow water on noise propagation is clearly seen in the simulations.

Sipilä *et al*. (2019) measured the propagation loss from noise measurements of an icebreaker. The noise measurements were repeated at varying by-pass distances of the ship and the measurement location. The propagation loss was calculated from the measurements. The water depth was about 25 meters in the measurement area. There was a slope in the seabed between the ship route and the measurement location. The propagation loss was also calculated using a range dependent parabolic equation model. Figure 47 shows comparison of geometrical transmission loss at a range of frequencies determined from the measurements and simulations. The two approaches show similar behavior for the transmission loss. The paper also studies the effect of different bottom sediment type and seabed slope on the transmission loss in shallow water.

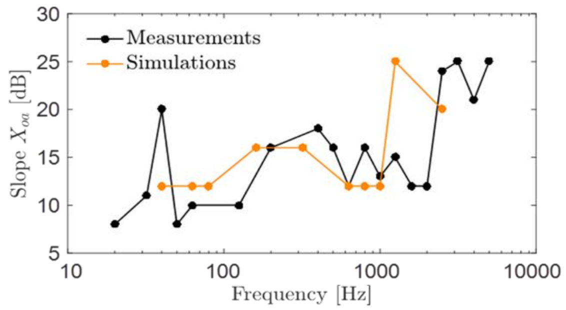

Figure 47. Measured and calculated propagation loss factor X , with propagation loss defined as X $\log_{10}$ R, at different frequencies determined for a distance of about 150 m. Figure taken from Sipilä *et al*. (2019).

Gaggero *et al*. (2016) calculated the transmission loss in shallow water to compare the model test results of noise emitting from a marine propeller to full-scale results. The conclusion was that careful determination of transfer function in model-scale and transmission loss in full-scale is required to make comparisons of source level at different scales. However, more data is needed to gain further confidence on the procedures and on the complex mechanisms of cavitating propeller noise generation.

7. BENCHMARKING (MV)

The Specialist Committee on Hydrodynamic Noise of the 29th ITTC was tasked to identify a benchmarking case for model-scale underwater radiated noise (URN) measurements. The requirements for the test-case were that:

a. full-scale underwater radiated noise measurements are available.
b. it is a representative merchant vessel.
c. the geometry and measurement data can be shared with the whole ITTC community.

In the present paragraph, the proposed candidate ship is presented, reporting the reasons for the choice (Section 7.1). In order to setup the test matrix, two activities have been carried out, i.e., a questionnaire among a list of possible participants and some calculations carried out by members of the Committee; the results of both activities are summarised (Section 7.2). Finally, the complete structure of the proposed benchmark activity is described (Section 7.3).

7.1 Proposed candidate ship

A review of possible benchmark cases for model-scale noise measurements has been carried out by the Committee in order to propose a suitable candidate. The most relevant cases considered are summarised in the following:

- Olympus (AQUO Project) – Coastal Tanker - L = 116.9 m – Displacement 13250 t – Speed 14 kn – 1 CPP (D = 4.80 m): geometries not available to all participants, only separate agreements (ref.: Johansson *et al*, 2015; Tani *et al*, 2016b)

- Nawigator (EFFORT and AQUO Projects) – Research Vessel – L = 60.3 m – Displacement 1150 t – Speed 13 kn – 1 CPP (D = 2.26 m) (Ref.: Gaggero *et al*, 2016)

- Princess Royal (SONIC Project) – Research Vessel (catamaran) – L = 18. 9 m –

Displacement 40 t – Speed 20 kn – 2 FPP (D = 0.75 m) (ref.: Aktas *et al.*, 2016b)

- Princess Royal (SONIC Project) propeller in open water conditions (Hydro Testing Forum test case) (ref.: Aktas *et al.*, 2016a; Hallander, 2017; Lafeber & Lloyd, 2017; Sakamoto *et al.*, 2017; Tani *et al.*, 2017; Tani *et al.*, 2020)

- Other cases were also considered, but they were either lacking URN data (REGAL used in LR CFD workshop), had noise measured with hull mounted transducers only (Seiun Maru), or URN measurements and geometries could not be made publicly available (Combi-Freighter)

Among the above mentioned cases, the research vessel Nawigator XXI has been selected, since it is the only case for which hull/propeller geometries and measurement data in full-scale can be shared with the ITTC Community. Moreover, Nawigator has a hull form and a propeller geometry that is representative of a merchant vessel. Therefore, despite its relatively small size, this ship is considered the best candidate for the benchmark activity.

In the following, a brief outline of the ship characteristics and the measurements available in full-scale is reported.

7.1.1 Ship characteristics

In Figure 48 a photograph of the ship is reported, while main ship characteristics are listed below.

Figure 48. Nawigator XXI Research Vessel.

- Ship name: Nawigator XXI
- Type / Year of building: Research Vessel built in 1998
- Owner: Maritime University of Szczecin
- Length overall: 60.3 m (LOS)
- Beam: 10.5 m
- Draft: 3.15 m
- Displacement: about 1150 t
- Speed: 13 kn (max)

Propulsion plant and other machineries characteristics are listed below:

- 1 Controllable Pitch Propeller (CPP), D = 2.26 m, P/D(design) = 0.942, 4 blades
- Main Engine: SULZER Cegielski 8S20D (4 stroke, 8 cyl L) resilient mounted, 1120 kW, 900 RPM, reduction rate: 3.75
- Auxiliary Engines: Caterpillar SR4: (4 stroke, 8 cyl L) resilient mounted, 2 x 240 kW + 1 x 85 kW, 1500 RPM
- Bow thruster: 110 kW, abt. 500 RPM (propeller)

7.1.2 Full-scale measurement campaign

URN measurements at sea have been carried out during the EU-FP7 AQUO project; the campaign took place in the Baltic Sea and the following data were recorded:

- Power, rpm, pitch, speed over ground
- Cavitation observations
- Vibrations
- URN
- Pressure pulses

Measurements have been performed at one ship draught (namely, 3.2 m at stern, 3.15 m at bow), mainly varying pitch at constant RPM (8 different pitch settings); in addition to this, in correspondence to one pitch setting two different propeller RPM have been considered (navigation and maximum)

It has to be kept in mind that the measurement campaign presents some shortcomings. In particular, information on blade pitch angle is only obtained from the bridge, thus there is some uncertainty on the exact value. Moreover, cavitation photographs using hull windows are available, but the quality is not enough to capture correctly the cavity extents. Finally, the URN measurements have been performed in shallow (24 m) water, requiring the use of a computational method to convert the radiated noise levels to source levels.

For what regards possible conditions of interest, considering the whole set of measurements, the signal to background noise ratio of the URN measurements is acceptable at maximum speed condition (maximum RPM) and for the conditions with lowest pitch tested. Model tests carried out during the AQUO project (propeller at UNIGE cavitation tunnel behind wake screen) suggest that in correspondence to maximum speed condition attached tip-vortex cavitation is present, plus very limited sheet cavity at tip, as reported in Figure 49; in correspondence to the lower pitch condition pressure side cavitation is present (tip vortex, vortex from sheet face and pressure side sheet cavitation)

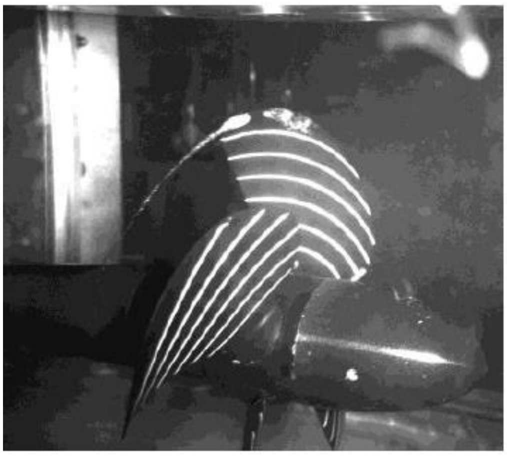

Figure 49. Cavitation observations at UNIGE cavitation tunnel (max. speed condition) (Gaggero *et al.*, 2016).

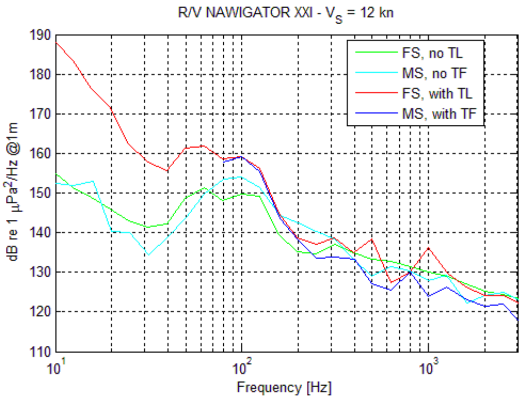

Figure 50. Model-scale vs Full-scale measurements (Gaggero *et al.*, 2016).

Notwithstanding the above-mentioned shortcomings, a good agreement between model tests and sea trials has been obtained, as reported in Figure 50. Therefore, the Committee considered it worthwhile to proceed with this candidate, keeping in mind that comparison between results of different cavitation test facilities is an important aspect of the benchmarking study.

7.2 Definition of the test matrix

In the following paragraphs, the results of the questionnaire and numerical calculations conducted by the Committee with the aim of defining the most suitable test matrix for the benchmarking activity are summarised.

7.2.1 Questionnaire

A questionnaire was circulated among possible participants to the benchmark activity, in order to get an insight into the number of facilities interested and the extent of their possible involvement in terms of number and complexity of tests.

The questionnaire obtained 20 answers, with 19 facilities confirming their interest in the benchmark activity. The Committee considers this result very encouraging in view of the forthcoming activity, with a large interest spread basically over the entire model testing community.

In particular, two conditions [12] were indicated as "mandatory", as follows:

- Condition A: 79% pitch and max shaft rate (860 RPM) / full-scale data available
- Condition B: 79% pitch, identical propeller loading (thrust coefficient value) as Condition A, but reduced cavitation number in order to enlarge sheet cavitation extent (together with tip–vortex cavitation) / no full-scale data available.

In addition to this, participants were asked to indicate their possible interest on different additional tests (e.g., at lower pitch [13], with reduced propeller loading, in different wakes).

Among the participants which provided a positive response, the following answers to specific questions were given:

- 100% agreed with the proposed "mandatory" conditions.
- 12 participants (63%) expressed interest in carrying out tests at reduced pitch; among these, 3 participants indicated the interest on the use of one additional pitch, 3 on two additional pitches, only one was in favour of more than two additional pitches; moreover, some participants proposed to use CPP model and not different FPP models in order to limit costs.
- 17 participants (89%) expressed interest in carrying out tests at constant pitch and reduced K_T; this kind of test of course does not reproduce the same phenomenon but has the advantage of investigating pressure side phenomena with low additional cost.
- 12 participants (63%) expressed interest in carrying out tests in open water condition; among these, all participants indicated interest in tests without shaft inclination, 6 participants indicated interest in investigating inclined shaft conditions (about 4° plus an higher inclination, with variable values); 1 participant indicated interest in testing propeller in pulling and pushing condition.
- Among facilities which use wake screens to reproduce the ship wake, 8 participants (42% of the total, 73% of facilities using wake screens) expressed interest in reproducing in addition to the full-scale wake also the model-scale wake.

Further possible interesting investigations suggested by some participants included the possibility to use the smart dummy concept (Schuiling *et al.*, 2011), to also measure propeller-induced hull-pressure fluctuations, and to increase the number of conditions in order to investigate tip vortex - sheet cavitation interactions.

Finally, considering all the participants (including the single negative answer), 58% confirmed to have an established procedure to determine the facility transfer function; this result confirms that this practice is becoming widespread, despite further efforts are still needed in order to make it a standard procedure for almost all facilities.

[12] For both conditions, tests have to be carried out reproducing ship wake (directly with models or with wake screens).

[13] Considering that a new propeller model for each additional pitch angle has to be manufactured to avoid uncertainties in the pitch setting.

The results of the questionnaire have been utilised in order to propose the conditions for the benchmark activity.

7.2.2 Numerical calculations

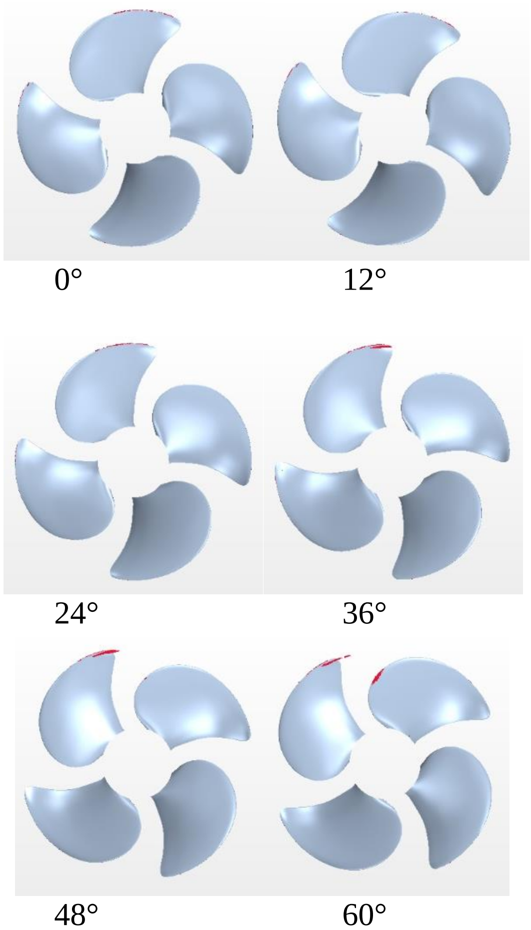

Figure 51. Cavitation predictions @ condition A1 with RANS code (courtesy of CSSRC).

In order to establish the conditions for the benchmarking activity, a series of numerical calculations have been carried out. In particular, Marin and UNIGE used BEM potential codes and CSSRC used a RANS code. The results of these calculation have been used to decide further conditions with respect to those tested at full-scale, reducing and increasing load to stimulate pressure side cavitation and increase suction side cavitation extent respectively. Moreover, calculations allowed to suggest a condition with very limited cavitation (slightly below inception) at rather large cavitation number.

In Figure 51 and Figure 52 results in correspondence to condition A1 only are reported. Numerical results confirm the expected extent of cavitation reported in Figure 49, with lower extent predicted by RANS calculations and higher extent predicted by BEM calculations.

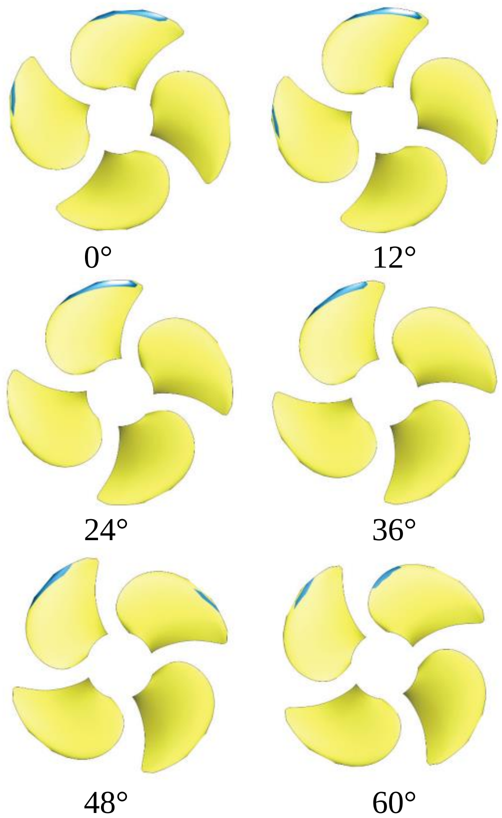

Figure 52. Cavitation predictions @ condition A1 with BEM code (courtesy of UNIGE).

7.3 **Proposed benchmark**

Considering the results of the questionnaire and of the numerical calculations, the Committee proposes the following conditions for the benchmark activity, as summarised in Table 11.

Table 11. Proposed test-conditions for the Nawigator XXI benchmarking studies.

Condition	P/D	K_T	σ_N (tip)	Type
A1[14]	0.91	0.22	2.79	Mandatory
A2	0.91	0.26	2.79	
A3	0.91	0.22	4.2	
A4	0.91	0.08	2.79	Suggested
B1[15]	0.464	0.08	3.58	Additional (lower pitch)
C1	0.91	0.22	2.79	Additional (uniform flow, no shaft inclination)
C2	0.91	0.26	2.79	
C3	0.91	0.22	4.07	
C4	0.91	0.08	2.79	
D1	0.91	0.22	2.79	Additional (uniform flow, 8° shaft inclination)
D2	0.91	0.26	2.79	
D3	0.91	0.22	4.07	
D4	0.91	0.08	2.79	
E1	0.91	0.22	2.79	Additional (wake sensitivity study)
E2	0.91	0.26	2.79	
E3	0.91	0.22	4.07	
E4	0.91	0.08	2.79	

The test-conditions consist of:

- Three "mandatory" conditions (condition A indicated above, named A1, condition A2 obtained with higher loading at constant cavitation number, condition A3 with reduced cavitation, near inception)
- One "suggested" condition (condition A4 with reduced loading at fixed pitch)
- Possible "additional conditions", such as:
  - tests at reduced pitch (31% in order to have reference full-scale tests), with a dedicated FPP model (condition B1)
  - tests in open water: basic tests with no shaft inclination (conditions C1-C4) plus additional tests at large shaft inclination, suggested value 8° (conditions D1-D4)
  - for smaller facilities using wake screens, additional tests with model-scale wake (conditions E1-E4

The tests must be performed according to normal procedures by all participants. For conditions A1-A4 and B1 the complete hull model or smart dummy will be used for larger facilities, dummy models or wake screens for smaller facilities. In the case of wake screens, the full-scale wake will be reproduced. For conditions E1-E4 (smaller facilities only), the model-scale wake will be reproduced.

Some further remarks must be considered when the benchmarking activity will be undertaken:

- in correspondence to lower pitch (condition B1), possible further conditions might be tested.
- for cases "C", "D", "E", all conditions proposed for case "A" are currently reproduced in the table, however the number of tests could be reduced.

[14] For this condition full-scale measurements are available; propeller revolution rate at full-scale was 230 RPM, with a correspondent $\sigma_{N\ (shaft)} = 3.09$

[15] For this condition full-scale measurements are available; propeller revolution rate at full-scale was 203 RPM, with a correspondent $\sigma_{N\ (shaft)} = 3.96$

8. SUMMARY AND CONCLUSIONS

The conclusions of the 29th Specialist Committee on Hydrodynamic Noise are presented here, ordered by the Terms of Reference.

1. An outline of the ITTC model-scale guidelines has been submitted to the IMO by the ITTC secretary in December 2017 without input from the Specialist Committee. The URN of shipping has until the moment of writing not been on the agenda of IMO MEPC meetings, even though a submission by Canada, Australia and the US, supported by the EU, asked for action. Therefore, the Specialist Committee did not consider another submission by the ITTC to be of value to the community within IMO.

2. Some progress on full-scale URN measurement procedures has been made, with an ISO regulation for shallow water noise measurements still in development. At present, a total of six classification societies have rules on URN emission with URN limits, some of which include procedures for the noise measurement in shallow water. Within the EU several URN monitoring programs have started in order to measure the present ambient noise levels in European waters needed for compliance with the Good Environmental Status. Some Canadian harbours have introduced measures to promote quieting ships which has resulted into an increase of the number of ships that hold an URN class.

3. A review of the recent published literature on model-scale noise measurements has been made in the areas of

   Facility reverberation: It appears that in the last years sufficient information has become available to measure and apply transfer functions. The Committee thus recommends that the determination of facility transfer functions becomes mandatory if the source level is to be determined. It should be noted that some issues are still present which need to be further studied.

   Tip-vortex scaling: Methods to account for the effect of Reynolds number on vortex cavity size and on the underwater radiated noise in model tests are proposed in the literature but further validation studies are required.

   Water quality: There is a general acknowledgement of the significance of water quality on cavitation behaviour and noise propagation, but this is generally not quantified. There is ongoing interest in the further development and application of, particularly optical based, techniques for the measurement of nuclei size distribution.

   Measurement techniques: Further progress has been made with respect to transducer calibration and in the use of pressure sensors, hydrophone arrays and dedicated signal processing techniques. Adding uncertainties in decibels of a measurement chain for noise measurements should be done with care.

   Benchmarking activity (HTF round robin test for a propeller in open water): Discrepancies between different facilities can be as high as 10 dB.

   Validation studies for propellers operating behind a ship hull: It is found that full-scale noise levels can be predicted within 5 to 10 dB by model-scale tests.

4. Progress on computational prediction methods has been made, especially in modelling cavitation and turbulence structures in the flow field. Guidelines to couple CFD with FWHE are given to capture the relevant noise sources and to omit spurious noise in the simulations. Semi-empirical models predict noise from different cavitation patterns so appropriate combination of models is needed to deal with the whole spectrum of URN. Data driven models seem a promising option for

cavitation noise predictions but should be applied carefully. Vibroacoustic models are used to predict the structure born noise from ships. The models are used by specialists for dedicated purposes and there is a limited number of papers in open literature. The models have matured from other application areas. Propagation loss models give more insight to propagation loss at different frequencies in shallow water (and in deep water). The approach seems promising and is recommended by Bureau Veritas for noise measurement analyses in shallow water. The propagation loss models are not yet widely used for ship source level determination but are more commonly used for noise mapping.

5. A review of possible benchmark cases for model-scale noise measurements has been carried out. Among them, the research vessel Nawigator XXI (considered during AQUO project) has been selected. As requested, hull/propeller geometries and measurements data in full-scale can be shared with the ITTC Community. Nawigator XXI ship has a hullform and propeller geometry that is representative of a merchant vessel, despite having a small size (L = 60.3 m – Displacement 1150 t). The ship has a maximum speed of about 13 kn and is equipped with 1 CPP (D = 2.26 m).

   A proposal for test conditions to be considered is presented by the Specialist Committee, considering also the results of a questionnaire among potential participants to the benchmarking activity and of ad hoc numerical calculations. The proposed conditions include minimal required tests corresponding to maximum speed at sea trials plus conditions with increased and decreased suction side cavitation and a condition with pressure side cavitation.

6. The guideline 7.5-02-01-05 for model-scale noise measurements has been updated, particularly with regards to facility reverberation and the facility transfer function describing the relation between acoustic source levels and measured radiated noise levels. New methods to account for the Reynolds number scaling of tip-vortex cavitation have been described. Note that guideline 7.5-02-01-05 has been renumbered to 7.5-02-03-03.9.

   The guideline 7.5-04-04-01 for full-scale noise measurements has been updated, particularly with regards to class rules on URN and corrections for the Lloyd-mirror effect.

9. RECOMMENDATIONS

The 29th Specialist Committee on Hydrodynamic Noise recommends adopting the following guidelines:

- ITTC guideline 7.5-02-01-05: Model-Scale Propeller Cavitation Noise Measurements.
- ITTC guideline 7.5-04-04-01: Underwater Noise from Ships, Full-Scale Measurements.

The recommendations for future work are:

- To organize the proposed round-robin test case.
- Further monitor and investigate specific aspects of model-scale noise measurements including reverberation, tip vortex scaling, water quality and the effect on uncertainty.
- Continue monitoring progress on shipping noise measurement procedures for shallow water and regulations as developed by ISO, classification societies and regulatory agencies.
- Continue monitoring progress on ship noise prediction by computational methods with emphasis on the prediction of cavitation noise using CFD methods and methods such as data driven models and machine learning techniques, and noise propagation modelling, especially for shallow waters.

10. REFERENCES

Aktas, B., 2016, "A Systematic Experimental Approach to Cavitation Noise Prediction on Marine Propellers", PhD Thesis (Newcastle University).

Aktas, B., Atlar, M., Turkmen, S., Korkut, E. and Fitzsimmons, P., 2016a "Systematic cavitation tunnel tests of a propeller in uniform and inclined flow conditions as part of a round robin test campaign", Ocean Engineering, Vol. 120, pp. 136–151.

Aktas, B., Atlar, M., Turkmen, S., Shi, W., Sampson, R., Korkut, E. and Fitzsimmons, P., 2016b, "Propeller Cavitation Noise Investigations of a Research Vessel Using Medium Size Cavitation Tunnel Tests and Full-Scale Trials", Ocean Engineering, Vol. 120, pp. 122-135.

Alexander, W.N., Hickling, C., Balantrapu, N.A. and Devenport, W.J., 2020, "Ingestion of non-uniform turbulent inflow by a rotor: sound production and propagation", 33rd Symposium on Naval Hydrodynamics, Osaka, Japan, October 2020.

Amailland, S., Thomas, J.-H., Pézerat, Ch. and Boucheron, R., 2018, "Boundary layer noise subtraction in hydrodynamic tunnel using robust principal component analysis", Journal of the Acoustical Society of America, Vol. 143, pp. 2152-2163.

ABS, 2018, Guide for the classification notation - Underwater Noise, American Bureau of Shipping.

Ando, S., Kimura, K., Segawa, K. and Yamamoto, K., 2018, "Study on the Hybrid Method of CFD and Bubble Dynamics for Marine Propeller Cavitation Noise Prediction", Tenth International Symposium on Cavitation (CAV2018).

ANSI/ASA S12.64-2009: Part 1, 2009, Quantities and procedures for description and measurement of underwater sound from ships, Part 1: General requirements.

AQUO-SONIC, 2015, Guidelines for regulation on UW noise from commercial shipping, Prepared by Bureau Veritas and DNV-GL.

Arndt, R.E.A. and Keller, A.P., 1976, "Free gas content effects on cavitation inception and noise in a free shear flow", Symposium on two phase flow and cavitation in power generation systems, Grenoble, France, Societe Hydrotechnique de France. Paris, pp. 3-16.

Arveson, P. T. and Vendittis, D. J., 2000, "Radiated noise characteristics of a modern cargo ship", Journal of the Acoustical Society of America, Vol. 107, no. 1, pp 118-129.

Audoly, C. and Meyer, V., (2017). "Measurement of radiated noise from surface ships – Influence of the sea surface reflection coefficient on the Lloyd's mirror effect", Acoustics 2017 Perth: Sound, Science and Society, Perth, The Australian Acoustical Society: Paper 20.

Bahtarian, M., 2019, "Quieting ships to protect the marine environment - workshop final report". ACENTECH Inc., Report #481 Cambridge, USA.

Baiter, H.J., 1989, "On cavitation noise scaling with the implication dissimilarity in cavitation inception", ASME International symposium on cavitation noise and erosion in fluid systems.

Baraniuk, R.G., Jones, D.L., 1995, "Unitary equivalence: a new twist on signal processing", IEEE Transactions on signal processing, Vol. 43, no. 10, pp. 2269-2282.

Bark, G., 1985, "Prediction of Propeller Cavitation Noise from Model Tests and its Comparison with Full Scale Data", Journal of Fluids Engineering, Vol. 107, pp. 112-

119.

Belibassakis, K. and Politis, G., 2019, "Generation and propagation of noise from cavitating marine propellers", Sixth International Symposium on Marine Propulsors - smp'19, Rome, Italy.

Binnerts, B., Jong, C., Karasalo, I., Östberg, M., Folegot, T., Clorennec, D., Ainslie, M., Warner, G. and Wang, L., 2019, "Model Benchmarking Results for Ship Noise in Shallow water", https:// northsearegion.eu/ media/ 9884/binnerts-et-al-2019-uace-jomopans-model-benchmarking.pdf

Birvalski, M. and van Rijsbergen, M.X., 2018a, "Application of Interferometric Particle Imaging to cavitation nuclei measurements in a ship model basin", 19th International Symposium on the Application of Laser and Imaging Techniques to Fluid Mechanics, Lisbon, Portugal, July 2018.

Birvalski, M. and van Rijsbergen, M.X., 2018b, "Size and concentration measurements of cavitation nuclei in the wake of a ship model", 10th International Symposium on Cavitation – CAV2018, Baltimore, May 2018.

Blake, W.K., 2017, "Mechanics of flow-induced sound and vibration". 2nd edition, Academic Press.

Blake, W.K. and Sevik, M.M., 1982, "Recent developments in cavitation noise research", International Symposium on Cavitation Noise, Phoenix, Arizona.

Bosschers, J., 2018a, "Propeller Tip-Vortex Cavitation and its Broadband Noise". PhD Thesis, University of Twente, Enschede, The Netherlands.

Bosschers, J., 2018b, "A Semi-Empirical Prediction Method for Broadband Hull-Pressure Fluctuations and Underwater Radiated Noise by Propeller Tip Vortex Cavitation", Journal of Marine Science and Engineering, Vol. 6, art. 49.

Bosschers, J., 2020, "The effect of Reynolds number on a developed tip-vortex cavity and its radiated noise", 33rd Symposium on Naval Hydrodynamics, Osaka, Japan.

Bosschers, J. and van Wijngaarden, E., 2012, "Scale effects on hull pressure fluctuations due to cavitating propellers", 10th International Conference on Hydrodynamics, St. Petersburg, Russia.

Boucheron R., 2016, "About Doppler-Fizeau effect on radiated noise from a rotating source in cavitation tunnel", 22nd International Congress on Acoustics, Buenos Aires, Argentina, September 2016.

Boucheron R., 2017, "Over-sampling improv ement for acoustic triangulation using Barker code or Schroeder code audio signals", 5th International Conference on Advanced Model Measurement Technology for the Maritime Industry AMT'17, Glasgow.

Boucheron, R., 2019a, "Adaptation of the Schroeder frequency to the case of acoustic propagation in duct", 6th International Conference on Advanced Model Measurement Technology for the Maritime Industry AMT'19, Rome, Italy.

Boucheron, R., (2019b), "Development of a demodulation method for acoustic propagation in ducts with unknown impedance conditions for both modal magnitude and wall impedance estimate", 26th International Congress on Sound and Vibration - ICSV26, Montreal, Canada.

Boucheron, R., 2020a, "About acoustic field characteristics in the test section of a cavitation tunnel", Ocean Engineering, Vol. 211, art. 107616.

Boucheron, R., 2020b, "Modal decomposition method in rectangular ducts in a test-section of a cavitation tunnel with a simultaneous estimate of the effective wall impedance", Ocean Engineering, Vol. 209, art. 107491.

Boucheron R., 2020c, "Influence of the warping time parameters on dedopplerization efficiency in the case of a rotating source in a cavitation tunnel", 179th Meeting of the Acoustical Society of America, Acoustics Virtually Everywhere, December 2020.

Boucheron, R., Amailland, S., Thomas, J.-H., Pézerat, Ch., Fréchou, D. and Briançon-Marjollet, L., 2017, "Experimental modal decomposition of acoustic field in cavitation tunnel with square duct section", 173rd Meeting of Acoustical Society of America – 8th Forum Acusticum, Boston, June 2017.

Boucheron R., Aumelas V., Donnet, M., Fréchou, D. and Poidatz, A., 2018, "Comparative study of optical experimental methods for micro-bubble sizing", 19th International Symposium on the Application of Laser and Imaging Techniques to Fluid Mechanics, Lisbon, Portugal, July 2018.

Breeding Jr., J.E., Pflug, L.A., Bradley, M., Walrod, M.H., McBride, W., 1996. "Research Ambient Noise Directionality (RANDI) 3.1 Physics Description". Naval Research Laboratory, Stennis Space Center, Report, No. NRL/FR/7176-95-9628.

Brennen, C.E., 1995, "Cavitation and Bubble Dynamics". Oxford University Press, New York.

Briancon-Marjollet, L. and Michel, J. M., 1990, "The hydrodynamic tunnel of I.M.G.: Former and recent equipments." Journal of Fluids Engineering, Vol. 112, no. 3, pp. 338-342.

Briançon, L., Fournier, P. and Frechou, D., 2013, "Marine propeller noise measurements techniques in hydroacoustics tunnel", 3rd International Conference on Advanced Model Measurement Technology for the EU Maritime Industry AMT'13.

Brown, N.A., 1976, "Cavitation noise problems and solutions", International Symposium on Ship-board Acoustics, Noordwijkerhout, The Netherlands.

BV, 2018, "Underwater Radiated Noise (URN)", Rule Note, NR 614 DT R02 E, Bureau Veritas.

Carlton, J.S., 2018, "Marine Propellers & Propulsion", Butterworth-Heinemann Ltd, Oxford, UK, 4th E.

CCS, 2018, "Guideline for ship underwater radiated noise", China Classification Society.

Ceccio, S.L. and Brennen, C.E., 1991, "Observations of the dynamics and acoustics of travelling bubble cavitation", Journal Fluid Mechanics, Vol. 233, pp. 633–660.

Chen L., Zhang L., Peng, X. and Shao X., 2019, "Influence of water quality on the tip vortex cavitation inception", Physics of Fluids, Vol. 31, art. 023303.

Chmelnitsky, E. and Gilbert, M., 2016, "Vessel quieting design, technology, and mainten-ance options for potential inclusion in EcoAction Program". Report 302-045.03, Hemmera Envirochem Inc.

Cho, S., Kang, D., Park, J.S. and Hahn, J., 2018, "Spatial mapping of underwater noise radiated from passing vessels using automatic identification system data", Japanese Journal of Applied Physics, Vol. 57, no. 7S1, art. 07LG07.

Cianferra, M, Petronio, A. and Armenio, V., 2019, "Numerical prediction of ship propeller noise through acoustic analogy", Sixth International Symposium on Marine Propulsors - smp'19, Rome, Italy.

Colbert, B.R., 2020, "Trends and developments in international regulation of anthropogenic sound in aquatic habitats". Journal of the Acoustical Society of America Vol. 147, no. 5, pp. 3100-3107.

Collins, M. D., 1993, " A split-step Padé solution for the parabolic equation method ", Journal of the Acoustical Society of America, Vol. 93, no. 4, pp. 1736-1742.

Collins, M. D., Cederberg, R. J., King, D. B. and Chin-Bing, S. A., 1996, "Comparison of algorithms for solving parabolic wave equations", Journal of the Acoustical Society of America, Vol. 100, no. 1, pp. 178-182.

Dinsenmeyer, A., Antoni, J., Leclère, Q. and Pereira, A., 2020, "A probabilistic approach for cross-spectral denoising: benchmarking with some recent methods", Journal of the Acoustical Society of America, Vol. 147, no. 5, pp. 3108-3127.

DNV-GL, 2019, Class Guideline DNVGL-CG-0313, Edition July 2019, "Measurement procedures for noise emission", Det Norske Veritas and Germanischer Lloyd.

DNV-GL, 2020, Rules for classification – Ships, DNVGL-RU-Ship Pt.6 Ch.7, Section 6 "Underwater Noise Emission – Silent", Det Norske Veritas and Germanischer Lloyd.

Dowling, A.P. and Ffowcs Williams, J.E., 1983, "Sound and Sources of Sound", John Wiley & Sons.

Duarte, C.M., Chapuis, L., Collin, S.P., Costa, D.P., Devassy, R.P., Eguiluz, V.M., Erbe, C., Gordon, T.A.C., Halpern, B.S., Harding, H.R., Havlik, M.N., Meekan, M., Merchant, N.D., Miksis-Olds, J.L., Parsons, M., Predragovic, M., Radford, A.N., Radford, C.A., Simpson, S.D., Slabbekoorn, H., Staaterman, E., Van Opzeeland, I.C., Winderen, J., Zhang, X. and Juanes, F., 2021, "The soundscape of the Anthropocene ocean", Science, Vol. 371, no. 6529, art. eaba4658.

Ebert, E., Kleinwächter, A., Kostbade, R. and Damaschke, N., 2018, "Dynamic water quality measurements on the full scale ferry ship "Loch Seaforth" by the Hydrodynamic Nuclei Concentration (HDNC) technique", 32nd Symposium on Naval Hydrodynamics, Hamburg, Germany, August 2018.

Erbe, C., Marley, S.A., Schoeman, R.P., Smith, J.N., Trigg, L.E. and Embling, C.B., 2019, "The Effects of Ship Noise on Marine Mammals—A Review", Frontiers in Marine Science, Vol. 6: art. 606.

Etter, P.C., 2013, "Underwater Acoustic modeling and simulation", 4th Edition, CRC Press.

Food and Agriculture Organization of the United Nations (FAO), 2019, Joint GFCM/ OceanCare Workshop on anthropogenic underwater noise and impacts on fish, invertebrates and fish resources, FAO headquarters, Rome, Italy, 21-22 February 2019.

Farassat, F., 1981, "Linear acoustic formulas for calculation of rotating blade noise", AIAA Journal, Vol. 19, no. 9, pp. 1122–1130.

Farassat, F., 2007, "Derivation of formulations 1 and 1A of Farassat", Technical Memorandum (TM) L-19318 NASA/TM-2007-214853.

Felli, M., Grizzi, S. and Falchi, M., 2014, "Novel approach for the isolation of the sound and pseudo-sound contributions from near field pressure fluctuation measurements: Analysis of the hydroacoustic and hydrodynamic perturbation in a propeller-rudder system", Experiment in Fluids, Vol. 55, no. 1, art. 1651.

Felli M., Falchi M. and Dubbioso, G., 2015, "Experimental approaches for the diagnostics of hydroacoustic problems in naval propulsion", Ocean Engineering, Vol. 106, pp. 1-19.

Feltane, A., Fayee, Boudreaux-Bartels, G. and Boudria, Y., 2018, "Using the Lambert-W function to create a new class of warped time-frequency representations", Circuits, Systems, and Signal Processing, Vol. 37, pp. 3191-3205.

Ffowcs Williams, J.E. and Hawkings, D.L., 1969, "Sound Generated by Turbulence and Surfaces in Arbitrary Motion", Philosophical Transactions of the Royal Society. Series A, Vol. 264, no. 1151, pp. 321-342.

Fischer, R. and Brown, N.A., 2005, "Factors affecting the underwater noise of commercial vessels operating in environmentally sensitive areas", OCEANS 2005, Proceedings of MTS/IEEE, Vol. 3, pp. 1982-1988.

Foeth, E.J. and Bosschers, J., 2016, 'Localization and Source-Strength Estimation of Propeller Cavitation Noise using Hull Mounted Pressure Transducers', 31st Symposium on Naval Hydrodynamics, Monterey, California.

Franc, J.-P. and Michel, J.-M., 2004, "Fundamentals of Cavitation", Kluwer Academic Press, Dordrecht.

Gaggero, S., Gaggero, T., Rizzuto, E., Tani, G., Villa, D. and Viviani, M., 2016, "Ship propeller side effects: pressure pulses and radiated noise", Noise Mapping, Vol. 3, no. 1, pp. 295-315.

Gao, J., Yu, L. and Jiang, W., 2019, "Extraction of target sources from incoherent and partially coherent background noise using low-rank and sparse decomposition of the cross-spectral matrix", Inter-noise 2019, Madrid, Spain, June 2019.

Gassman, M., Kindberg, L.B., Wiggins, S.M. and Hildebrand, J.A., 2017a, "Underwater noise comparison of pre- and post-retrofitted Maersk G-class container vessels", Marine Physical Laboratory, Scripps Institute of Oceanography, Report MPL-TM-616.

Gassmann, M., Wiggins, S.M. and Hildebrand, J.A., 2017b, "Deep-water measurements of container ship radiated noise signatures and directionality", Journal of the Acoustical Society of America, Vol. 142, no. 3, pp. 1563-1574.

Gedamke, J., Harrison, J., Hatch, L. et al. (2016). "Ocean noise strategy roadmap", NOAA report, USA.

Gennaretti, M., Luceri, L. and Morino, L., 1997, "A Unified Boundary Integral Methodology for Aerodynamics and Aeroacoustics of Rotors", Journal of Sound and Vibration, Vol. 200, no. 4, pp. 461–489.

Greco, L., Muscari, R., Testa, C. and Di Mascio, A., 2014, "Marine Propellers Performance and Flow-Field Features Prediction by a Free-Wake Panel Method", Journal of Hydrodynamics, Ser.B, Vol. 26, no. 5, pp. 780-795.

Hald, J., 2017, "Removal of incoherent noise from an averaged cross-spectral matrix", Journal of the Acoustical Society of America, Vol. 142, no. 2, pp. 846-854.

Hald, J., 2019, "Denoising of cross-spectral matrices using canonical coherence", Journal of the Acoustical Society of America, Vol. 146, no. 1, pp. 399-408.

Hallander, J., 2017, "Systematic cavitation tunnel tests with a propeller in uniform and inclined flow conditions as part of a round robin campaign", 5th International Conference on Advanced Model Measurement Technologies for the Maritime Industry - AMT'17 (Glasgow, UK).

Halliday, W., Insley, S., Hilliard, C., de Jong, T. and Pine, M., 2017, "Potential impacts of shipping noise on marine mammals in the western Canadian Arctic", Marine Pollution Bulletin, Vol. 123, pp. 73-82.

Hannay, D., MacGillivray, A., Wladichuk, J., Pace, F. and Frouin-Mouy, H., 2019, "Comparison of Class Society Quiet Notation maximum noise levels with ECHO program measurements" [presentation], Quieting Ships to Protect the Marine Environment: Technical Workshop. Hosted by the International Maritime Organization (IMO), 30 Jan to 1 Feb 2019, London, U.K.

Harrison, C.H. and Harrison, J.S., 1995, "A simple relationship between frequency and range averages for broadband sonar", Journal of Acoustical Society of America, Vol. 97, no. 2, pp.1314-1317.

Haver, S.M., Fournet, M.E.H., Dziak, R.P., Gedamke, J., Hatch, L.T., Haxel, J., Heppell, S.A., McKenna, M.F., Mellinger, D.K. and Van Parijs, S.M., 2019, "Comparing the underwater soundscapes of four US national parks and marine sanctuaries", Frontiers in Marine Science, Vol. 6, art. 500.

He, T., Humphrey, V.F., Mo S. and Fang, E., 2020, "The effect of water surface roughness on the measurement of radiated ship noise", Proceedings of Meetings on Acoustics, Vol. 40, no. 1, art. 070019.

Heinke, H.-J., 2003, "The influence of test parameters and wake field simulation on the cavitation and the propeller induced pressure fluctuations", STG-Sprechtag Kavitation, Hamburg.

Heinke, H.-J., Johannsen, C., Kröger, W., Schiller, P. and Weitendorf, E.-A., 2012, "On cavitation nuclei in water tunnels", Eighth International Symposium on Cavitation - Cav2012. Singapore: Paper No. 270.

Howe, M., 2002, "Frontmatter. In Theory of Vortex Sound" Cambridge Texts in Applied Mathematics, pp. I-Viii, Cambridge University Press. Cambridge.

Hynninen, A., Tanttari, J., Viitanen, V.M. and Sipilä, T., 2017, "On predicting the sound from a cavitating marine propeller in a tunnel", 5th International Symposium on Marine Propulsors, SMP'17, Espoo, Finland, June 2017.

Ianniello, S., 2015, "Sheet Cavitation Noise Prediction from A Marine Propeller", 22nd International Congress on Sound and Vibration (ICSV22), Florence, Italy.

Ianniello, S., 2016, "The Ffowcs Williams–Hawkings equation for hydroacoustic analysis of rotating blades. Part 1. The rotpole", Journal of Fluid Mechanics, Vol. 797, pp. 345-388.

Ianniello, S., Muscari, R. and Di Mascio, A., 2013, "Ship Underwater Noise Assessment by the Acoustic Analogy. Part I: Nonlinear Analysis of a Marine Propeller in a Uniform Flow", Journal of Marine Science and Technology, Vol. 18, no. 4, pp 547-570.

Ianniello, S., Muscari, R. and Di Mascio, A., 2014, "Ship Underwater Noise Assessment by the Acoustic Analogy part II: Hydroacoustic Analysis of a Ship Scaled Model", Journal of Marine Science Technology, Vol. 19, pp:52–74.

Ianniello, S. and De Bernardis, E., 2015, "Farassat's Formulations in Marine Propeller Hydroacoustics", International Journal of Aeroacoustics, Vol. 14, no. 1 & 2, pp. 87 – 103.

ISO, 2016, ISO 17208-1:2016, "Underwater acoustics – Quantities and procedures for description and measurement of underwater sound from ships – Part 1: Requirements for precision measurements in deep water used for comparison purposes", ISO Procedure.

ISO, 2019a, ISO 17208-2:2019, "Underwater acoustics – Quantities and procedures for description and measurement of underwater sound from ships – Part 2: Determination of source level from deep water measurements", ISO Procedure.

ISO, 2019b, ISO 20233-2:2019(E), "Ships and marine technology – Model test method for propeller cavitation noise evaluation in ship design – Part 2: Noise source localization", ISO Procedure.

ITTC, 2014, 27th ITTC Conference, Copenhagen, Denmark.

ITTC, 2017a, 28th ITTC Conference, Wuxi, China.

ITTC, 2017b, Recommended Procedures and Guidelines 7.5–04 04-01 Underwater Noise from Ships, Full Scale Measurements.

Jensen, F.B., Kuperman, W.A., Porter, M.B. and Schmidt, H., 2011, Computational Ocean Acoustics, 2nd Edition, Springer.

Jiang, P., Lin, J., Sun, J., Yi, X. and Shan, Y., 2020, "Source spectrum model for merchant ship radiated noise in the Yellow Sea of China", Ocean Engineering, Vol. 216, art. 107607.

Johannsen, C., 1998, "Investigation of propeller-induced pressure pulses by means of high-speed video recording in the three-dimensional wake of a complete ship model", 22nd Symposium on Naval Hydrodynamics, Washington, D.C.

Johansson T, Hallander J, Karlsson R, Långström A. and Turesson, M., 2015 "Full scale measurements of underwater radiated noise from a coastal tanker". OCEANS 2015 MTS/IEEE Conference, Genova, May 18-21, 2015.

Joy, R., Tollit, D., Wood, J., MacGillivray, A., Li, Z., Trounce, K. and Robinson O., 2019, "Potential benefits of vessel slowdowns on endangered southern resident killer whales". Frontiers in Marine Science, Vol. 6, Article 344.

Kamiirisa, H., 2001, "The effect of water quality characteristics on cavitation noise", Fourth International Symposium on Cavitation, California Institute of Technology.

Kendrick, A. and Terweij, R. 2019, "Ship underwater radiated noise", Report Vard Marine Inc.

Kerwin, J.E., 1986, "Marine Propellers", Annual Reviews of Fluid Mechanics, Vol. 18, pp. 367–403.

Khoo, M. T., Venning, J. A., Pearce, B. W., Brandner, P. A. and Lecoffre, Y., 2016, "Development of a Cavitation Susceptibility Meter for Nuclei Size Distribution Measurements", 20th Australasian Fluid Mechanics Conference, Perth, Australia, AFMS.

Khoo, M. T., Venning, J. A., Pearce, B. W., Takahashi, K., Mori T. and Brandner, P. A., 2020a, "Natural nuclei population dynamics in cavitation tunnels", Experiments in Fluids, Vol. 61, art. 34.

Khoo, M. T., Venning, J. A., Pearce, B. W. and Brandner, P. A., 2020b, " Statistical aspects of tip vortex cavitation inception and desinence in a nuclei deplete flow", Experiments in Fluids, Vol. 61, art. 145.

Kim, D., Seong, W., Choo, Y. and Lee, J., 2015, "Localization of incipient tip vortex cavitation using ray based matched field inversion method", Journal of Sound and Vibration, Vol. 354, pp. 34-46.

Kinnas, S.A. and Fine, N.E., 1992, ''A Nonlinear Boundary Element Method for the Analysis of Propeller Sheet Cavitation,'' 19th Symposium on Naval Hydrodynamics, ONR, Seoul Korea, pp. 1–17.

Kinnas, S. and Pyo, S., 1999, "Cavitating propeller analysis including the effects of wake alignment", Journal of Ship Research, Vol. 43, pp. 38–47.

Kinnas, S., Lee, H.S. and Young, Y.L., 2003, "Modeling of Unsteady Sheet Cavitation on Marine Propeller Blades", International Journal of Rotating Machinery, Vol. 9, pp. 263–277.

Kleinsorge, L., Schemmink, S., Klose, R. and Greitsch, L., 2017, "Case study for the determination of propeller emitted noise by experimental and computational methods", 5th International Symposium On Marine Propulsors - SMP'17, Espoo, Finland, June 2017.

Knapp, R.T., Daily, J.W. and Hammitt, F.G., 1970, "Cavitation", McGraw-Hill Book Company, New York.

Kozaczka, E. and Grelowska, G., 2018. "Propagation of ship-generated noise in shallow sea", Polish Maritime Research, Vol. 25, pp. 37-46.

Kuttruff, H., 2009, "Room acoustics", Fifth edition, Spon Press, Taylor & Francis, U.K.

Lafeber, F.H., Bosschers, J., de Jong, C. and Graafland, F., 2015, "Acoustic reverberation measurements in the Depressurized Towing Tank", 4th International Conference on Advanced Model Measurement Technologies for the Maritime Industry AMT'15, Istanbul, Turkey.

Lafeber, F.H. and Bosschers, J., 2016, "Validation of Computational and Experimental Prediction Methods for the Underwater Radiated Noise of a Small Research Vessel", PRADS, Copenhagen, Denmark.

Lafeber, F.H. and Lloyd, T., 2017, "Round robin test on the underwater radiated noise of a cavitating ship propeller in open water". 5th International Conference on Advanced Model Measurement Technologies for the Maritime Industry -AMT'17, (Glasgow, UK).

Lampe, T., Radtke, L., Göttsche, U., Düster, A. and Abdel-Maksoud, M., 2019, "Evaluation of performance and acoustic signature of flexible marine propellers under consideration of fluid-structure interaction by means of partitioned simulation", Sixth International Symposium on Marine Propulsors - smp'19, Rome, Italy.

Lebrun, D., Allano, D., Méès, L., Walle, F., Corbin, F., Boucheron, R. and Fréchou, D., 2011, "Size measurement of bubbles in a cavitation tunnel by digital in-line holography", Applied Optics, Vol. 50, no. 34, pp. H1—H9.

Lecoffre, Y., 1987, "Procedures and Instrumentation for monitoring gas content in cavitation test loops", ASME International Symposium on Cavitation Research Facilities and Techniques, December 1987.

Lee, J.T., 1987, "A Potential Based Panel Method for the Analysis of Marine Propellers in Steady Flow", Tech. Rep. 87-13, Department of Ocean Engineering, MIT, Cambridge, Massachusetts USA.

Lee, J.H., Jung, J.K., Lee, K.J., Han, J.M., Park, H.G. and Seo, J.S., 2012, "Experimental Estimation of a Scaling Exponent for Tip Vortex Cavitation via Its Inception Test in Full- and Model-ship", Journal of Hydrodynamics, Vol. 24, no. 5, pp. 658-667.

Li, D.Q., Hallander, J. and Johansson, T., 2018, "Predicting underwater radiated noise of a full scale ship with model testing and numerical methods". Ocean Engineering, Vol. 161, pp. 121–135.

Lidtke, A.K., Humphrey, V.F. and Turnock, S.R., 2016, "Feasibility study into a computational approach for marine propeller noise and cavitation modelling", Ocean Engineering, Vol. 120, pp. 152–159.

Lidtke, A., Lloyd, T. and Vaz, G., 2019, "Acoustic modelling of a propeller subject to non-uniform inflow", Sixth International Symposium on Marine Propulsors, smp'19, Rome, Italy.

Lighthill M.J., 1952, "On sound generated aerodynamically: 1. general theory", Proceeding of The Royal Society A, Vol. 211, pp. 564–578.

Lloyd, T.P., Rijpkema, D. and van Wijngaarden, E., 2014, "Implementing the Ffowcs Williams-Hawkings acoustic analogy into a viscous CFD solver", Numerical Towing Tank Symposium, Marstrand, Sweden.

Lloyd, T.P., Lidtke, A.K., Rijpkema, D., van Wijngaarden, E., Turnock, S.R. and Humphrey, V.F., 2015a, "Using the FW-H equation for hydroacoustics of propellers", 15th Numerical Towing Tank Symposium. Cortona.

Lloyd, T., Rijpkema, D. and van Wijngaarden, E., 2015b, "Marine propeller acoustic modelling: comparing CFD results with an acoustic analogy method". Fourth International Symposium on Marine Propulsors, spm'15, Austin, Texas.

Lloyd, T., Lafeber, F.H. and Bosschers, J., 2018, "Investigation and Validation of Procedures for Cavitation Noise Prediction from Model-Scale Measurements", 32nd Symposium on Naval Hydrodynamics, Hamburg, Germany, 5-10 August 2018.

Løvik, A., 1981, "Scaling of Propeller Cavitation Noise", Noise sources in ships, Nordforsk, Stockholm, Sweden.

LR, 2017, ShipRight - Design and Construction - Additional Design and Construction Procedure for the Determination of a Vessel's Underwater Radiated Noise, Lloyd's Register.

Lyon, R.H. and DeJong, R.G., 1995, "Theory and Application of Statistical Energy Analysis", Second Edition, Butterworth-Heinemann, Boston, 1995, 227 p.

McCormick Jr., B.W., 1962, "On cavitation produced by a vortex trailing from a lifting surface", Journal of Basic Engineering, Vol. 84, no. 3, pp. 369-379.

Méès, L., Lebrun, D., Allano, D., Walle, F., Lecoffre, Y., Boucheron, R. and Fréchou, D., 2010, "Development of interferometric techniques for nuclei size measurement in cavitation tunnel", 28th Symposium on Naval Hydrodynamics, Pasadena, California, September 2010.

Mendez, S., Sharma, A., Shoeybi, M. and Lele, S.K., 2009, "Post-processing of large eddy simulations for jet noise predictions," CTR Annual Research Briefs.

Mendez, S., Shoeybi, M., Lele, S.K. and Moin, P., 2013, "On the Use of the Ffowcs Williams-Hawkings Equation to Predict Far-Field Jet Noise from Large-Eddy Simulations", International Journal of Aeroacoustics, Vol. 12, no. 1, pp 1-20.

Merkle, C.L. and Athavale, M., 2012, "Time-accurate unsteady incompressible flow algorithm based on artificially compressibility". AIAA paper 87-1137.

Meyer, V. and Audoly, C., 2019, "A parametric study of the environment and the array configuration for underwater noise measurement from ships in shallow water", 26th International Congress on Sound and Vibrations, Montréal, Canada, 7-11 July 2019.

Meyer, V. and Audoly, C., (2020). "Accounting for sea floor properties in the assessment of underwater noise radiated from ships in shallow water." Proceedings of Meetings on Acoustics, Vol. 40, no. 1, art. 070007.

MacGillivray, A.O., Zizheng, L., Hannay, D.E., Trounce, K.B. and Robinson, O.M., 2019, "Slowing deep-sea commercial vessels reduces underwater radiated noise". Journal of the Acoustical Society of America., Vol. 146, no. 1, pp. 340-351.

McHorney, D.H., Pelella, G.M., Hilliard, L.C. and Palmieri, M.R., 2018, "Methods to Minimize Commercial Vessel-Generated Marine Acoustic Pollution", Retrieved from https://digitalcommons.wpi.edu/iqp-all/5247

Miglianti, F., Cipollini, F., Oneto, L., Tani, G. and Viviani, M., 2019a, " Model scale cavitation noise spectra prediction: Combining physical knowledge with data science", Ocean Engineering, Vol. 178, pp. 185-203.

Miglianti F., Tani G., Viviani M., Cipollini F. and Oneto L., 2019b, "Data driven models for propeller cavitation noise in model scale", Sixth International Symposium on Marine Propulsors (smp'19).

Mitson, R.B., (Ed), 1995, "Underwater noise of research vessels: Review and recommendations", ICES Study Group Report.

Moreno, A., (Ed.), 2014, "European URN Standard Measurement Method", AQUO EU FP7 Project, Deliverable 3.1.

Morino, L., Chen, L.T. and Suciu, E.O., 1975, ''Steady and Oscillatory Subsonic and Supersonic Aerodynamics Around Complex Configurations,'' AIAA Journal, Vol. 13, pp. 368–374.

Morino, L. and Gennaretti, M, 1992, "Boundary Integral Equation Methods for Aerodynamics", Computational Nonlinear Mechanics in Aerospace Engineering, Atluri, S.N. (ed), Progress in Aeronautics & Astronautics, AIAA, Washington, DC, Vol. 146, pp. 279-320.

Morse, P.M. and Ingard, K.U., 1968, "Theoretical acoustics", Princeton University Press.

Nitzkorski, Z. and Mahesh, K., 2014, "A dynamic end-cap technique for sound computation using the Ffowcs Williams and Hawkings equations", Physics of Fluids Vol. 26, no. 11, art. 115101.

Okamura, N. and Asano, T., 1988, "Prediction of Propeller Cavitation Noise and Its Comparison with Full-Scale Measurements", Journal of Naval Architects of Japan, Vol. 164, pp.19-33

Oshima, A., 1990, "A study on correlation of vortex cavitation noise of propeller measured in model experiments and full scale". Journal of the Society of Naval Architects of Japan, Vol. 168, no. 1, pp. 89–96.

Oshima, A., 1994, "Scaling of Tip Vortex Cavitation Noise of Propeller", Technical report, Vol. 31, No. 3, Mitsubishi Heavy Industries, Ltd., Nagasaki, Japan.

Pang, Y., Liu, J., Yu, M. and Wu, W., 2020a, "Propagation loss analysis using ship radiated noise in shallow water." Proceedings of Meetings on Acoustics, Vol. 40, no. 1, art. 070010.

Pang, Y., Yu, M., Wu, W. and Wang, S., 2020b, "Ship noise source level measurement in shallow water based on experimental propagation loss", ResearchGate, Doi:10.13140/RG.2.2.31101.38883.

Papoulis, A., 2002, "Probability, random variables and stochastic processes", 4th edition, McGraw-Hill.

Park, C., Kim, G., Park, Y., Lee, K. and Seong, W., 2016, "Noise Localization Method for Model Tests in a Large Cavitation Tunnel Using Hydrophone Array", Remote Sensing, 2016, Vol. 8, no. 3, art. 195.

Park, C., Kim, G.-D., Park, Y.-H., Jang, H.-G. and Jang, Y.H., 2018, "A Study on the Model Test for the Twin Propeller Cavitation Noise" (in Korean). Journal of the Society of Naval Architects of Korea, Vol. 55, no. 1, pp. 28-36.

Park, C., Kim, G. D., Yim, G.-T., Park, Y., and Moon, I.-S., 2019, "The validation of model test method for propeller cavitation noise prediction". 6th International Conference on Advanced Measurement Technology for the Maritime Industry, AMT'19, Rome, Italy.

Park, C., Kim, G.D., Yim, G.T., Park, Y.H. and Moon, I., 2020, "A validation study of the model test method for propeller cavitation noise prediction", Ocean Engineering, Vol. 213, art. 107655.

Park, J. and Seong, W., 2017, "Novel scaling law for estimating propeller tip vortex cavitation noise from model experiment". Journal of Hydrodynamics, Vol. 29, no. 6, pp. 962–971.

Poinsot, T.J. and Lele, S.K., 1992, "Boundary conditions for direct simulations of compressible viscous flows", Journal of Computational Physics, Vol. 101, no. 1, pp. 104-129.

Popper, A.N. and Hastings, M.C., 2009, "The effects of anthropogenic sources of sound on fishes", Journal of Fish Biology, Vol. 75, pp. 455-589.

Renilson, M. 2009, "Reducing underwater noise pollution from large commercial vessels". Report to IFAW, ISBN: 978-1-906920-02-9.

Rijpkema D., Starke B. and Bosschers J., 2013, "Numerical simulation of propeller-hull interaction and determination of the effective wake field using a hybrid RANS-BEM approach", Third International Symposium on Marine Propulsors smp'13, Launceston, Tasmania, Australia.

van Rijsbergen, M.X. and Beelen, S., 2019, "A Lagrangian analysis of scale effects on sheet cavitation inception", 6th International Symposium on Marine Propulsors SMP-19, Rome, Italy, May 2019.

RINA, 2017, Amendments to Part A and Part F of "Rules for the Classification of Ships" - New additional class notation: "DOLPHIN QUIET SHIP" and "DOLPHIN TRANSIT SHIP", Registro Italiano Navale.

Robinson, S.P., Lepper, P.A. and Hazelwood, R.A., 2014, "Good Practice Guide for Underwater Noise Measurement". NPL Good Practice Guide No. 133, National Measurement Office, Marine Scotland, The Crown Estate, ISSN:1368-6550.

Ross, D., 1976, "Mechanics of Underwater Noise", Pergamon Press.

Russell, P., Venning, J., Pearce, B.W. and Brandner, P.A., 2020a, "Calibration of Mie scattering imaging for microbubble measurement in hydrodynamic test facilities", Experiments in Fluids, Vol. 61, art. 93.

Russell, P.S., Barbaca, L., Venning, J.A., Pearce, B.W. and Brandner, P.A., 2020b, "Measurement of nuclei seeding in hydrodynamic test facilities", Experiments in Fluids, Vol. 61, art. 79.

Sakamoto, N., Fujisawa, J., Sawada, Y., Ukon, Y. and Kamiirisa, H., 2017, "Measurement of cavitation noise radiated from a marine propeller with and without shaft inclination" 5th International Conference on Advanced Model Measurement Technologies for the Maritime Industry - AMT'17, Glasgow, UK.

Salvatore, F. and Esposito, P.G., 2001, "An improved boundary element analysis of cavitating three-dimensional hydrofoils", Fourth International Symposium on Cavitation - CAV2001, California Institute of Technology.

Salvatore, F. and Ianniello, S., 2003, "Preliminary Results on Acoustic Modelling of Cavitating Propellers", Journal of Computational Mechanics, Vol. 32, pp. 291–300.

Salvatore, F., Testa, C. and Greco, L., 2003, "A Viscous/Inviscid Coupled Formulation for Unsteady Sheet Cavitation Modelling of Marine Propellers", Fifth International Symposium on Cavitation - Cav2003, Osaka, Japan.

Salvatore, F., Streckwall, H. and van Terwisga, T., 2009a, "Propeller cavitation modelling by CFD-results from the VIRTUE 2008 Rome workshop", 1st International Symposium on Marine Propulsors, Trondheim, Norway.

Salvatore, F., Testa, C. and Greco, L., 2009b, "Coupled Hydrodynamics–Hydroacoustics BEM Modelling of Marine Propellers Operating in a Wakefield", 1st International Symposium on Marine Propulsors, Trondheim, Norway.

Schuiling, B., Lafeber, F.H., van der Ploeg, A. and van Wijngaarden, E., 2011, "The Influence of the Wake Scale Effect on the Prediction of Hull Pressures due to Cavitating Propellers", Second International Symposium on Marine Propulsors SMP'11, Hamburg, Germany, June 2011.

Seol H., 2013, "Time Domain Method for the Prediction of Pressure Fluctuation Induced by Propeller Sheet Cavitation: Numerical Simulations and Experimental Validation", Ocean Engineering, Vol. 72, pp. 287-296.

Seol, H., Jung, B., Suh, J-C. and Lee, S., 2002, "Prediction of Non–Cavitating Underwater Propeller Noise", Journal of Sound and Vibration, Vol. 257, no. 1, pp. 131–156.

Seol, H., Suh, J-C. and Lee S., 2005, "Development of Hybrid Method for the Prediction of Underwater Propeller Noise", Journal of Sound and Vibration, Vol. 288, pp 345–360.

Seol, H., Paik, B.G., Park, Y.H., Kim, K.Y., Ahn, J.W., Park, C., Kim, G.D. and Kim, K.S., 2015, "Propeller Cavitation Noise Model Test in KRISO Large Cavitation Tunnel and Its comparison with Full-Scale Results", 4th International Conference on Advanced Model Measurement Technology for the Maritime Industry, Gdansk, Poland.

Shorter, P.J. and Langley, R.S., 2005a, "Vibro-acoustic analysis of complex system", Journal of Sound and Vibration, Vol. 288, no. 3, pp. 669-699.

Shorter, P.J. and Langley, R.S., 2005b, "On the reciprocity relationship between direct field radiation and diffuse reverberant loading", Journal of the Acoustical Society of America, Vol. 117, no. 1, pp. 85-95.

Shur, M.L., Spalart, P.R., and Strelets, M.K., 2005, "Noise prediction for increasingly complex jets. Part I: Methods and tests", International Journal of Aeroacoustics, Vol. 4, no. 3, pp. 213–246.

Sipilä, T., Viitanen V., Uosukainen, S. and Klose, R., 2019. "Shallow Water Effects on Ship Underwater Noise Measurements", Proceedings of Internoise 2019.

Southall, B.L., Bowles, A.E., Ellison, W.T., Finneran, J.J., Gentry, R.L., Greene Jr., C.R., Kastak, D., Ketten, D.R., Miller, J.H., Nachtigall, P.E., Richardson, W.J., Thomas, J.A. and Tyack, P.L., 2008, "Marine mammal noise exposure criteria: Initial scientific recommendations", Aquatic Mammals, Vol. 33, no. 4, pp. 411-521.

Spence, J., Fisher, R., Bahtiarian, M., Boroditsky, L., Jones, N. and Dempsey, R., 2007, "Review of existing and future potential treatments for reducing underwater sound from oil and gas industry activities", NCE Report 07-001, Noise Control Engineering, Inc., 185 p.

Strasberg, M., 1977, "Propeller Cavitation Noise after 35 Years of Study", ASME symposium on Noise and Fluids Engineering, Atlanta, USA.

Tani, G., Viviani, M., Armelloni, E. and Nataletti, M., 2016a, "Cavitation Tunnel Acoustic Characterisation and Application to Model Propeller Radiated Noise Measurements at Different Functioning Conditions", Proceedings of the Institution of Mechanical Engineers, Part M: Journal of Engineering for the Maritime Environment, Vol. 230, no. 2, pp. 250–266.

Tani, G., Viviani, M., Hallander, J., Johansson,

T. and Rizzuto, E., (2016b), "Propeller underwater radiated noise: a comparison between model scale measurements in two different facilities and full scale measurements", Applied Ocean Research, Vol. 56, pp. 48–66.

Tani, G., Aktas, B., Viviani, M. and Atlar, M., 2017, "Two medium size cavitation tunnel hydro-acoustic benchmark experiment comparisons as part of a round robin test campaign", Ocean Engineering, Vol. 138, pp. 179-207.

Tani, G., Aktas, B., Viviani, M., Yilmaz, N., Miglianti, F., Ferrando, M. and Atlar, M., 2019a, "Cavitation tunnel tests for "The Princess Royal" model propeller behind a 2-dimensional wake screen", Ocean Engineering, Vol. 172, pp. 829–843.

Tani, G., Viviani, M., Ferrando, M. and Armelloni, E., 2019b, "Aspects of the measurement of the acoustic transfer function in a cavitation tunnel", Applied Ocean Research, Vol. 87, pp. 264–278.

Tani, G., Viviani, M., Felli, M., Lafeber, F.H., Lloyd, T., Aktas, B., Atlar, M., Turkmen, S., Seol, H., Hallander, J. and Sakamoto, N., 2020, "Noise measurements of a cavitating propeller in different facilities: results of the round robin test programme", Ocean Engineering, Vol. 213, art. 107599.

Testa, C., Ianniello, S., Salvatore, F. and Gennaretti, M., 2008, "Numerical approaches for hydroacoustic analysis of marine propellers", Journal of Ship Research, Vol. 52, no. 1, pp. 57–70.

Testa, C., Ianniello, S. and Salvatore, F., 2018a, "A Ffowcs Williams and Hawkings formulation for hydroacoustic analysis of propeller sheet cavitation", Journal of Sound and Vibration, Vol. 413, pp. 421-441.

Testa, C., Porcacchia, F., Greco, L. and Muscari, R, 2018b, "Effectiveness of Boundary Element Method Hydrodynamic", A. Yücel Odabaşı Colloquium Series 3rd International Meeting Progress in Propeller Cavitation and its Consequences: Experimental and Computational Methods for Predictions, 5th–16th November 2018, Istanbul, Turkey.

Thomson, D.J.M. and Barclay, D.R., 2020, "Real-time observations of the impact of COVID-19 on underwater noise", Journal of the Acoustical Society of America, Vol. 147, no. 5, pp. 3390-3396.

Traverso, F., Gaggero, T., Tani, G., Rizzuto, E., Trucco, A. and Viviani, M., 2017, "Parametric Analysis of Ship Noise Spectra", IEEE Journal of Oceanic Engineering, Vol. 42, no. 2, pp. 424-438.

UNCLOS, 2018, United Nation Convention of Law of the Sea.

Ward J. and Robinson S., 2019, "Low frequency hydrophone calibration with a Laser interferometer", Underwater Acoustics Conference and Exhibition (UACE) 2019, Hersonissos, Greece.

Wang, L., Heaney, K., Pangerc, T., Theobald, P., Robinson, S. and Ainslie, M., 2014, "Review of underwater acoustic propagation models", NPL Report. AC 12

Wang, M., Lele, S. and Moin, P., 1996, "Computation of quadrupole noise using acoustic analogy", AIAA Journal, Vol. 34, no. 11, pp. 2247-2254.

Weitendorf, E.-A., 1981, "Cavitation phenomena, propeller excited hull pressure amplitudes and cavitation scale effect." Ocean Engineering, Vol. 8, no. 5, pp. 517-539

Weitendorf, E.-A. and Tanger, H., 1999, "Cavitation Investigations in Two Conventional Tunnels and in the Hydrodynamics and Cavitation Tunnel HYKAT", Ship Technology Research, Vol. 46, pp. 43-56

Weston, D.E., 1971, Intensity-range relations in oceanographic acoustics. Journal of Sound and Vibration, Vol. 18, no. 2, pp. 271-287.

Urick, R.J., 1983, "Principles of Underwater Sound", McGraw-Hill.

Young, Y.L. and Kinnas S.A., 2003, "Numerical Modeling of Supercavitating Propeller Flows", Journal of Ship Research, Vol. 47, pp. 48-62.

Zhang, B., Xiang, Y., He, P., and Zhang, G.-J., 2019, "Study on prediction methods and characteristics of ship underwater radiated noise within full frequency", Ocean Engineering, Vol. 174, pp. 61-70.

Appendix A: Review of rules on full-scale noise measurements

Organization	Classification Societies						ISO	ANSI/ASA
	DNV-GL	BV	RINA	LR	ABS	CCS		
Rule number	**CG-0313**	**NR 614**	**/**	**/**	**295**	**GD28-2018**	**17208**	**S12.64**
Notation	Silent-E:Transit Silent-E:Quiet Silent-R / Silent-S Silent-F / Silent-A	URN - controlled vessel URN - advanced vessel URN - specified vessel	Dolphin Transit Dolphin Quiet	T for Transit Q for quiet R for research	UWN(Type) UWN+(Type)	Underwater Noise 1 Underwater Noise 2 Underwater Noise 3		
Year	2010 2019 v2	2014 2017 v2 2018 v3	2017	2018	2018	2016 2018 v2	2016 (part 1) 2019 (part 2)	2009
Water depth	Min 30 m under keel, and h> 0.64 v^2, with sloping seabed preferred	Shallow: 60 m <h <200 m and h> 0.3 v^2; Deep: >200 m and >1.5L	>150 m	Shallow: 60 m or 0,3v^2<h<150 m or 1.5L ; Deep: >150 m and >1.5L	Shallow: 60 m < h<150 m, h> 0.3 v^2; Deep: >150 m and >1.5L	Single Hydrophone: max(40 m , 0.64v^2); multiple hydrophone: max(60m , 0.3v^2).	>Max(150m,1.5L)	3 Grades A: >Max(300m,3L); B: >Max(150m,1.5L);; C: >Max(75m,1L);
Hydrophone depth(s)	0.2 m above seabed	Shallow: 3 hydrophones spaced at 15 m~20 m, with bottom 3 m~5 m from sea bottom Deep: 3 hydrophones spaced at more than 30 m, with top >40 m from surface	3 hydrophones at depths for: 15°, 30°, and 45°? below horizontal	Shallow: 3 hydrophones at h/10, h/2, and 5 m above seabed Deep: 3 hydro-phones at depths for: 15°, 30°, and 45° below horizontal	3 hydrophones at depths for: 15°, 30°, and 45° below horizontal	1 hydrophone:< 0.5 m above bottom; 3 hydrophones: spaced at 15 m~20 m, with bottom 3 m~5 m from sea bottom	3 hydrophones at depths for: 15°, 30°, and 45° below horizontal	Grade A and B: 3 hydrophone depth, 15°, 30°, and 45°; Grade C: 1 hydrophone, 20°.
CPA Distance	100 m~200 m	d_{CPA}=Max(200 m, 1L)(nominal), Max(100 m, 1L)(silent ship), 3 distances: d_{CPA},Min(400 m, 1.5 d_{CPA}), Min(500 m,2 d_{CPA})	Greater than 150 m	Greater than 100 m and ship length	Greater than 100 m and ship length	Transit:150m to 250m Quiet: d_{CPA}=Max(200 m, 1L)(nominal), Max(100 m, 1L)(silent ship),3 distances: d_{CPA},Min(400 m, 1.5 d_{CPA}), Min(500 m,2 d_{CPA})	Greater than 100 m or 1L	Greater than 100 m or 1L
Averaging time	≤ 5 kts, ship length/speed > 5 kts, 2 x ship length/speed	Time for passing ±45° of CPA, with a step of 5°	Time to travel 1.5 x ship length	Time for passing ±30° of CPA	Time for passing ±30° of CPA	2x ship length	Time for passing ±30°of CPA	Time for passing ±30°of CPA
Propagation adjustment factor	18 log r	Acoustic model ; 19 log r(water depth < 100 m);20 log r(water depth)>100 m);	20 log r	Shallow: measured or modelled Deep: 20 log r	20 log r	H<100m: 18 log r H>100m: 20 log r	20 log r	20 log r
Sea surface adjustment	None	Acoustic model	None	Shallow: measured or modelled Deep: Angle-dependent formula	None	none	angle dependent formulae (part 2)	none
Seabed reflection adjustment	-5dB	Acoustic model	None	Shallow: measured or modelled Deep: none	0.5 dB if hydrophone less than 20 cm off bottom	none	none	none
Number of passes	1 port + 1 starboard	6 port + 6 starboard, 2 at each of 3 CPA distances	2 port + 2 starboard	2 port + 2 starboard	2 port + 2 starboard	1 port + 1starborad	2 port + 2 starboard	2 port + 2 starboard
Frequency range	10 Hz to 100 kHz	10 Hz to 50 kHz	10 Hz to 40 kHz	10 Hz to 100 kHz	Commercial vessels:10 Hz to 50 kHz; Research vessels: 10 Hz to 100, 000 Hz	10 Hz to 50 kHz	10 Hz to 20 / 50 kHz	10 Hz to 10 / 25 / 50 kHz (depending on grade)
Vessel speed	Transit: 80% MCR Quiet Cruise: 11 knots for L>50 m;8 knots for L<50 m	According to the contract specifications or, by default, at NCR.	Not specified	Typically:85% MCR, Research vessels: 11 knots; Seismic vessels:5 knots; DP mode: 40% nominal load	Transit: 85% MCR Quiet: 3.1 m/s + 0.0084L	11 knots(L>50m), 8 knots (L<50m)	not specified	not specified
Measurement Result type	RNL (modified)	RNL	RNL	MSL	RNL(modified)	RNL	RNL(part 1) MSL(part 2)	RNL

L= Overall ship length; h= Water depth; RNL= Radiated Noise Level; MSL= Monopole Source Level; MCR= Maximum Continuous Rating